Universität Stuttgart

Analytical Energy Gradients for Open-Shell Local Second-Order Møller-Plesset Perturbation Theory and Applications to large Molecules

Von der Fakultät Chemie der Universität Stuttgart zur Erlangung der Würde eines Doktors der Naturwissenschaften (Dr. rer. nat.) genehmigte Abhandlung

Vorgelegt von
Mark Julian Dornbach
aus Esslingen a. N.

Hauptberichter: Prof. Dr. Hans-Joachim Werner

Mitberichter: Prof. Dr. Willem Klopper

Tag der mündlichen Prüfung: 31. Juli 2018

Institut für Theoretische Chemie

2018

Contents

Acknowledgements

By signing the declaration of authorship below I am certifying that this dissertation is 'entirely my own work'. This is of course only true in a very narrow sense, as there are many, many people that supported me during this work, without whom I would have not managed to investigate the topics below in such a productive manner. Therefore, I want to briefly express my gratitude to all of them.

First of all, I want to thank my supervisor Prof. Dr. Hans-Joachim Werner for countless discussions, an always open door, for his patience, and for providing me with all means necessary to conduct my research.

Furthermore, a very big thank you to Prof. Dr. Peter Schwerdtfeger for welcoming me into his group in Auckland, and his ideas, hints and frequent good advice. Thank you as well to Prof. Dr. Ricardo Mata for sharing the details of Molpros COSMO implementation, and to Dr. Max Schwilk for a machine-readable version of the FH-set geometries. I also want to thank Prof. Dr. Willem Klopper for agreeing to be my external examiner and everyone involved in proofreading this work.

Let me additionally express my gratitude to Prof. Dr. László v. Szentpály for good discussions, even better wine, and counselling whenever needed, and to my fellow PhDs Christine Krause and Dr. Max Schwilk for a lot more than just sharing an office with me.

Finally, and maybe most important, I want to thank Anna Madeo and my parents Hanne and Dr. Josef Dornbach for their continued love and support, especially during – but not limited to – the last four years.

Zusammenfassung

Die Nutzung lokaler Näherungen zur Berechnung der dynamischen Elektronenkorrelation ermöglicht es, Energien für Moleküle mit einigen hundert Atomen vorherzusagen. Über diese Methoden zur Berechnung von Energien hinausgehend existieren jedoch kaum niedrig skalierende *ab initio* Modelle um weitere Eigenschaften, wie beispielsweise Dipolmomente oder Gleichgewichtsgeometrien, zu berechnen. Analytische Gradienten, basierend auf lokaler Møller-Plesset-Störungstheorie (LMP2), waren ursprünglich nur für geschlossenschalige Moleküle mit Pipek-Mezey-Lokalisation (PM) im besetzten Raum verfügbar; der virtuelle Raum wird dabei durch aus projizierten Atomorbitalen (PAOs) generierten Domänen beschrieben. Die Nutzung von PM ist teilweise problematisch, da bei der Verwendung diffuser Funktionen im Basissatz Konvergenzprobleme auftreten können.

In dieser Arbeit wurden daher offen- und geschlossenschalige LMP2-Gradienten basierend auf intrinsischen Bindungsorbitalen (IBOs) implementiert. IBOs sind ein alternativer Ansatz zur Lokalisierung besetzter Räume. Im Gegensatz zur weit verbreiten PM-Methode sind sie schneller zu berechnen und sehr stabil gegenüber Änderungen des verwendeten Basissatzes. IBOs vermeiden Lokalisierungsartefakte und zeigen das von qualitativen chemischen Konzepten bekannte Bindungsbild. Sie werden durch Projektion der besetzten Orbitale auf eine minimale Basis von Atomorbitalen generiert, was in einem Zwischenschritt zu so genannten intrinsischen Atomorbitalen (IAOs) führt. Die Lokalisierung des besetzten Raumes erfolgt dann auf der Basis dieser IAOs. Grundsätzlich machen es diese Projektionen aufwändiger, analytische Gradienten abzuleiten und am Ende effizient zu implementieren. Dies ist im Rahmen dieser Arbeit dennoch gelungen.

Zusätzlich können in dem neuen (L)MP2 Programm nicht nur Eigenschaften geschlossenschaliger, sondern auch high-spin offenschaliger Systeme, berechnet werden. Der Formalismus zur Behandlung offenschaliger Systeme ist dabei um einiges komplizierter als die entsprechende geschlossenschalige Theorie, der Rechenaufwand bei geschickter Formulierung der Theorie jedoch ähnlich. Die neu implementierten Gradienten sind in einer integraldirekten Variante oder mit Dichtefitting verfügbar. Des Weiteren können Lösungsmittel über einen elektrostatischen Ansatz während der Gradientenberechnung berücksichtigt werden (COSMO).

Neben einer umfangreichen Betrachtung der Theorie beinhaltet die vorliegende Arbeit auch einige Untersuchungen verschiedener Systeme basierend auf den neuen Gradientenmethoden. Hierbei wurden ausführliche Tests zur Genauigkeit der neuen IBO Gradienten durchgeführt. Für die geschlossenschalige Implementierung geschah dies anhand eines Testsets für kleine bis mittelgroße Moleküle mit über 100 verschiedenen Systemen. Ferner wurden Radikalstabilisierungsenergien für insgesamt 30 verschiedene Reaktionen berechnet, um auch die Anwendbarkeit und Präzision der offenschaligen lokalen Gradienten zu demonstrieren. Neben diesen rein theoretischen Benchmarks enthält die Arbeit auch verbesserte Ionisierungspotentiale eines Satzes von 24 Molekülen, die im Bereich organischer Photovoltaikzellen und -elektronik Anwendung finden. Hierbei werden erstmals neben vertikalen Ionisierungspotentialen auch adiabatische berechnet und mit verfügbaren experimentellen Daten abgeglichen. Zuletzt wird die Anwendbarkeit der neuen Gradientenmethode für ein System mit 175 Atomen anhand der Geometrieoptimierung von $FeC_{72}N_2H_{100}$ demonstriert. Es handelt sich hierbei um einen Komplex mit quintett-Grundzustand.

Die Arbeit befasst sich darüber hinaus mit dem Einfluss von Basissatzsuperpositionsfehlern auf nicht-kovalente Wechselwirkungen. Die Untersuchung erfolgt anhand von sechs ausgewälten Dimeren mittels verschiedener lokaler und explizit korrelierter MP2 methoden.

Abstract

The use of local approximations to calculate the dynamic electron correlation makes it possible to predict single-point energies for large molecules with hundreds of atoms. However, beyond these methods for calculating energies, there are hardly any low-scaling *ab initio* models to compute other properties, such as dipole moments or equilibrium geometries. For example, analytical gradients based on local Møller-Plesset perturbation theory (LMP2) were initially only available for closed-shell molecules with Pipek-Mezey localization (PM) in the occupied space; the virtual space is described by domains generated from projected atomic orbitals (PAOs). The use of PM localization can be problematic, as convergence problems may occur when using basis sets containing diffuse functions.

Therefore, open- and closed-shell LMP2 gradients based on intrinsic bond orbitals (IBOs) were implemented in this work. IBOs are an alternative approach for localization of occupied spaces. In contrast to the well known PM method, they are faster to calculate and very stable with respect to basis set changes. IBOs avoid localization artefacts and show the binding pattern known from qualitative chemical concepts. They are generated by projecting the occupied orbitals to a minimal basis of atomic orbitals, resulting in an intermediate step in so-called intrinsic atomic orbitals (IAOs). The localization of the occupied space will then be based on these IAOs. Due to these projections, both the derivation and efficient implementation of analytical gradients are more involved. Still, this has been achieved in the context of this work.

In addition, the new (L)MP2 program can not only calculate the properties of closed-shell but also high-spin open-shell systems. The formalism for the treatment of open-shell systems is much more complicated than the corresponding closed-shell theory, but the computational effort is similar when the theory is formulated properly. The newly implemented gradients are available in an integral direct version or with density fitting. Furthermore, solvents can be considered via an electrostatic approach during the gradient calculation (COSMO).

In addition to an extensive discussion of the underlying theory, the present work also includes some investigations of different systems based on the new gradient methods and thorough tests were performed on the accuracy of the new IBO gradients. The closed-shell implementation

was tested using a set for small to medium sized molecules with over 100 different systems. Furthermore, radical stabilization energies were calculated for a total of 30 different reactions in order to demonstrate the applicability and precision of our local open-shell gradients. In addition to these purely theoretical benchmarks, the work also includes improved ionization potentials of a set of 24 molecules used in the field of organic photovoltaic cells and electronics. For the first time not only vertical but also adiabatic ionization potentials for this set are calculated and compared against available experimental data. Finally, we demonstrate the applicability of the new gradient method for a system of 175 atoms through geometry optimization of $FeC_{72}N_2H_{100}$, a complex with quintett ground state.

The dissertation additionally discusses the influence of basis-set superposition errors on noncovalent interactions. The investigation is based on six selected dimers using different local and explicitly correlated MP2 methods.

Notation

Index notation used for different orbital spaces:

Indices	Orbital Space
i, j, k, l	doubly occupied orbitals ('closed orbitals')
t, u	singly occupied orbitals ('active orbitals')
m, n	singly and doubly occupied orbitals
a, b, c, d	virtual orbitals
x, y	virtual and singly occupied orbitals
p, q	any orbital, occupancy unspecified
r, s	projected atomic orbitals (PAOs) and active orbitals
μ, ν, τ, υ	AO basis functions $\in B_1$
ρ, σ	AO basis functions $\in B_2$
ρ', σ'	Intrinsic Atomic Orbitals

Index notation used for other quantities:

Indices	Quantity
A, B	current atom
	or auxiliary basis used for density-fitting
i	iterative steps during the inversion of the iterative subspace (DIIS)
x	current number of iterations in DIIS
	or coupled perturbed Hartree-Fock (CPHF)
γ, θ	surface segments in the conductor-like screening model (COSMO)

Throughout this work, summation over repeated indices (Einstein summation) is implied.

Abbreviations

AO	Atomic Orbital
AVnZ	correlation-consistent, augmented n-tuple zeta Dunning basis set
AVnZ'	AVnZ, H=VnZ basis set
BSSE	Basis Set Superposition Error
CCSD(T)	Coupled-Cluster Singles and Doubles with perturbative Triples correction
COSMO	COnductor-like Screening MOdel
CP	CounterPoise correction
CPHF	Coupled Perturbed Hartree-Fock
CPL	Coupled Perturbed Localization
CSF	Configuration State Function
DIIS	Direct Inversion in the Iterative Subspace
DF	Density Fitting
DFT	Density Functional Theory
HF	Hartree-Fock
HOMO	Highest Occupied Molecular Orbital
IAO	Intrinsic Atomic Orbital
IBO	Intrinsic Bond Orbital
IP	Ionization Potential
irrep	IRreducible REPresentation
LCAO	Linear Combination of Atomic Orbitals
LMP2	Local Second-order Møller-Plesset perturbation theory
LMO	Localized Molecular Orbital
LRMP2	Local Restricted Second-order Møller-Plesset perturbation theory
MAE	Mean Absolute Error
MAX	MAXimum error
MO	Molecular Orbital
MP2	Second-order Møller-Plesset perturbation theory
OSV	Orbital-Specific Virtual

PAO	Projected Atomic Orbital
PES	Potential Energy Surface
PM	Pipek-Mezey
PNO	Pair-Natural Orbital
RCCSD(T)	Restricted Coupled-Cluster Singles and Doubles
	with perturbative Triples correction
RHF	Restricted Hartree-Fock
RMP2	Restricted Second-order Møller-Plesset perturbation theory
RMS	Root-Mean-Square deviation
SCF	Self-Consistent Field
UCCSD(T)	Unrestricted Coupled-Cluster Singles and Doubles
	with perturbative Triples correction
UHF	Unrestricted Hartree-Fock
VnZ	correlation-consistent n-tuple zeta Dunning basis set

List of Tables

List of Tables in Appendices

List of Figures

List of Figures in Appendices

1 Introduction

A molecule's wave function and energy are fundamental quantities ultimately determining the macroscopic behaviour of matter. Both the wave function and energy are directly available from electronic structure calculations, yet hard or impossible to measure experimentally. To bridge this gap between theory and experiment, it is thus required to compute experimentally accessible quantities. Some quantities of interest such as activation barriers or dissociation energies can be easily found by calculating energy differences of the systems investigated. Others, as for instance excitation energies, require information on transitions between different electronic states. The third and last type of properties – the ones this work is concerned with – are molecular properties specific for a given electronic state at a fixed point on the potential energy surface. They can be found by a theoretical framework called molecular response theory [1–3].

Response theory describes a molecule's response to a perturbation of its current equilibrium state. The perturbation, be it time-dependent or independent, may be for instance an external electromagnetic field or the change of nuclear coordinates within the atomic structure of the molecule. We can use these molecular responses to calculate quantities such as molecular equilibrium structures or dipole moments. If the observables in question are time-independent, the molecule is in a stationary state [1, 4]. In order to compute a stationary state we consider the molecule's response to a perturbation as a change in the molecular energy. If the perturbation is small, it can be described by a Taylor expansion around the unperturbed value. The first-order term in this expansion then expresses the linear response and contains the first energy derivative with respect to the perturbation, the second-order term expresses the quadratic response containing the second derivative and so on [1–4]. The first-order electronic energy derivative with respect to the nuclear coordinates, referred to as the nuclear energy gradient, is a force acting on the nuclei and can be used for molecular geometry optimization, whereas a first-order derivative with respect to a uniform external electric field will give the molecular dipole moment [1, 3, 5, 6]. In the present work we will limit the discussion to such time-independent real perturbations, thereby excluding properties either depending on magnetic fields as for instance NMR shifts or frequency-dependent properties such as dynamic dipole polarizabilities [1, 4].

Looking at the current literature, various different response property implementations for closed-

shell electron correlation methods exist [1, 7–12] – less present, however, are response properties of open-shell molecules. The description of molecules with unpaired electrons often requires a multi-reference treatment as one configuration state function (CSF) may be not enough to describe the molecules (near-) degenerate electronic configuration [13]. However, even if a single CSF sufficiently describes the open-shell system, it cannot necessarily be treated by the self-consistent field method (SCF) commonly used to solve the Hartree-Fock eigenvalue problem. This is due to the SCF Fock operator being defined as an effective one-electron operator; this definition fails for rotations in the active-active space if they are non-redundant. Such non-redundant rotations can occur if singly occupied alpha and beta spin-orbitals are mixed [13]. This problem is avoided if all unpaired electrons have either alpha or beta spin only, called a high-spin configuration. High-spin configurations are often described sufficiently by just a single Slater determinant, and so extended versions of single-reference methods can be used [14–22]. Such an extension is not as straight forward as the derivation of the underlying closed-shell theories, but once implemented, gradients designed for high-spin open-shell molecules enable us to investigate a rather large amount of chemical problems already, without the need for more complicated and expensive methods. Being more involved in derivation and implemantation, there are fewer implementations for different flavours of high-spin open-shell Hartree-Fock and Møller-Plesset gradients available than there are closed-shell codes [7, 23–27]. Also, to our knowledge, none of them involve local electron correlation treatment as discussed below.

Despite the straight forward perturbative approach used in response theory, it is challenging to find a suitable theoretical framework to predict such molecular properties with chemical accuracy and at the same time at affordable computational costs [1, 6, 28, 29]. This becomes apparent if one looks at the computational costs just for the molecular energy calculation, which is preceding the calculation of any response property. Calculating for instance molecular energies using highly accurate *ab initio* methods results in a steep increase of computational cost with increasing molecular size: second-order Møller-Plesset perturbation theory (MP2) scales as $\mathcal{O}(N^5)$ in computational time, and the coupled-cluster singles and doubles method with perturbative triples correction – the current 'gold standard' of quantum chemistry – even as $\mathcal{O}(N^7)$, with N being the number of electrons [30, 31]. This scaling is due to the number of possible electron configurations growing rapidly with the system's size. Introducing a local electron correlation treatment, which takes advantage of the locality of dynamic electron correlation, is one way to reduce the effort with increasing molecular or basis set size down to even linear scaling by restricting the number configurations [30, 32–41]. Another approach in reducing the formal scaling are fragmentation methods, in which a molecule is divided into smaller pieces, treating each of these fragments independently. The main advantage of such fragmentation methods over local electron correlation treatment is the less complex implementation [42, 43]. However, as dividing a molecule severely affects its dynamic correlation, the generated fragments must strongly overlap; this leads to a lot of redundant computational work [40]. This redundancy also

affects dipole moments and nuclear gradients based on fragmentation methods – if not the full gradient, at least the expensive two-electron integral contributions [11, 44, 45]. Consequently, this work will focus on local electron correlation treatment as suggested by Pulay [30], since it is well established and without computational redundancy.

The idea of local correlation treatment can be briefly summarized as follows: if an electron can be localized within a specific part of the molecule, its interaction with electrons in other, more distant regions will decrease quickly with increasing interelectronic distance. We can thus omit or simplify treatment of all electron pairs with electrons sufficiently far apart, which is called the pair approximation. Also, the excitation of an electron to a virtual orbital is more important if the orbitals in question are in the same vicinity. The domain approximation exploits this by limiting electron excitations from an occupied orbital to a local subspace of the available virtual orbitals only [30–32]. The localization usually takes place after the initial Hartree-Fock treatment prior to calculation of the correlation energy and possible derivatives. Local correlation treatment thereby cannot only be applied to energies in an effective manner, but to response property predictions as well [9, 10, 29, 46–49]. Local gradients are in general similar to their respective canonical counterparts, but with additional contributions due to orbital localization and local approximations. Furthermore, as the local pair and domain approximations are based on distance or connectivity criteria, and the molecular geometry is subject to change during a geometry optimization, one can end up with domains being different at the beginning and end of a calculation. This poses a problem, as the potential energy surface on which the nuclei move experiences a discontinuity whenever domains change, independent of the localization method used. There are different approaches to avoid such discontinuities; in this work, the local domains will be frozen once the gradient is small enough to ensure smooth convergence close to the equilibrium geometry [50–52].

Today, various different response property implementations for closed-shell local electron correlation methods exist, but none of them is based on intrinsic bond orbitals (IBOs) [53]. IBOs are a recently developed ansatz for occupied space localization, similar to the well known Pipek-Mezey scheme [54]. The differences between the two methods are that IBOs are more stable with respect to basis set changes, show the bonding picture expected from qualitative chemical concepts, and are faster to compute [53]. IBOs are based in intrinsic atomic orbitsals (IAOs) which in turn are closely related to quasiatomic orbitals but do not need an iterative procedure for generation [55, 56]. Complementary, projected atomic orbitals (PAOs) are an ansatz to generate a local correlation space for each pair of occupied orbitals [30]. Further details on the different localization schemes of occupied orbitals, the modification of the correlation space as well as the thereby introduced approximations, their physical justification, and extension to open-shell systems can be found in chapter 3.

Having obtained the energy of an unperturbed molecule using a method of choice, the required derivatives of the energy functional needed to describe the perturbation can be found by using either analytical or numerical differentiation. Numerical differentiation has the advantage of almost zero implementation effort, but suffers from numerical errors and can come at the cost of very high computational demand for certain properties. Finite difference numerical nuclear energy gradients for instance are at least $2 \cdot 3 N_{at}$ times as expensive as the underlying energy calculation, with N_{at} the number of atoms in the system [1, 6]. Still, numerical methods can at least be used to test a method's accuracy prior to analytic implementation. Analytic differentiation on the other hand can lead to efficient and exact algorithms, but the implementation and debugging may be tedious. And, depending on the type of perturbation, each energy derivative will lead to different response properties [1, 3, 4]. The derivatives will also differ for every correlation method and type of localization, as the generating energy functional is influenced by the ansatz and type of approximations chosen. In this work we will present the implementation of both, restricted closed- and high-spin open-shell analytic IBO energy gradients for local second-order Møller-Plesset perturbation theory (LRMP2). We have implemented analytic gradients for first order properties only; second- and higher-order properties such as force constants or polarizabilities can then be found by numerical differentiation [6]. The gradients are available via the program package MOLPRO [57].

During the process, canonical open-shell gradients on the restricted MP2 level have been implemented as an intermediate step [24, 25]. Additionally, local restricted open-shell Pipek-Mezey gradients at the MP2 level as well as density fitting (DF) for local, and COSMO for all gradients are available. In order to fully understand the newly developed gradient methods and all approximations employed, this thesis will first briefly introduce the well-known closed-shell Hartree-Fock and MP2 methods for calculating molecular energies [58, 59] and then extend them for use in restricted high-spin open-shell cases. In the following chapter, we will discuss local electron correlation approximations, before proceeding to the canonical Hartree-Fock and MP2 gradients in chapter 4, and finally closed- and open-shell local RMP2 gradients in chapter 5. All gradients are derived using the z-vector method of Handy and Schaefer [28], and we will additionally discuss the density fitting approximation and its application to gradient methods [60–62], as well as an electrostatic method for treating solvent effects (COSMO) [63]. Having established nuclear energy gradients at the (local, restricted) MP2 level in this thesis, other response properties besides dipole moments and equilibrium structures can be found as well, and higher levels of theory – such as local open-shell coupled cluster gradients – can be implemented in the future.

In order to augment our theoretical considerations, the last chapter provides some example calculations to demonstrate the gradient's precision and scaling. The newly developed closed-shell IBO gradients are tested against a test set of 102 small to medium-sized molecules as

published by Friedrich and Hähnchen [64]; the set was futher augmented by three molecules from the ISOL24 test set [65] as molecules with more than 30 atoms would else have been under-represented. Additionally, vertical ionization potentials (IPs) of 24 molecules as reported by Sherrill and co-workers [66] were improved and, using our open-shell gradients, adiabatic IPs were calculated after relaxing the cations geometries. Some IPs are available for comparison in the NISTs database of experimental properties [67]. Subsequently, radical stabilization energies for a set of 30 reactions as discussed by Liu [21] were obtained using LRMP2-gradient based geometries. Those stabilization energies are compared against calculations based on DFT and RCCSD(T) level geometry optimizations. Finally, we investigated the ground state of an iron complex discussed in [68] and [69] in order to demonstrate the gradients overall scaling and applicability to larger molecules – in this case containing 175 atoms and five unpaired electrons.

2 Molecular Orbital Theory

This chapter will first introduce the Born-Oppenheimer approximation as a foundation of the geometry optimization algorithm used later in this work [2, pp. 24]. We then proceed to discuss the closed-shell Hartree-Fock theory (HF) [58], which is solved using the Roothaan-Hall self-consistent field approach (SCF) [70], and subsequently high-spin unrestricted and restricted open-shell Hartree-Fock methods (UHF, RHF) [14–16]. In the next step, with HF and RHF wave functions as a reference, second-order Møller-Plesset perturbation theory (MP2) can be applied to address electron correlation beyond the (R)HF level. MP2 is a special case of many-body perturbation theory which will be introduced first, followed by closed-shell MP2 and restricted open-shell MP2 (RMP2) in sections 2.4 and 2.4.3 [17–19, 59].

2.1 The Born-Oppenheimer Approximation

We would like to calculate the wave function Ψ and energy E of a many-body quantum system by solving the time-independent Schrödinger equation

$$\hat{H}\Psi = E\Psi. \tag{2.1}$$

In above equation, $\hat{H} = \hat{H}_{el} + \hat{T}_{nuc}$ denotes the system's Hamilton operator. Its electronic part may be written as a sum over one- and two-particle operators:

$$\hat{H}_{el} = \sum_{i=1}^{N_{el}} \hat{h}_i + \sum_{j>i}^{N_{el}} \hat{g}_{ij} + E_{nuc} \tag{2.2}$$

$$\hat{h}_i = -\frac{1}{2}\nabla_i^2 - \sum_{A=1}^{N_{at}} \frac{Z_A}{|R_A - r_i|} \tag{2.3}$$

$$\hat{g}_{ij} = \frac{1}{|r_i - r_j|} \tag{2.4}$$

The one-electron operator $\hat{h}_i$ describes the motion of electron i in the external field of all nuclei A in a system with N_{at} atoms. It also includes the non-relativistic kinetic energy of the electron. $\hat{g}_{ij}$ is the two-electron Coulomb operator accounting for the electron-electron repulsion, with summation running over $j > i$ only to avoid double counting and self-repulsion of the N_{el} electrons. Both operators have been denoted in atomic units which we will always use during this work unless stated otherwise. The nuclear repulsion energy

$$E_{nuc} = \sum_{B>A}^{N_{at}} \frac{Z_A Z_B}{|R_A - R_B|} \tag{2.5}$$

with nuclear charge Z_A is independent of the electrons' coordinates $r = \{r_i\}$ and can therefore be added as a constant in the end; it is also a Coulomb type interaction. Missing in the electronic Hamiltonian above is a kinetic energy term for the nuclear motion

$$\hat{T}_{nuc} = -\frac{1}{2} \sum_A^{N_{at}} \frac{1}{M_A} \nabla_A^2, \tag{2.6}$$

as the nuclei are kept fixed during the calculation. This separation of the electronic from the nuclear motion is called the Born-Oppenheimer approximation [71, 72], [3, pp. 88], and [73, pp. 41].

Using the Born-Oppenheimer approximation, an electronic Schrödinger equation for every set of fixed nuclear coordinates $\bar{R} = \{R_A\}$ is solved:

$$\hat{H}_{el}\Psi_{el}(r, \bar{R}) = E_{el}(\bar{R})\Psi_{el}(r, \bar{R}) \tag{2.7}$$

In a second step, the nuclear kinetic energy is then reintroduced within a nuclear Schrödinger equation, describing the molecule's translation, rotation, and vibration:

$$\hat{H}_{nuc}\Psi_{nuc} = E\Psi_{nuc} \tag{2.8}$$

The nuclear Hamilton operator $\hat{H}_{nuc} = \hat{T}_{nuc} + E_{el}(\bar{R})$ includes the previously omitted nuclear kinetic energy term and the solution of eq. 2.7, $E_{el}(\bar{R})$, as an average electronic potential acting on the nuclei at their current positions $\bar{R}$. If calculated for different sets of nuclear coordinates, $E_{el}(\bar{R})$ can be seen as an electronic potential energy surface (PES) on which the nuclei move. This motion decoupling is physically justified, as a nucleus is more heavy than an electron and thus moves slower. Hence, the nuclei only feel an average influence from the fast electronic motion and electrons adapt to slow nuclear motion almost instantaneously. The approximation to the time-independent Schrödinger equation's total wave function is $\Psi(r, \bar{R}) = \Psi_{nuc}(\bar{R})\Psi_{el}(r, \bar{R})$, see [73, pp. 43] and [74, pp. 258].

The Born-Oppenheimer approximation is a very common tool in quantum chemistry and will be valid as long as the states obtained from the solution of the electronic Schrödinger equation are well separated [3, p. 85]. For adjacent electronic states, the non-adiabatic coupling terms neglected in eq. 2.8, however, will be large and the approximation fails. Those coupling terms arise from the fact that $\hat{T}_{nuc}$ actually acts on the total wave function Ψ instead of Ψ_{nuc}. The geometry optimization algorithm and underlying gradients discussed in chapters 4 and 5 are also based on the separation of electronic and nuclear motion: For a molecular geometry optimization, one first solves eq. 2.7 for a suitable starting geometry to obtain $E_{el}(\bar{R})$. The nuclear gradient acting on nucleus A at this geometry is then defined as $g_A = dE_{el}(\bar{R})/dR_A$, and the nuclei can be moved accordingly. Then the electronic Schrödinger equation is solved again for the new set of $\{\bar{R}\}$, the nuclei moved, and repeated until a stationary point on the potential energy surface is reached. This approach simplifies the solution of the Schrödinger equation as compared to taking the nuclear motion into account at the same time as the electronic motion [6], [2, pp. 24].

2.2 The Hartree-Fock Method

The electronic Schrödinger equation, eq. 2.7, can be solved for instance using the Hartree-Fock method [58]. HF introduces additional approximations in order to simplify the many-body problem at hand: The first is called the 'mean-field approximation' and neglects the dynamic electron correlation. Dynamic correlation describes the instantaneous electron-electron repulsion due to negative charges. Disregarding it, all electrons of opposite spin can move independently from each other. The electron-electron interaction can be partially recovered by considering the motion of a single electron in the mean field of all other electrons, but the average inter-electronic distance is still systematically underestimated, which in turn leads to an overestimation of the energy. For electrons with parallel spin the approximation has a smaller effect, as the Pauli principle forbids two such electrons to be in the same spatial location at the same time, and HF follows this principle strictly. Overall, the error introduced by omitting the dynamic correlation is too large for the results to remain chemically accurate and usually some form of correlation correction is performed after the HF treatment [3, pp. 80], [13, pp. 170].

The second and less grave approximation is the neglect of static electron correlation, making HF a 'single-reference method'. Static correlation arises in situations where more than one orbital configuration is required to describe a molecule's ground state wave function qualitatively correct [13, p. 162]. An orbital configuration is the spin-independent distribution of a number of electrons on a set of orbitals. Each configuration is described by one or more configuration state functions (CSFs) which in turn are eigenfunctions of the total spin operator $\hat{S}^2$ [13, pp.

51]. CSFs Ψ are generated from linear combinations of Slater determinants [75] and Slater determinants Φ themselves describe how a number of electrons N_{el} is distributed over a set of spin-orbitals ψ_i:

$$\Phi_{ij...p} = \frac{1}{\sqrt{N_{el}!}} \begin{vmatrix} \psi_i(1) & \psi_j(1) & \dots & \psi_p(1) \\ \psi_i(2) & \psi_j(2) & \dots & \psi_p(2) \\ \vdots & \vdots & \ddots & \vdots \\ \psi_i(N_{el}) & \psi_j(N_{el}) & \dots & \psi_p(N_{el}) \end{vmatrix} = ||\psi_i(1)\psi_j(2)\dots\psi_p(N_{el})|| \qquad (2.9)$$

Each spin-orbital can be seen as a product of a spatial and a spin-eigenfunction and is occupied by a single electron. The spin-orbitals are grouped in Slater determinants, as determinants will change their sign if two rows are swapped. This corresponds to the total wave function being anti-symmetric for the exchange of two electrons. Also, if two rows in a Slater determinant are equal, the resulting wave function is zero as required by the Pauli principle. Slater determinants are enumerated by the secondary spin quantum number M_S and are generally eigenfunctions of the spin-projection operator $\hat{S}_z$, but not of $\hat{S}^2$. A spin- and possibly symmetry-adapted linear combination of Slater determinants sharing the same orbital occupation numbers, yet with electrons distributed over different spin-orbitals form a CSF [13, pp. 46, 51], [3, p. 87].

It is worth noting that closed-shell molecules always have a singlet configuration with $S = 0$, which implies that there is just one ground state Slater determinant existent with $M_S = 0$. This determinant, called the HF determinant, is an eigenfunction of both $\hat{S}_z$ and $\hat{S}^2$. In general, Φ is a simultaneous eigenfunction of $\hat{S}_z$ and $\hat{S}^2$ whenever $M_S = \pm S$. The only other electronic configuration besides $S = 0$ for which this is true is called a high-spin configuration, in which all unpaired electrons share the same spin. Discussions on open-shell methods in this work will be limited to such high-spin configurations only. If there are more spin-orbitals ψ_p available than electrons in the system, the spin-orbitals contributing to the HF Slater determinant will be called occupied or internal orbitals, the remaining ones virtual or external orbitals. The full set of internal and external orbitals is called the spin orbital basis and is taken to be orthonormal

$$\langle\psi_p|\psi_q\rangle = \delta_{pq}, \; \delta_{pq} = \begin{cases} 1 \; \forall \; p = q \\ 0 \; \forall \; p \neq q \end{cases}. \qquad (2.10)$$

The pointed brackets denote integration over all electronic coordinates and δ_{pq} is called the 'Kronecker delta' [3, p. 87], [13, pp. 434].

Based on eqs. 2.2 and 2.9, and approximating $\Psi_{el} \approx \Phi$, the system's energy expression, eq. 2.7, can be rewritten as

$$E_{HF} = \langle\Phi|\hat{H}|\Phi\rangle = \sum_{i=1}^{N_{el}} h_i + \sum_{j>i}^{N_{el}} (J_{ij} - K_{ij}) + E_{nuc}. \qquad (2.11)$$

In this equation, $h_i = \langle \psi_i(1)|\hat{h}_i|\psi_i(1)\rangle$ denotes an integral over the one-electron operator and $J_{ij} = \langle \psi_i(1)\psi_j(2)|\hat{g}_{ij}|\psi_i(1)\psi_j(2)\rangle$ is the Coulomb integral over the two-electron operator. A further term arises from the wave function's anti-symmetry; it is called the exchange term as the electrons on the Ket-side are swapped: $K_{ij} = \langle \psi_i(1)\psi_j(2)|\hat{g}_{ij}|\psi_j(1)\psi_i(2)\rangle$. Due to the last two integrals' structure, one needs to know the form of all other occupied orbitals $j \neq i$ before calculating the energy of orbital i [3, pp. 89]. This problem originates from the mean-field approximation discussed above and requires an iterative solution of the equation system. Writing the spin-orbitals as products of spin functions and spatial orbitals, and subsequent spin integration yields for closed-shell regimes

$$E_{HF} = 2 \sum_{i=1}^{N_{el}/2} h_{ii} + \sum_{ij}^{N_{el}/2} \left(2(ii|jj) - (ij|ij)\right) + E_{nuc}. \tag{2.12}$$

Here we have assumed that all internal orbitals are generated from pairs of spin-orbitals sharing the same spatial function but differing in the spin-eigenfunction. The orbitals are thus doubly occupied with two electrons of opposite spin. After spin integration the one- and two-electron integrals are independent of the spin-eigenfunctions leaving us with spatial molecular orbitals ϕ_i only:

$$h_{ij} = \langle i|\hat{h}|j\rangle = \langle \phi_i(1)|\hat{h}|\phi_j(1)\rangle \tag{2.13}$$

$$(ik|jl) = \langle \phi_i(1)\phi_j(2)|\hat{g}_{ij}|\phi_k(1)\phi_l(2)\rangle \tag{2.14}$$

The orthonormality condition still holds as $\langle p|q\rangle = \delta_{pq}$ [2, pp. 13].

2.2.1 Variation of the Hartree-Fock Energy

HF orbitals are defined to be the subset of orbitals yielding the lowest possible energy in a given basis set with N_{AO} basis functions if $\Psi_{el} \approx \Phi$ [2, p. 15]. They can be determined variationally by setting up a Lagrangian $\mathcal{L}$ containing the HF closed-shell energy eq. 2.12 (or in general eq. 2.11) as the function to be optimized and the orthonormality condition eq. 2.10 as a constraint in order to keep the MOs orthonormal, so

$$\mathcal{L} = E_{HF} - 2 \sum_{ij}^{N_{el}/2} \lambda_{ij} \left(\langle i|j\rangle - \delta_{ij}\right). \tag{2.15}$$

Variation of the HF energy in an orthonormal basis set is performed by unitary rotation $\mathbf{U}$ of the orbitals, mixing the initial internal and external spaces

$$|q\rangle = \sum_p^{N_{AO}} U_{pq}|p\rangle. \tag{2.16}$$

This way, the new MOs q can conveniently be described in the basis of the old MOs p. At the expansion point $\mathbf{U} = \mathbf{1}$, the derivative of $\mathcal{L}$ with respect to $\mathbf{U}$ takes the form

$$\left.\frac{d\mathcal{L}}{dU_{pi}}\right|_{\mathbf{U=1}} = 4\left\{h_{pi} + \sum_j^{N_{el}/2}[2(pi|jj) - (pj|ji) - \delta_{pj}\lambda_{ji}]\right\} = 0. \tag{2.17}$$

The derivative needs to be equal to zero, as we are looking for a minimum [3, pp. 90]. Defining a 'Fock matrix' as

$$f_{pq} = h_{pq} + \sum_j^{N_{el}/2}[2(pq|jj) - (pj|jq)] \tag{2.18}$$

simplifies the above expression to be

$$f_{pi} = \sum_j^{N_{el}/2} \delta_{pj}\lambda_{ji}. \tag{2.19}$$

The so-called Hartree-Fock equations, eq. 2.19, show that the Lagrangian multipliers in the occupied-occupied space correspond to the respective Fock matrix elements, as $f_{ki} = \lambda_{ki} \, \forall \, p = k$. Thus, we can conclude that we are free in the choice of Lagrangian multipliers, respective Fock matrix elements of the internal space – as long as the associated MOs can be generated by a unitary rotation in order to preserve orthonormality. Or in other words, E_{HF} is invariant with respect to unitary rotations within the occupied-occupied space (and similarly also in the virtual-virtual space as there is no contribution from orbitals outside the Slater determinant to E_{HF}). If $p = a$ however, we obtain the so called Brillouin condition with $f_{ai} = 0$ (as $\delta_{ai} = 0$); a is a virtual space index. The mixing of internal and external orbital spaces will thus change the energy and we are required to find a solution that satisfies $f_{aj} = 0$ [13, pp. 441].

One way to solve eq. 2.19 is by transforming it into a 'canonical' basis, thereby requiring the Lagrangian multipliers to be $\lambda_{pp} = \epsilon_p$ and $\lambda_{pq} = 0$ ($p \neq q$). The diagonalization of the Lagrangian multipliers (and thereby the Fock matrix) is an arbitrary choice and there are other possible definitions that fulfil the requirements for optimized HF orbitals; it is sufficient for the $f_{pq} = \lambda_{pq}$ to form a block-diagonal matrix to fulfil the Brillouin condition [13, p. 449]. Yet, the canonical ansatz is very convenient, as it reduces the HF equations to a simple eigenvalue problem:

$$f_{pq} = \epsilon_p\delta_{pq} \tag{2.20}$$

The resulting eigenvalues ϵ_i are the energies of the associated orbitals (the eigenvectors) ϕ_i', which are called 'canonical orbitals'. Although they are different from the non-canonical orbitals ϕ_i, the prime will be omitted in the notation from now on. It will be apparent from the context which orbitals are meant [73, pp. 120]. It should also be noted that due to the double counting of electron repulsion in the Fock operator, the sum of single orbital energies ϵ_i is not simply equal to the total electronic energy of the system, E_{HF}, but is given by eq. 2.12, which can be rewritten as

$$E_{HF} = 2 \sum_i^{N_{el}/2} \epsilon_i - \sum_{ij}^{N_{el}/2} \left(2(ii|jj) - (ij|ij)\right) + E_{nuc} \tag{2.21}$$

with

$$\epsilon_i = f_{ii} = h_{ii} + \sum_j^{N_{el}/2} \left(2(ii|jj) - (ij|ij)\right). \tag{2.22}$$

2.2.2 The Self-Consistent Field Equations

Prior to proceeding to open-shell HF, it makes sense to have a look at the mathematical form of the MOs employed, as this will not only enable us to derive the actual HF working equations, but it will also be of importance for the gradient expressions later on. Usually, MOs are approximated by expanding them in a finite set of N_{AO} non-orthogonal atom-centred basis functions $|\mu\rangle = |\chi_\mu\rangle$, called the atomic orbital (AO) basis:

$$|p\rangle = \sum_{\mu=1}^{N_{AO}} |\mu\rangle C_{\mu p} \tag{2.23}$$

This expansion is known as 'linear combination of atomic orbitals' (LCAO) approximation and was first suggested by Roothaan and Hall in 1951 [70, 76]. The expansion coefficients $C_{\mu p}$ are called MO-coefficients, and being non-orthonormal the AO functions have the overlap $S_{\mu\nu} = \langle \mu | \nu \rangle$. $\mathbf{C}$ is a square matrix, as there are as many linear independent combinations (MOs) as there are AO basis functions in a linear independent basis [73, pp. 136]. The orthonormality condition (eq. 2.10) can be expressed in matrix notation as

$$\mathbf{C}^\dagger \mathbf{S} \mathbf{C} = \mathbf{1}. \tag{2.24}$$

Inserting eq. 2.23 into eq. 2.18 we get

$$f_{pq} = C_{\mu p} F_{\mu\nu} C_{\nu q} = [\mathbf{C}^\dagger \mathbf{F} \mathbf{C}]_{pq} \tag{2.25}$$

with

$$F_{\mu\nu} = h_{\mu\nu} + D_{\tau\upsilon}^{(0)} \left[(\mu\nu|\tau\upsilon) - \frac{1}{2}(\mu\tau|\nu\upsilon) \right] \tag{2.26}$$

the Fock matrix in AO basis [2, pp. 15]. In closed-shell regimes the zeroth-order density matrix $D_{\mu\nu}^{(0)}$ takes the form $D_{\mu\nu}^{(0)} = 2C_{\mu i}C_{\nu i}$. Einstein summation over repeated indices in above and all following equations is implied. In the canonical case and for orthonormal MOs, $f_{pq} = \delta_{pq}$ and $[\mathbf{C}^\dagger]^{-1} = \mathbf{SC}$. Applying these conditions to eq. 2.25, we arrive at the most famous Hartree-Fock-Rothaan equations [70]

$$\mathbf{FC} = \mathbf{SCE}. \tag{2.27}$$

$E_{pq} = \delta_{pq}\epsilon_p$ is a diagonal matrix containing the orbital energies as defined earlier in eq. 2.22. The above mentioned equations are of pseudo-eigenvalue form, as the Fock matrix generating the MO coefficients $\mathbf{C}$ depends on the density matrix $\mathbf{D}^{(0)}$; the density matrix itself is in turn generated by the very coefficients that $\mathbf{F}$ is supposed to act on – the MO coefficients. Subsequently, the Hartree-Fock-Rothaan equations, also known as self-consistent field (SCF) equations, are a non-linear system of equations with an infinite number of solutions and have to be solved iteratively for self-consistence. Contrary to eq. 2.19, eq. 2.27 can be solved in a non-orthonormal basis [73, pp. 136, 142, 145].

2.3 High-Spin Open-Shell Hartree-Fock Theory

In section 2.2 it was assumed that every internal orbital should be occupied by two electrons, one with α- and one with β-spin. This is obviously not true for many chemical systems, as there are unpaired electrons present. As mentioned above, we will limit the discussion to high-spin open-shell systems, as this is the only open-shell electron configuration which can be described by a single Slater determinant [13, pp. 53]. If there is no external magnetic field present, the energy is degenerate for $M_S = S$ or $M_S = -S$, and thus all unpaired electrons can be assumed to have α-spin; subsequently $N_\alpha > N_\beta$ [74, p. 249]. Constructing the wave function from a Slater determinant containing spin-orbitals, there are now two main approaches: On the one hand, every electron could occupy its own independent spin-orbital, leading to an approach called unrestricted HF (UHF). On the other hand, the first N_β orbitals could satisfy the previous occupation condition of two electrons per spatial orbital, leaving $N_\alpha - N_\beta$ singly occupied orbitals. This is named the restricted ansatz (RHF), as the occupation condition effectively restricts the spatial part of pairs of spin-orbitals to be equivalent. Both, UHF and RHF are size-extensive, but only UHF is also generally size-consistent, a property needed to describe dissociation qualitatively correct. Yet, only for restricted methods the HF wave function is an eigenfunction of $\hat{S}^2$. UHF thus suffers from an effect called spin contamination, where excited spin-states mix into the ground state wave function, see [3, p. 100] and [73, p. 206]. For geometry optimizations of the ground state molecule close to the equilibrium geometry, it is

more important to have a non-contaminated ground state wave function, hence our gradients will be based on a restricted HF reference. Still, as UHF serves as a theoretical bridge between closed-shell HF and RHF, it will be briefly introduced before proceeding further [77].

2.3.1 The Unrestricted Hartree-Fock Model

If we lift the previous occupation condition of two electrons per orbital, the spatial part of the spin-orbitals is no longer restricted and it is possible to find two different sets of MOs for α- and β-spin electrons. As a result, the generated wave function may be no longer transforming as irreducible representation of the molecule's point group and mixing with higher states can lead to spin contaminated wave functions [13, p. 170]. This is a serious drawback and can lead to results that are physically not justified. As the number of electrons with α- and β-spin does not change, however, the wave function remains an eigenfunction of $\hat{S}_z$. The UHF ansatz leads to two formally independent sets of SCF equations,

$$\mathbf{F}^\alpha \mathbf{C}^\alpha = \mathbf{S}\mathbf{C}^\alpha \mathbf{E}^\alpha \text{ and } \mathbf{F}^\beta \mathbf{C}^\beta = \mathbf{S}\mathbf{C}^\beta \mathbf{E}^\beta, \tag{2.28}$$

that are just coupled via the total charge density $\mathbf{D}^{(0)+} = \mathbf{D}^{(0)\alpha} + \mathbf{D}^{(0)\beta}$ in the Fock operators

$$F^\alpha_{\mu\nu} = h_{\mu\nu} + \left[D^{(0)+}_{\tau\upsilon}(\mu\nu|\tau\upsilon) - D^{(0)\alpha}_{\tau\upsilon}(\mu\tau|\nu\upsilon) \right] \tag{2.29}$$

and

$$F^\beta_{\mu\nu} = h_{\mu\nu} + \left[D^{(0)+}_{\tau\upsilon}(\mu\nu|\tau\upsilon) - D^{(0)\beta}_{\tau\upsilon}(\mu\tau|\nu\upsilon) \right]. \tag{2.30}$$

The equations are referred to as Pople-Nesbet equations and are the equivalent to the closed-shell Hartree-Fock-Roothaan equations 2.27 [14, 15]. Definition of the UHF MO coefficients and thus densities and orthonormality conditions are completely separated as

$$
\begin{aligned}
|\phi_p^\alpha\rangle &= |\mu\rangle C_{\mu p}^\alpha, \ D_{\mu\nu}^{(0)\alpha} = C_{\mu m}^\alpha C_{\nu m}^\alpha, \ (\mathbf{C}^\alpha)^\dagger \mathbf{S}\mathbf{C}^\alpha = \mathbf{1}, \\
|\phi_p^\beta\rangle &= |\mu\rangle C_{\mu p}^\beta, \ D_{\mu\nu}^{(0)\beta} = C_{\mu i}^\beta C_{\nu i}^\beta, \ \text{and} \ (\mathbf{C}^\beta)^\dagger \mathbf{S}\mathbf{C}^\beta = \mathbf{1}.
\end{aligned} \tag{2.31}
$$

While solving for self-consistency, both sets of equations have to be computed simultaneously in order to update the total density, but apart from that a closed shell code can be used with only minor modifications [73, pp. 209]. The UHF energy is

$$E_{UHF} = \frac{1}{2} \text{tr} \left\{ \mathbf{D}^{(0)\alpha} \left(\mathbf{h} + \mathbf{F}^\alpha \right) \right\} + \frac{1}{2} \text{tr} \left\{ \mathbf{D}^{(0)\beta} \left(\mathbf{h} + \mathbf{F}^\beta \right) \right\} + E_{nuc}. \tag{2.32}$$

It is also possible to define a Fock operator that is similar to the one in closed-shell HF, called $\mathbf{F}^+$ and its compliment $\mathbf{F}^-$, which will be useful later on:

$$\mathbf{F}^+ = \frac{1}{2}(\mathbf{F}^\alpha + \mathbf{F}^\beta) \text{ and } \mathbf{F}^- = \frac{1}{2}(\mathbf{F}^\alpha - \mathbf{F}^\beta) \tag{2.33}$$

$\mathbf{F}^+$ is now only dependent on the charge density $\mathbf{D}^{(0)+}$, whereas $\mathbf{F}^-$ only depends on the spin density $\mathbf{D}^{(0)-} = \mathbf{D}^{(0)\alpha} - \mathbf{D}^{(0)\beta}$:

$$F_{\mu\nu}^+ = h_{\mu\nu} + D_{\tau\upsilon}^{(0)+} \left[(\mu\nu|\tau\upsilon) - \frac{1}{2}(\mu\tau|\nu\upsilon) \right] \tag{2.34}$$

$$F_{\mu\nu}^- = -\frac{1}{2} D_{\tau\upsilon}^{(0)-} (\mu\tau|\nu\upsilon) \tag{2.35}$$

The UHF energy expression now takes the form

$$E_{UHF} = \frac{1}{2} \operatorname{tr} \left\{ \mathbf{D}^{(0)+} \left(\mathbf{h} + \mathbf{F}^+ \right) \right\} + \frac{1}{2} \operatorname{tr} \left\{ \mathbf{D}^{(0)-} \mathbf{F}^- \right\} + E_{nuc}. \tag{2.36}$$

By comparing eqs. 2.26 and 2.34 as well as 2.12 and 2.36, we can immediately see the close relation between HF and UHF. They are not necessarily the same however, as in certain systems $\mathbf{D}^{(0)+} \neq \mathbf{D}^{(0)}$ and $\mathbf{D}^{(0)-} \neq \mathbf{0}$. This is due to the missing spatial restriction in UHF.

2.3.2 The Restricted Hartree-Fock Model

In order to find a solution that is an eigenfunction of both spin operators, $\hat{S}_z$ and $\hat{S}^2$, we need to design a wave function that is restricted in the spatial part of the spin-orbitals. The Fock operators for RHF are formally equivalent to UHF eqs. 2.34 and 2.35 but the definition of the densities is different [16]:

$$D_{\mu\nu}^{(0)+} = 2C_{\mu i}C_{\nu i} + C_{\mu t}C_{\nu t} \tag{2.37}$$

$$D_{\mu\nu}^{(0)-} = C_{\mu t}C_{\nu t} \tag{2.38}$$

Due to the spatial restriction, there is again just one set of MO coefficients, similar to closed-shell HF. In open-shell cases, the notation will now distinguish between doubly occupied orbitals (closed orbitals) denoted as i, j, k, l and singly occupied open shell (active) orbitals t, u containing just one electron with α-spin. The variational conditions

$$2(\mathbf{F}^+\mathbf{C})_{\mu i} = 2(\mathbf{SC})_{\mu i}\epsilon_i + (\mathbf{SC})_{\mu t}\epsilon_{ti} \tag{2.39}$$

$$\left[(\mathbf{F}^+ + \mathbf{F}^-)\mathbf{C} \right]_{\mu t} = (\mathbf{SC})_{\mu t}\epsilon_t + (\mathbf{SC})_{\mu i}\epsilon_{it} \tag{2.40}$$

are now directly coupled and the energy takes the form

$$E_{RHF} = \frac{1}{2} \operatorname{tr} \left\{ \mathbf{D}^{(0)+}(\mathbf{h} + \mathbf{F}^+) \right\} + \frac{1}{2} \operatorname{tr} \left\{ \mathbf{D}^{(0)-} \mathbf{F}^- \right\} + E_{nuc}. \tag{2.41}$$

Comparing again with closed-shell HF theory and assuming no unpaired electrons are present, $\mathbf{D}^{(0)+} \to \mathbf{D}^{(0)}$ and $\mathbf{D}^{(0)-} \to \mathbf{0}$; eqs. 2.26 and 2.34, 2.27 and 2.39, as well as 2.12 and 2.41, are now equivalent. Thus RHF can be considered a direct extension of the well known closed-shell HF theory. All above equations can be derived analogously to the closed-shell case with the Lagrangian ansatz

$$\mathcal{L} = E_{RHF} - 2\lambda_{ij} \left(\langle i|j \rangle - \delta_{ij} \right) - \lambda_{tu} \left(\langle t|u \rangle - \delta_{tu} \right) - 2\lambda_{ti} \langle t|i \rangle \tag{2.42}$$

and subsequently including the LCAO approximation [16], [2, pp. 68].

As for closed-shell HF, unitary rotations within each of the three orbital spaces – occupied, active and virtual – will not affect the RHF energy, but rotations in between the spaces will change it. Without further restrictions, as for closed-shell systems, this leads to diagonal Fock matrix blocks that are not uniquely defined. Again, this freedom can be used to construct a canonical solution, even if it is more involved in the Fock matrix definition:

$$\check{\mathbf{f}} = \begin{array}{c} occ \\ act \\ vrt \end{array} \begin{pmatrix} \overset{occ}{\mathbf{f}^+} & \overset{act}{\mathbf{f}^+ - \mathbf{f}^-} & \overset{vrt}{\mathbf{f}^+} \\ \mathbf{f}^+ - \mathbf{f}^- & \mathbf{f}^+ + \mathbf{f}^- & \mathbf{f}^+ + \mathbf{f}^- \\ \mathbf{f}^+ & \mathbf{f}^+ + \mathbf{f}^- & \mathbf{f}^+ + \mathbf{f}^- \end{pmatrix} = \begin{array}{c} occ \\ act \\ vrt \end{array} \begin{pmatrix} \overset{occ}{\check{\epsilon}^c} & \overset{act}{0} & \overset{vrt}{0} \\ 0 & \check{\epsilon}^o & 0 \\ 0 & 0 & \check{\epsilon}^a \end{pmatrix} \tag{2.43}$$

The labels *occ, act, vrt* have been added for convenience to visualize the different subspaces. The Fock operators $f^+_{pq} = C_{\mu p} F^+_{\mu\nu} C_{\nu q}$ and $f^-_{pq} = C_{\mu p} F^-_{\mu\nu} C_{\nu q}$ are the MO basis equivalents to their respective AO representations $F^+_{\mu\nu}$ and $F^-_{\mu\nu}$. The RHF Brillouin theorem [16, 78] is

$$f^+_{ai} = f^+_{at} + f^-_{at} = f^+_{it} - f^-_{it} = 0. \tag{2.44}$$

2.4 Second-Order Møller-Plesset Perturbation Theory

This section will give a brief introduction to Møller-Plesset perturbation theory which addresses dynamic electron correlation beyond HF [59]. Even if the HF method recovers about 99% of the exact energy within the basis set limit, the remaining contribution $E_{corr} = E_{exact} - E_{HF}$ is in the same order of magnitude as most effects chemists are interested in [3, p. 133]. The deviation is caused by the HF mean-field approximation underestimating dynamic electron correlation, *cf.* section 2.2. There are many methods to approximate the correlation energy

in a better way, with second-order Møller-Plesset perturbation theory (MP2) among the most commonly used *ab initio* methods. MP2 is reasonably accurate but not as complicated and expensive as for instance coupled cluster theory. For that reason it is a good choice if we are interested in properties requiring advanced calculations beyond molecular energies. After a general introduction to many-body perturbation theory we will, as for HF, first discuss the closed-shell case before proceeding to the more involved treatment of open-shell systems.

2.4.1 Many-Body Perturbation Theory

In perturbation theory it is assumed that the unperturbed reference system, described by an unperturbed Hamiltonian $\hat{H}^{(0)}$ and a corresponding wave function $\Psi^{(0)}$, is close to the perturbed system of interest. The perturbed system has the Hamilton operator

$$\hat{H} = \hat{H}^{(0)} + \Lambda \hat{H}^{(1)}, \tag{2.45}$$

where $\hat{H}^{(1)}$ describes a time-independent perturbation and Λ is the perturbation strength parameter. Inserting $\hat{H}$ into the time-independent Schrödinger equation, eq. 2.1, and setting $\Lambda = 0$ the unperturbed case is obtained as

$$\hat{H}^{(0)}|\Psi^{(0)}\rangle = E^{(0)}|\Psi^{(0)}\rangle. \tag{2.46}$$

Instead of using the total Schrödinger equation, perturbation theory could also be applied to the electronic or nuclear Schrödinger equations. The only limitations are that the reference system has to be non-degenerate and we are only looking for the ground state of the perturbed system [3, pp. 159]. If the perturbation parameter Λ now is increased towards a finite value, the system's wave function and energy will change, which can be expressed as a Taylor expansion in powers of Λ:

$$\Psi = \Lambda^0 \Psi^{(0)} + \Lambda^1 \Psi^{(1)} + \Lambda^2 \Psi^{(2)} + \Lambda^3 \Psi^{(3)} + \ldots \tag{2.47}$$

$$E = \Lambda^0 E^{(0)} + \Lambda^1 E^{(1)} + \Lambda^2 E^{(2)} + \Lambda^3 E^{(3)} + \ldots \tag{2.48}$$

In order to simplify the derivation and find a unique solution, the perturbed wave function Ψ can be chosen to be intermediately normalized

$$\langle \Psi | \Psi^{(0)} \rangle = \langle \Psi^{(0)} | \Psi^{(0)} \rangle + \Lambda \langle \Psi^{(1)} | \Psi^{(0)} \rangle + \Lambda^2 \langle \Psi^{(2)} | \Psi^{(0)} \rangle + \cdots = 1 \tag{2.49}$$

such that

$$\langle \Psi^{(n)} | \Psi^{(0)} \rangle = \delta_{n0}. \tag{2.50}$$

Inserting eqs. 2.45, 2.47 and 2.48 into eq. 2.1 and collecting all terms with the same power of Λ yields the nth-order perturbation equations:

$$\hat{H}^{(0)}\Psi^{(0)} = E^{(0)}\Psi^{(0)} \qquad \text{for } \Lambda^0$$
$$\hat{H}^{(0)}\Psi^{(1)} + \hat{H}^{(1)}\Psi^{(0)} = E^{(0)}\Psi^{(1)} + E^{(1)}\Psi^{(0)} \qquad \text{for } \Lambda^1$$
$$\hat{H}^{(0)}\Psi^{(2)} + \hat{H}^{(1)}\Psi^{(1)} = E^{(0)}\Psi^{(2)} + E^{(1)}\Psi^{(1)} + E^{(2)}\Psi^{(0)} \quad \text{for } \Lambda^2 \tag{2.51}$$
$$\vdots$$

If all possible solutions of the unperturbed Schrödinger equation generate an (almost) complete set of orthonormal functions $\{\Phi^\lambda\}$, the first-order corrected wave function $\Psi^{(1)}$ can be expressed as a linear combination of all unperturbed configurations Φ^λ:

$$|\Psi^{(1)}\rangle = t_\lambda|\Phi^\lambda\rangle = t_\lambda\hat{e}_\lambda|\Phi\rangle \tag{2.52}$$

The configurations Φ^λ are excited determinants which are generated from the ground state reference by an excitation operator $\hat{e}_\lambda$, and by definition it is $\Psi^{(0)} = \Phi$. After inserting eq. 2.52 into eq. 2.51 (second line, Λ^1) and multiplying from the left by $\langle\Phi|$, the first order energy correction is obtained as

$$E^{(1)} = \langle\Psi^{(0)}|\hat{H}^{(1)}|\Psi^{(0)}\rangle = \langle\Phi|\hat{H}^{(1)}|\Phi\rangle. \tag{2.53}$$

Thus, one can calculate $E^{(1)}$ by applying the perturbed Hamiltonian to the unperturbed wave function, without needing to know the form of $\Psi^{(1)}$ beforehand. In general, knowing the nth-order wave function is sufficient to calculate the $(2n+1)$th-order energy correction, thus a second-order energy correction for instance requires the first-order wave function to be found (Wigners rule, [2, pp. 25]). Multiplying with a function other than $\langle\Phi|$ will determine the expansion coefficients of the first order wave function in the basis of all unperturbed states:

$$t_\lambda = \frac{\langle\Phi^\lambda|\hat{H}^{(1)}|\Phi\rangle}{E_0 - E_\lambda} = \frac{\langle\Phi^\lambda|\hat{H}|\Phi\rangle}{E_0 - E_\lambda} \ \forall \ \lambda \neq 0 \tag{2.54}$$

Here E_0 is the solution of the unperturbed ground state, E_λ the solution associated with the unperturbed configuration Φ^λ, and $\hat{H}^{(0)}$ is assumed to be diagonal:

$$\langle\Phi^\lambda|\hat{H}^{(0)}|\Phi^{\lambda'}\rangle = E_\lambda\delta_{\lambda\lambda'} \tag{2.55}$$

The second-order energy correction can be found in the same manner to be

$$E^{(2)} = \langle\Psi^{(0)}|\hat{H}^{(1)}|\Psi^{(1)}\rangle = \langle\Psi^{(0)}|\hat{H}|\Psi^{(1)}\rangle = t_\lambda\langle\Phi|\hat{H}|\Phi^\lambda\rangle = t_\lambda K_\lambda. \tag{2.56}$$

The expansion coefficients t_λ are usually referred to as amplitudes and the integrals can be collected in a matrix K_λ [3, pp. 159].

In eq. 2.52 we have silently introduced a formalism called 'second quantization' by using excitation operators $\hat{e}^\lambda$ to generate excited configurations Φ^λ from some form of ground state reference determinant Φ [79]. The excitation operators themselves are composed of creation and annihilation operators, denoted $\hat{a}_p^\dagger$ and $\hat{a}_p$ respectively. If acting on a spin-orbital p, those operators either create or remove an electron if allowed by the Pauli principle, else they will return zero. The operators also observe the anti-commutation relation to ensure the wave function's anti-symmetry whenever necessary, so the sequence in which the operators are applied to a wave function matters. If now an annihilation operator $\hat{a}_i$ acts on an occupied spin-orbital i, and a creation operator $\hat{a}_a^\dagger$ on a virtual orbital a, this corresponds to a single excitation $a \leftarrow i$ of an electron from orbital i to a:

$$\hat{e}_{ai} = \hat{a}_a^\dagger \hat{a}_i \tag{2.57}$$

The general index λ in above equation has been replaced by the indices of the manipulated orbitals. Similar double excitations $a \leftarrow i \wedge b \leftarrow j$ are possible using operators $\hat{a}_a^\dagger, \hat{a}_b^\dagger, \hat{a}_i, \hat{a}_j$, and equivalently triple and higher order excitations. Additionally, the operators can be restricted to only act on orbitals with a given spin, indicated using a tilde for α- and bar for β-spin quantities. This can be used to construct spin-free excitation operators:

$$\hat{E}_{ai} = \tilde{e}_{ai} + \bar{e}_{ai} = \tilde{a}_a^\dagger \tilde{a}_i + \bar{a}_a^\dagger \bar{a}_i \tag{2.58}$$

2.4.2 Closed-Shell Second-Order Møller-Plesset Perturbation Theory

Closed-shell Møller-Plesset perturbation theory is many-body perturbation theory applied to the electronic Schrödinger equation with the unperturbed (zeroth-order) Hamilton operator defined to be the closed-shell Fock operator

$$\hat{H}_{el}^{(0)} = f_{pq} \hat{E}_{pq}. \tag{2.59}$$

Perturbation theory is a reasonably good approach, as we expect $\hat{H}_{el}^{(0)}$ to be close to the exact solution already [3, pp. 163]. The zeroth-order wave function is the HF Slater determinant $\Psi^{(0)} = \Phi$, and so for a canonical reference with $f_{ij} = \delta_{ij}\epsilon_i$, the zeroth-order energy $E^{(0)}$ is just the sum of all MO energies ϵ_i:

$$E^{(0)} = \langle \Phi | \hat{H}_{el}^{(0)} | \Phi \rangle = \sum_{pq}^{N_{el}/2} f_{pq} \langle \Phi | \hat{E}_{pq} | \Phi \rangle = 2 \sum_i^{N_{el}/2} \epsilon_i \tag{2.60}$$

According to eq. 2.45, the Hamiltonian's first-order correction is the difference between $\hat{H}_{el}^{(0)}$ and the exact solution $\hat{H}_{el}$ (eq. 2.2)

$$\langle\Phi|\hat{H}_{el}^{(1)}|\Phi\rangle = \langle\Phi|\hat{H}_{el} - \hat{H}_{el}^{(0)}|\Phi\rangle = E_{HF} - E^{(0)} = E^{(1)} \tag{2.61}$$

The nuclear energy contribution E_{nuc} has been omitted for now and will be simply added later. In consequence, the first-order energy correction then removes the Fock operator's doubly-counted average electron interaction (*cf.* eqs. 2.21, 2.22)

$$E^{(1)} = \langle\Phi|\hat{H}_{el}^{(1)}|\Phi\rangle = -\sum_{ij}^{N_{el}/2} \left(2(ii|jj) - (ij|ij)\right) \tag{2.62}$$

which results in the HF energy E_{HF} (for instance eq. 2.12) to be recovered as

$$E_{HF} = E^{(0)} + E^{(1)} + E_{nuc}. \tag{2.63}$$

That is to say, the first 'real' perturbative correction to the Hartree-Fock energy happens at second-order level [59], [3, p. 163].

The expression for the second-order energy correction eq. 2.56 requires the calculation of a first-order wave function $\Psi^{(1)}$, eq. 2.52. The excited determinants Φ^λ which are spanning the first-order wave function are generated from the HF reference by a spin-free excitation operator, eq. 2.58. The index λ is replaced by all possible single excitations $a \leftarrow i$ as well as double excitations $a \leftarrow i \wedge b \leftarrow j$, and all higher orders [13, pp. 740]. Due to the Brillouin condition discussed in section 2.2, single excitations can be excluded in the closed-shell case, as for singly excited configurations (*cf.* eq. 2.54)

$$\langle\Phi_i^a|\hat{H}|\Phi\rangle = 2f_{ai} = 0. \tag{2.64}$$

Also all triply or higher excited determinants will not contribute to $\Psi^{(1)}$ as the acting Hamiltonian is a two-particle operator [13, p. 745]. So only doubly excited configurations $|\Phi_{ij}^{ab}\rangle := \hat{E}_{ai}\hat{E}_{bj}|\Phi\rangle$ remain for the closed-shell MP2 energy correction. Some of the remaining configurations, namely Φ_{ij}^{ab} and Φ_{ij}^{ba}, however, are not orthogonal. The general expansion coefficients over all excited states t_λ should thus be replaced with contravariant coefficients over doubly excited states only,

$$\tilde{T}_{ab}^{ij} = 2T_{ab}^{ij} - T_{ba}^{ij}. \tag{2.65}$$

The corresponding contravariant configurations are

$$|\tilde{\Phi}_{ij}^{ab}\rangle = \frac{1}{6}\left(2|\Phi_{ij}^{ab}\rangle + |\Phi_{ij}^{ba}\rangle\right). \tag{2.66}$$

Contravariant configurations span the same space as their covariant equivalents with the advantage of being orthogonal to the covariant ones for $i \geq j$ and $k \geq l$:

$$\langle \tilde{\Phi}^{ab}_{ij} | \Phi^{cd}_{kl} \rangle = \delta_{ac} \delta_{bd} \delta_{ik} \delta_{jl} + \delta_{ad} \delta_{bc} \delta_{il} \delta_{jk} \tag{2.67}$$

Contravariant quantities will be used for spin-integrated closed-shell systems only and the tilde does thus not indicate α-spin as compared to the spin-orbital based open-shell theory discussed in other parts of this work [80, pp. 7] and [79]. After spin-integration, the exchange matrix coefficients are found to be

$$K^{ij}_{ab} = \langle \Phi | \hat{H} | \tilde{\Phi}^{ab}_{ij} \rangle = (ai|bj). \tag{2.68}$$

The closed-shell MP2 energy correction thus is

$$E^{(2)}_{MP2} = \langle \Phi | \hat{H} | \Psi^{(1)} \rangle = \langle \Phi | \hat{H} | \tilde{\Phi}^{ab}_{ij} \rangle \tilde{T}^{ij}_{ab} = K^{ij}_{ab} \tilde{T}^{ij}_{ab}. \tag{2.69}$$

If MP2 is based on a canonical HF reference, the amplitudes T^{ij}_{ab} can be directly calculated as

$$T^{ij}_{ab} = -\frac{K^{ij}_{ab}}{\epsilon_a + \epsilon_b - \epsilon_i - \epsilon_j}. \tag{2.70}$$

If a non-diagonal occupied Fock matrix block is used as zeroth-order Hamiltonian, the amplitudes are not readily available in a closed expression as eq. 2.54 cannot be fully decoupled. They instead have to be found in an iterative manner:

$$\Delta T^{ij}_{ab} \approx \frac{-R^{ij}_{ab}}{\epsilon_a + \epsilon_b - f_{ii} - f_{jj}} \tag{2.71}$$

The new amplitudes are generated by adding the amplitude update ΔT^{ij}_{ab} to the amplitudes of the previous iteration. The contribution

$$R^{ij}_{ab} = \frac{1}{2} \frac{\partial E^{(2)}}{\partial \tilde{T}^{ij}_{ab}} = [\mathbf{K}^{ij} + \mathbf{T}^{ij}\mathbf{F} + \mathbf{F}\mathbf{T}^{ij} - f_{ik}\mathbf{T}^{kj} - \mathbf{T}^{ik}f_{kj}]_{ab} := 0 \tag{2.72}$$

is called the residuum and will vanish for fully optimized amplitudes [80, pp. 7]. In the residual equations, F_{ab} denotes the virtual-virtual subspace of the Fock matrix in MO basis. The residuum's general form is

$$R_\lambda = \frac{1}{2} \frac{\partial E^{(2)}}{\partial t_\lambda} = \langle \Phi^\lambda | \hat{H} | \Phi \rangle + \langle \Phi^\lambda | \hat{H}^{(0)} - E^{(0)} | \Psi^{(1)} \rangle := 0. \tag{2.73}$$

As eq. 2.69 (or in general eq. 2.56) depends linearly on the amplitudes a small error in the amplitudes will lead to significant deviations in the energy correction. This problem can be

overcome by instead using the Hylleraas functional [31]:

$$E_2 = 2\langle\Phi^\lambda|\hat{H}|\Phi\rangle + \langle\Phi^\lambda|\hat{H}^{(0)} - E^{(0)}|\Psi^{(1)}\rangle = t_\lambda(K_\lambda + R_\lambda) \tag{2.74}$$

We can determine the amplitudes by minimizing the Hylleraas functional with respect to all t_λ. The functional is designed to have a minimum for the exact first order wave function, in which case $E^{(2)} = E_2$ [13, pp. 734]. Applying the MP2 excitation operator eq. 2.58 to eq. 2.74 leads to the explicit Hylleraas energy expression for closed-shell MP2 as

$$E_2 \;=\; \tilde{T}^{ij}_{ab}\left[K^{ij}_{ab} + R^{ij}_{ab}\right]. \tag{2.75}$$

2.4.3 Restricted Open-Shell Second-Order Møller-Plesset Perturbation Theory

Deriving Møller-Plesset perturbation theory using a RHF reference, several different approaches for defining the zeroth-order Hamiltonian can be taken [17–19, 77]. Seven of them are summarized in a very good review by Crawford and Schaefer [81]. All of them have different strengths and weaknesses and we have chosen restricted MP2 (RMP2) [18] as method of choice for deriving gradients. RMP2 offers the advantage of orbital invariance towards all rotations that are allowed within the RHF reference – which will be important for introducing local approximations later on – and leads to straightforward gradient expressions. Its ansatz as a simple sum of both RHF Fock operators, $\mathbf{f}^\alpha$ and $\mathbf{f}^\beta$, however, renders the zeroth-order Hamiltonian spin-dependent [81]:

$$\hat{H}^{(0)} = f^\alpha_{mn}\tilde{e}_{mn} + f^\beta_{ij}\bar{e}_{ij} + f^\alpha_{ab}\tilde{e}_{ab} + f^\beta_{xy}\bar{e}_{xy} \tag{2.76}$$

The indices m, n used above run over both occupied spaces, including doubly (i, j) and singly (t, u) occupied orbitals; indices x, y include active (t, u) and virtual (a, b) orbitals. If $\hat{H}^{(0)}$ is not spin-free, the later generated first order wave function $|\Psi^{(1)}\rangle$ may be spin-contaminated, even though the method is called restricted MP2 (RMP2). Conveniently, this contamination has only minor influence on the second-order energy correction $E^{(2)} = \langle\Phi|\hat{H}|\Psi^{(1)}\rangle$, as $\hat{H}$ and Φ still remain spin-free. Most of the perturbed wave function's spin-contamination is then eliminated due to the projection included in $E^{(2)}$, and only higher order energies, which are not of interest here, may be directly contaminated [81, 82].

The definition of the first-order wave function, eq. 2.52, is formally unchanged no matter which ansatz for $\hat{H}^{(0)}$ is used. However one should note that the off-diagonal blocks of $\mathbf{f}^\alpha$ and $\mathbf{f}^\beta$ are now non-zero as the simple closed-shell Brillouin condition is no longer fulfilled (see eq. 2.44). As the off-diagonal blocks are not included in eq. 2.76, this leads to additional single excitations $\tilde{t}^m_a$ for α-spin and $\bar{t}^i_x$ for β-spin electrons that were previously zero. This can be avoided by

diagonalizing the Fock operators prior to MP2 treatment, which then leads to two different sets of MO coefficients, similar to UHF. This is called different orbitals for different spins (DODS)[1] [81]. Yet for gradients, especially when aiming for local electron correlation treatment later on, including singles into the perturbation treatment is more favourable than employing the DODS formalism. The RMP2 excitation operators needed to generate the excited configurations for the first-order wave function are:

$$t_\lambda \hat{e}_\lambda \rightarrow \tilde{t}_a^m \tilde{e}_m^a + \bar{t}_x^i \bar{e}_i^x + \frac{1}{4}\tilde{T}_{ab}^{mn}\tilde{e}_m^a\tilde{e}_n^b + \frac{1}{4}\bar{T}_{xy}^{ij}\bar{e}_i^x\bar{e}_j^y + \check{T}_{ax}^{mi}\tilde{e}_m^a\bar{e}_i^x. \tag{2.77}$$

Here we have separated $\alpha\alpha$, $\beta\beta$, and mixed pair excitations into different amplitudes; a tilde denotes alpha-spin quantities, a bar beta-spin quantities, and a check mixed spin contributions. The factors 1/4 again account for the amplitude symmetries

$$\tilde{T}_{ab}^{mn} = -\tilde{T}_{ba}^{mn} = -\tilde{T}_{ab}^{nm} = \tilde{T}_{ba}^{nm} \tag{2.78}$$

$$\bar{T}_{xy}^{ij} = -\bar{T}_{yx}^{ij} \ = -\bar{T}_{xy}^{ji} \ = \bar{T}_{yx}^{ji}. \tag{2.79}$$

Inserting eq. 2.77 into eq. 2.56, the RMP2 second-order energy expression is

$$E_{RMP2}^{(2)} = \tilde{t}_a^m \tilde{f}_a^m + \bar{t}_x^i \bar{f}_x^i + \frac{1}{4}\left[\tilde{T}_{ab}^{mn}K_{ab}^{mn} + \bar{T}_{xy}^{ij}K_{xy}^{ij}\right] + \check{T}_{ax}^{mi}K_{ax}^{mi}. \tag{2.80}$$

With off-diagonal elements present in the Fock operators, the amplitudes have to be found iteratively. Applying the RMP2 excitation operator 2.77 to eq. 2.74 leads to the explicit Hylleraas energy expression for RMP2 as

$$
\begin{aligned}
E_2 &= \frac{1}{4}\left[\tilde{T}_{ab}^{mn}(K_{ab}^{mn} - K_{ba}^{mn} + \tilde{R}_{ab}^{mn}) + \bar{T}_{xy}^{ij}(K_{xy}^{ij} - K_{yx}^{ij} + \bar{R}_{xy}^{ij})\right] + \check{T}_{ax}^{mi}(K_{ax}^{mi} + \check{R}_{ax}^{mi}) \\
&+ \ \tilde{t}_a^m(\tilde{f}_a^m + \tilde{r}_a^m) + \bar{t}_x^i(\bar{f}_x^i + \bar{r}_x^i)
\end{aligned}
\tag{2.81}
$$

with

$$
\begin{aligned}
\tilde{R}_{ab}^{mn} &= [\mathbf{K}^{mn} - \mathbf{K}^{nm} + \tilde{\mathbf{T}}^{mn}\mathbf{F}^\alpha + \mathbf{F}^\alpha\tilde{\mathbf{T}}^{mn} - f_{mm'}^\alpha\tilde{\mathbf{T}}^{m'n} - \tilde{\mathbf{T}}^{mm'}f_{m'n}^\alpha]_{ab} \\
\bar{R}_{xy}^{ij} &= [\mathbf{K}^{ij} - \mathbf{K}^{ji} + \bar{\mathbf{T}}^{ij}\mathbf{F}^\beta + \mathbf{F}^\beta\bar{\mathbf{T}}^{ij} - f_{ik}^\beta\bar{\mathbf{T}}^{kj} - \bar{\mathbf{T}}^{ik}f_{kj}^\beta]_{xy} \\
\check{R}_{ax}^{mi} &= [\mathbf{K}^{mi} + \check{\mathbf{T}}^{mi}\mathbf{F}^\beta + \mathbf{F}^\alpha\check{\mathbf{T}}^{mi} - f_{mn}^\alpha\check{\mathbf{T}}^{ni} - \check{\mathbf{T}}^{mj}f_{ji}^\beta]_{ax} \\
\tilde{r}_a^m &= \left[(\mathbf{f}^\alpha)^m + \mathbf{F}^\alpha\tilde{\mathbf{t}}^m - f_{mn}^\alpha\tilde{\mathbf{t}}^n\right]_a \\
\bar{r}_x^i &= \left[(\mathbf{f}^\beta)^i + \mathbf{F}^\beta\bar{\mathbf{t}}^i - f_{ij}^\beta\bar{\mathbf{t}}^j\right]_x.
\end{aligned}
\tag{2.82}
$$

These are the working equations that are solved iteratively until the residuals vanish [21]. The fact that for converged amplitudes $2R_\lambda = \partial E_2/\partial t_\lambda = 0$ – the Hylleraas functional is stationary

---

[1]The DODS formalism should not be confused with block-diagonalzation of the Fock operators as used in other flavours of open-shell MP2!

with respect to small variations of the optimized amplitudes – is very convenient for deriving gradient expressions [29, 31]. To simplify notation in the residuals above and all following equations, it will be assumed that Pauli violating terms are set to zero from now on if summed over them. We can thus extend the contributions in eq. 2.82 to be

$$\tilde{R}_{xy}^{mn} = \begin{array}{c} \\ act \\ vrt \end{array} \overset{\begin{array}{cc} act & vrt \end{array}}{\begin{pmatrix} 0 & 0 \\ 0 & \tilde{R}_{ab}^{mn} \end{pmatrix}}, \; \check{R}_{xy}^{mn} = \begin{array}{c} \\ act \\ vrt \end{array} \overset{\begin{array}{cc} act & vrt \end{array}}{\begin{pmatrix} 0 & 0 \\ \check{R}_{at}^{mn} & \check{R}_{ab}^{mn} \end{pmatrix}} \; \text{and} \; \tilde{r}_x^m = \begin{array}{c} \\ act \\ vrt \end{array} \overset{\begin{array}{c} act \end{array}}{\begin{pmatrix} 0 \\ \tilde{r}_a^m \end{pmatrix}} \quad (2.83)$$

with $\check{R}_{xy}^{mn} = 0 \; \forall \; n \in t$. Beta-spin quantities $\bar{R}_{xy}^{mn}$ and $\bar{r}_x^m$ remain unchanged in the active indices, but $\bar{R}_{xy}^{mn} = \bar{r}_x^m = 0 \; \forall \; m, n \in t, u$. The open-shell amplitudes $\tilde{t}_x^m, \bar{t}_x^m, \tilde{T}_{xy}^{mn}, \bar{T}_{xy}^{mn}$, and $\check{T}_{xy}^{mn}$ can be extended equivalently.

3 Local Electron Correlation Methods

As discussed in chapter 2, there is no unique choice of orbitals that solve the HF equations. One may choose any linear combination, as long as the orbitals remain orthonormal and occupied and virtual orbitals do not mix. The canonical approach diagonalizing the Fock matrix had the advantage that the HF equations turned into a simple pseudo-eigenvalue problem. Also, in (R)MP2, the amplitudes generated from diagonal Fock matrices were directly available without solving a further set of equations. Yet, the disadvantage that comes with this choice of orbitals is the difficulty of introducing further approximations. Such approximations are necessary to limit the steep scaling of computational cost with increasing molecular size if dynamic electron correlation of post-HF precision is to be calculated. This steep scaling is physically not justified, as the dynamic correlation energy decreases with growing interelectronic distance r_{12} as r_{12}^{-6} [30, 32].

In order to save computational effort during a post-HF calculation, one possible approach is to reduce the level of theory or even completely omit the treatment of all electron pairs with an intereletronic distance above a certain threshold. For canonical MOs, this is difficult to implement, as the orbitals tend to be delocalized over the whole molecule, so every electron is spatially close to every other. Taking advantage of the energies' invariance with respect to unitary transformations however, the orbitals in the occupied block of the Fock matrix can be rearranged to fulfil arbitrary boundary conditions [30, 33, 83]. A suitable boundary condition could be, for instance, to minimize the spatial extent of the MOs during localization, as suggested by Foster and Boys [84, 85]. Boys' localization was initially developed to relate quantum chemical calculations to traditional chemical bonding theories and leads to 'banana'-shaped localized molecular orbitals (LMOs) [86]. In a related procedure called Edmiston-Ruedenberg localization, the electronic self-repulsion energy is maximized, which yields LMOs similar to the $\pi-$ and $\sigma-$bonds commonly used in many areas of chemistry [87]. From a computational point of view, both procedures suffer from convergence problems, as their solutions are not guaranteed to be unique [86]. Instead of localizing the spatial extent of the MOs in question as in the procedures above, one could also maximize the sum of Mulliken gross atomic charges, so every LMO is generated by AO basis functions residing at as few atoms as possible. This is known as the Pipek-Mezey (PM) localization scheme [54]. Section 3.1 will explain PM localization more detailed, as it is one of the two localization schemes used for our gradients.

The problem of building a localization algorithm based on Mulliken charges is that these charges are mathematically not well defined and can thus not be systematically improved towards the complete basis set limit [53, 88–90]. A solution being more stable with respect to basis set changes are Knizia's intrinsic bond orbitals (IBOs), which is the second localization scheme we have chosen [53]. IBOs follow the same idea as PM localization, but instead of Mulliken charges, partial charges generated from intrinsic atomic orbitals (IAOs) are used. A more in-depth discussion of IBO localization and implementation can be found in section 3.2. Of course there are many more methods and modifications of methods, with the field still under active research today, but a review of all of them would be beyond the scope of this thesis. Once the MOs are localized by a procedure of choice, spatial confinement of the electrons makes it possible to introduce a pair energy or distance criterion; all pairs above a certain distance or below a certain pair energy can then either be treated on lower levels of theory or neglected completely. This is called the pair approximation [30, 86].

Further computational effort can be saved by restricting the number of pair excitations used to generate the first order MP2 wave function $\Psi^{(1)}$, eq. 2.52. The contribution of a specific excitation $a \leftarrow i \wedge b \leftarrow j$ to the wave function will decrease the further the considered orbitals are apart, as the excitation will be less important [30, 32, 86]. This is due to the exponential decay of the integrals $(ai|bj)$ with increasing distance between the basis functions of $|i\rangle$ and $|a\rangle$ (and of course $|j\rangle$ and $|b\rangle$) [80, p. 10]. In order to exploit this effect, the canonical virtual MOs are replaced by a set of AOs from which the occupied space has been removed, called projected atomic orbitals (PAOs); localizing the virtual block using the same procedures as for the occupied MOs is usually not successful [30, 91]. But as the AO basis functions are assumed to be atom centred in this work, the PAOs are already a quite useful form of virtual space localization. Then excitations from every LMO i are restricted to a subset of PAOs called a domain. For the LMO's primary domain $[i]$, all PAOs located at atoms the LMO i is residing at are included; the selection criterion is usually an atomic partial charge threshold which needs to be exceeded. The union of two domains $[ij] = [i] \cup [j]$ then is called a pair domain and the domains can be increased even further by adding more virtual orbitals from neighbouring atoms, until in the limit of full domains (and including all pairs) the complete canonical correlation energy is recovered [86]. The domain approximation in local methods will, as a welcome side-effect, reduce the intramolecular basis set superposition error (BSSE) [32]. The most common method for virtual space localization has long been the aforementioned projected atomic orbitals, as they are simple to derive and implement. They will be discussed in more detail in section 3.3. A drawback of the PAO method is the slow convergence of the correlation energy towards the canonical solution if domain sizes are increased [92]. For energy calculations, other orbitals such as orbital-specific virtuals (OSVs) or pair-natural orbitals (PNOs) recently have found widespread use [37, 93–95]. The use of other virtual orbital methods than PAOs in gradient methods, however, is not as straight forward and their efficiency still has to be

proved [49, 96].

3.1 Pipek-Mezey Localization

For Pipek-Mezey localization one maximizes the square sum of the Mulliken gross atomic charges at every atom A [54]

$$P_{PM} = \frac{1}{4} \sum_{i'} \sum_{A}^{N_{at}} [s_{i'i'}^A]^2 \rightarrow \text{ max} \tag{3.1}$$

with the atom-specific gross charge

$$s_{i'i'}^A = \sum_{\mu \in A} [L_{\mu i'} S_{\mu\nu} L_{\nu i'} + L_{\mu i'} S_{\mu\nu} L_{\nu i'}]. \tag{3.2}$$

The occupied canonical MO coefficients populate a rectangular submatrix of $\mathbf{C}$ called $\mathbf{C}_0$, the new LMO coefficients populate a submatrix $\mathbf{L}_0$ with

$$|i'\rangle = |\mu\rangle [\mathbf{L}_0]_{\mu i'}. \tag{3.3}$$

As it will be clear from context if we refer to canonical MOs $|i\rangle$ or LMOs $|i'\rangle$, the prime denoting LMOs will be omitted from now on. Furthermore, all equations in this and the following sections can be used for active space localization if indices i, j are replaced by t, u. Virtual orbitals are assumed to be canonical with a submatrix $\mathbf{C_v}$ such that we can define two square matrices $\mathbf{C} = (\mathbf{C_0}|\mathbf{C_v})$ and $\mathbf{L} = (\mathbf{L_0}|\mathbf{C_v})$. Using this concatenation, we can extend the definition of eq. 3.2 for later use to full MO space as

$$S_{pq}^A = \sum_{\mu \in A} [L_{\mu p} S_{\mu\nu} L_{\nu q} + L_{\mu q} S_{\mu\nu} L_{\nu p}]. \tag{3.4}$$

The two sets of occupied MO coefficients are connected by a unitary rotation matrix $\mathbf{w}$

$$\mathbf{L}_0 = \mathbf{C}_0 \mathbf{w}. \tag{3.5}$$

which can be extended to a full space matrix by assuming the virtual-virtual block is the identity matrix and the elements of the off-diagonal blocks are zero. If P_{PM} is maximized, every LMO is spanned by AO basis functions that reside at as few atoms as possible. The stationary condition is the first derivative of eq. 3.1 with respect to a unitary rotation of the occupied orbitals. If the rotation matrix fulfils $\mathbf{U}^\dagger \mathbf{U} = \mathbf{1}$, it can be expanded as

$$\mathbf{U} = e^{\mathbf{V}} = \mathbf{1} + \mathbf{V} + \frac{1}{2}\mathbf{V}^2 + ... \text{ with } \mathbf{V} = -\mathbf{V}^\dagger. \tag{3.6}$$

At the expansion point, $\mathbf{V} = 0$, and due to $\mathbf{V}$s anti-symmetry, we can limit the stationary condition to all pairs $j > i$:

$$(g_{PM})_{ij} = \left(\frac{\partial P_{PM}}{\partial V_{ij}}\right)_{\mathbf{V}=0} = \frac{1}{2}\sum_{A}^{N_{at}}[s_{jj}^A - s_{ii}^A]s_{ij}^A = 0 \ \forall \ j > i. \tag{3.7}$$

Furthermore, by expanding the perturbed MO coefficients in $\mathbf{V}$, $\mathbf{L}(\mathbf{V}) = \mathbf{L}(\mathbf{0})(\mathbf{1} + \mathbf{V})$ can be conveniently described in the basis of the unperturbed coefficients $\mathbf{L}(0)$. In general, PM localization is a very efficient method to generate a unique set of localized orbitals. However, localization may fail in highly symmetric cases such as benzene, as there is more than one possible solution with maximum overlap. Also, diffuse basis sets or basis set changes during geometry optimization can lead to localization problems, as discussed earlier [9, 29, 53, 54].

3.2 Intrinsic Bond Orbitals

A possible alternative to PM localization are intrinsic bond orbitals (IBOs), where the localization is carried out based on a set of perturbed AOs called intrinsic atomic orbitals (IAOs) [53]. IAOs are generated by projections onto a minimal basis; they are closely related to quasiatomic orbitals which can be found in an iterative manner [56]. The minimal basis B_2 of free-atom AOs and the large basis set B_1 used for the preceding HF calculation are non-orthonormal with metric

$$[\mathbf{S}_1]_{\mu\nu} = \langle\mu|\nu\rangle, [\mathbf{S}_2]_{\rho\sigma} = \langle\rho|\sigma\rangle, \text{ and } [\mathbf{S}_{12}]_{\mu\rho} = [\mathbf{S}_{21}]_{\rho\mu} = \langle\mu|\rho\rangle. \tag{3.8}$$

AO basis functions throughout this work are indexed by μ, ν, τ, υ for the main basis B_1 and ρ, σ for the auxiliary basis B_2. To clarify which quantity is spanned by which basis, the main basis set overlap $\mathbf{S} = \mathbf{S}_1$ will be written using a basis set index as well whenever IBOs are discussed. To construct the IAOs $|\rho'\rangle$, the already existing canonical MOs $|i\rangle$ are depolarized by projecting them onto the minimal basis B_2 and back

$$\{|\tilde{i}\rangle\} = \text{orth}\{P_1 P_2 |i\rangle\} \tag{3.9}$$

with

$$P_1 = \sum_{\mu\nu\in B_1} |\mu\rangle[\mathbf{S}_1]_{\mu\nu}^{-1}\langle\nu| \tag{3.10}$$

$$P_2 = \sum_{\rho\sigma\in B_2} |\rho\rangle[\mathbf{S}_2]_{\rho\sigma}^{-1}\langle\sigma| \tag{3.11}$$

being the projectors onto bases B_1 and B_2, and $|\tilde{i}\rangle$ the depolarized canonical MOs.[1] $[\mathbf{S}_1]^{-1}_{\mu\nu}$ and $[\mathbf{S}_2]^{-1}_{\rho\sigma}$ are the respective inverse overlap matrices and 'orth' indicates symmetric orthogonalization within B_1 which can be achieved by applying

$$\mathbf{X} = \text{orth}\{\bar{\mathbf{X}}\} = \bar{\mathbf{X}} \left[\bar{\mathbf{X}}^\dagger \mathbf{S}_1 \bar{\mathbf{X}}\right]^{-1/2} \tag{3.12}$$

to an arbitrary matrix $\bar{\mathbf{X}}$. To differentiate between quantities already orthogonalized and their non-orthogonalized counterparts, the latter will be marked with a bar from now on.[2]

Two projectors describing the contribution of the polarized and depolarized MOs to the occupied space, O and $\tilde{O}$, can be constructed as

$$O = \sum_i |i\rangle\langle i| \text{ and } \tilde{O} = \sum_{\tilde{i}} |\tilde{i}\rangle\langle\tilde{i}| \tag{3.13}$$

for doubly occupied orbitals, and similarly

$$O = \sum_t |t\rangle\langle t| \text{ and } \tilde{O} = \sum_{\tilde{t}} |\tilde{t}\rangle\langle\tilde{t}| \tag{3.14}$$

for active orbitals if existent. The projectors in matrix notation correspond to the respective polarized and depolarized zeroth-order densities. As densities are invariant to unitary rotations within the occupied orbitals, both canonical MOs or LMOs can be used in the construction of density matrices $\mathbf{D}^{(0)}$ and $\tilde{\mathbf{D}}^{(0)}$, a relation which will be used in due time to simplify some of the upcoming derivative expressions. Using those projectors, the minimal set of perturbed IAOs which span the occupied MOs of the original HF wave function can be generated as

$$|\rho'\rangle = \text{orth}\left\{\left(O\tilde{O} + (1-O)(1-\tilde{O})\right) P_1|\rho\rangle\right\} \tag{3.15}$$

or

$$|\rho'\rangle = \text{orth}\left\{\left(1 + O - \tilde{O}\right) P_1|\rho\rangle\right\}. \tag{3.16}$$

We can now see that the IAOs are basically a polarized minimal basis, as eq. 3.15 describes the projection of the occupied free atom AOs (via $\tilde{O}$) and the virtual free atom AOs (via $1-\tilde{O}$) onto their respective polarized counterparts O and $1-O$. Almost the same effect can be achieved by adding the difference between the polarized and unpolarized densities (which is the polarization) to the unpolarized AOs, as in eq. 3.16. Although the latter equation may be inaccurate in the sense that it polarizes the virtual space in the wrong direction $1 + O$, the advantages of simplicity and faster computation outweigh this drawback, and eq. 3.16 will be used in this

---

[1] The tilde denoting depolarized canonical MOs should not be confused with the one used to indicate alpha-spin amplitudes, Fock matrices, or excitation operators in RMP2.

[2] This bar should not be confused with the one used to denote beta-spin amplitudes, Fock matrices, or excitation operators in RMP2.

work instead of eq. 3.15 [53, 56].

Having constructed the IAOs by either projection, the IBOs $|i\rangle$ (or $|t\rangle$) can be found by maximizing a functional very similar to eq. 3.1:

$$P_{IB} = \frac{1}{2p} \sum_i \sum_A^{N_{at}} \left(\sum_{\rho' \in A} \langle i | \rho' \rangle \langle \rho' | i \rangle \right)^p = \frac{1}{2p} \sum_i \sum_A^{N_{at}} \left(q_{ii}^A \right)^p \rightarrow \text{max} \tag{3.17}$$

with the localization exponent $p = 2$ or $p = 4$ and q_{ii}^A being the partial charge of orbital $|i\rangle$ at atom A. The difference between the localization exponents is that a higher exponent forces a more thorough localization by punishing so called localization tails. On the one hand this can sometimes yield better results, as the least localized orbital defines the overall locality; on the other hand higher exponents may over-localize systems resulting in unwanted physical effects [53, 91]. We will present and have implemented the gradients for both exponents. Using a different definition of charges as for PM localization, the overlap matrix elements Q_{pq}^A are now given as

$$Q_{pq}^A = \sum_{\rho' \in A} \left[\mathbf{L}^\dagger \mathbf{S}_1 \mathbf{B} \right]_{p\rho'} \left[\mathbf{B}^\dagger \mathbf{S}_1 \mathbf{L} \right]_{\rho' q} \tag{3.18}$$

where we have extended the definition of q_{ij}^A as in the previous section to full MO space for use in the local gradients later on.

For both, PM and IBOs, the LMO coefficient matrix $\mathbf{L}$ is defined equivalently, and similar to the LMO coefficient matrix there is a matrix of IAO coefficients $\mathbf{B}$, which corresponds to eq. 3.16 in matrix notation

$$\mathbf{B} = \text{orth} \left\{ \bar{\mathbf{B}} \right\} = \text{orth} \left\{ (\mathbf{S}_1^{-1} + \mathbf{C}\mathbf{C}^\dagger - \tilde{\mathbf{C}}\tilde{\mathbf{C}}^\dagger)\mathbf{S}_{12} \right\}. \tag{3.19}$$

It should be noted that in open-shell systems there exist two sets of IAOs, one generated for closed-shell and one for active orbitals; thus partial charges $\mathbf{q}^A$ for the two spaces are determined independently. The depolarized MOs eq. 3.9 can be represented as

$$\tilde{\mathbf{C}} = \text{orth} \left\{ \mathbf{S}_1^{-1} \mathbf{S}_{12} \mathbf{S}_2^{-1} \mathbf{S}_{21} \mathbf{C} \right\}. \tag{3.20}$$

Differentiation of eq. 3.17 with respect to an infinitesimal change of the occupied orbitals (via MO coefficient expansion using $\mathbf{U} = \mathbf{1} + \mathbf{V}$) leads to the residual equations

$$(g_{IB})_{ij} = \frac{1}{2} \sum_A^{N_{at}} \left([q_{jj}^A]^{p-1} - [q_{ii}^A]^{p-1} \right) q_{ij}^A = 0 \; \forall \; j > i \tag{3.21}$$

to be solved. For $p = 2$ this equation is formally equivalent to eq. 3.7 and the same algorithm of pair-wise orbital rotations can be used to solve both of them [86].

3.3 Projected Atomic Orbitals

To limit the number of excitations $\hat{e}_\lambda$ to the virtual space, they can be restricted to a set of virtual orbitals spatially close to the LMO in question. The most common ansatz for generation of such localized virtual orbitals is to simply project the generating AOs $|\mu\rangle$ against the localized occupied space [30]:

$$|r\rangle = \left[1 - \sum_m |m\rangle\langle m|\right] |\mu\rangle C_{\mu r}^{AO} \tag{3.22}$$

where usually $C_{\mu r}^{AO} = \delta_{\mu r}$ is used. Here the middle term describes the removal of all closed and active LMOs ($|m\rangle\langle m|$) out of the complete set of AOs $(1 - ...)$. The linear combinations of the remaining AOs are called projected atomic orbitals (PAOs) $|r\rangle$ and they populate a rectangular coefficient matrix $\mathbf{P}$:

$$\begin{aligned}
|r\rangle &= |\mu\rangle\, P_{\mu r} \tag{3.23}\\
\mathbf{P} &= \mathbf{1} - \mathbf{L}_0\mathbf{L}_0^\dagger\mathbf{S}_1 = \mathbf{C_v}\mathbf{C_v^\dagger}\mathbf{S}_1 = \mathbf{C_v}\mathbf{Q}. \tag{3.24}
\end{aligned}$$

The transformation matrix Q_{xr} is a rectangular matrix from which a submatrix for every domain $Q_{xr'}^m$ can be generated by restricting the right-hand index $r' \in [m]$. As the domains $Q_{xr'}^m$ are usually apparent from the neighbouring quantities $(\mathbf{t}^m, \mathbf{T}^{mn}, \mathbf{K}^{mn}, ...)$, we will in most cases omit the superscript. It is

$$\begin{aligned}
\mathbf{T}_{\mathrm{MO}}^{mn} &= \mathbf{Q}\mathbf{T}_{\mathrm{PAO}}^{mn}\mathbf{Q}^\dagger \tag{3.25}\\
\mathbf{t}_{\mathrm{MO}}^{m} &= \mathbf{Q}\mathbf{t}_{\mathrm{PAO}}^{m}. \tag{3.26}
\end{aligned}$$

In open-shell systems, $\mathbf{Q}$ is a mixed quantity, acting as transformation of the virtual subspace only:

$$\mathbf{Q} = \begin{array}{c} \\ act \\ \\ \\ vrt \end{array}\!\!\begin{pmatrix} 1 & 0 & 0 & & 0 \\ 0 & 1 & 0 & & 0 \\ 0 & 0 & 1 & & 0 \\ & & & \ddots & \\ 0 & 0 & 0 & & Q_{as'} \end{pmatrix} \text{ with } s' \notin act \tag{3.27}$$

In the active subspace, $\mathbf{Q}$ is a unit matrix. This arises from the fact that active orbitals are not transformed to PAO space. In all cases, PAOs are by definition orthonormal on the occupied

space but not amongst themselves:

$$\langle r|m \rangle \;\; = \;\; 0 \tag{3.28}$$

$$\langle r|s \rangle \;\; = \;\; \left[\mathbf{S}^{\mathrm{virt}}\right]_{rs} = \left[\mathbf{Q}^{\dagger}\mathbf{Q}\right]_{rs}. \tag{3.29}$$

They are linearly dependent and reside near the atom at which the generating AOs originate. Redundant PAOs can occur and need to be removed later in the individual domains. The primary domain generated in a subsequent step should include all PAOs that arise from basis functions that contribute to the considered LMO significantly [30, 97]. Unless noted otherwise, a significant contribution of basis functions at atom A to an LMO i is defined as an IAO partial charge $q_{ii}^A \geq 0.15$ in this work; if present, active orbitals are included into every domain, with r, s then running over both active orbitals and PAOs. PAOs are the virtual orbitals currently used in our method.

3.4 Local Second-Order Møller-Plesset Perturbation Theory

After discussing the different localization schemes above, this section will introduce local approximations to closed- and open-shell MP2 theory in a general manner [21, 34–36, 46, 98, 99]. The pair approximation limits the sum over the number of orbital pairs i, j in the MP2 energy Hylleraas functional. In practice, the pairs to retain are either selected by the spatial distance between the closest atoms in the primary domains of LMOs i and j, or by their connectivity. The connectivity is defined as the number of bonds between the closest atoms in the domains of both orbitals. Additionally, excitations to the virtual space are restricted to pair domains $[ij]$. The standard pair domains, as defined previously as union of two primary orbital domains, can be extended to systematically improve the resulting correlation energy [86, 97]. This is also done using a distance or connectivity criterion, thereby including all PAOs at neighbouring atoms to the domain with those neighbouring atoms either bound to an atom inside the domain or within a certain distance to it. For closed-shell MP2, eq. 2.75 can thus be altered to read

$$E_2 = \sum_{i \geq j}^{pairs} (2 - \delta_{ij}) \sum_{rs \in [ij]} \tilde{T}_{rs}^{ij} \left(K_{rs}^{ij} + R_{rs}^{ij} \right) \tag{3.30}$$

with $K_{rs}^{ij} = Q_{ar} K_{ab}^{ij} Q_{bs}$ and the PAO space transformation Q_{ar} implicitly defined in eq. 3.24. As the PAOs r, s are not necessarily orthogonal amongst themselves, overlap matrices $(\mathbf{S}^{\mathrm{virt}})_{rs}$, *cf.* eq. 3.29, need to be introduced to the residual equations 2.72:

$$R_{rs}^{ij} = [\mathbf{K}^{ij} + \mathbf{S}^{\mathrm{virt}} \mathbf{T}^{ij} \mathbf{F} + \mathbf{F} \mathbf{T}^{ij} \mathbf{S}^{\mathrm{virt}} - f_{ik} \mathbf{S}^{\mathrm{virt}} \mathbf{T}^{kj} \mathbf{S}^{\mathrm{virt}} - \mathbf{S}^{\mathrm{virt}} \mathbf{T}^{ik} \mathbf{S}^{\mathrm{virt}} f_{kj}]_{rs}, \; r, s \in [ij] \quad (3.31)$$

Similar to the integrals K_{rs}^{ij}, the virtual subspace of the Fock matrix, F_{ab}, has been transformed to the PAO basis to simplify above expression, with $F_{rs} = Q_{ar}F_{ab}Q_{bs}$. One should note that all matrix multiplications in above residual equations implicitly involve domains, for instance

$$[\mathbf{S}^{\text{virt}}\mathbf{T}^{kj}\mathbf{S}^{\text{virt}}]_{rs} = \sum_{r's'\in[kj]} S_{rr'}^{\text{virt}} T_{r's'}^{kj} S_{s's}^{\text{virt}}, \ r,s \in [ij]. \tag{3.32}$$

This is also true for all following matrix multiplications involving local quantities. For RMP2 the Hylleraas functional eq. 2.81 can be modified equivalently as

$$
\begin{aligned}
E_2 &= \sum_m \sum_{r\in[m]} \tilde{t}_r^m(\tilde{f}_r^m + \tilde{r}_r^m) + \bar{t}_r^m(\bar{f}_r^m + \bar{r}_r^m) \\
&+ \sum_{mn}^{pairs} \sum_{rs\in[mn]} \check{T}_{rs}^{mn}(K_{rs}^{mn} + \check{R}_{rs}^{mn}) \\
&+ \sum_{m>n}^{pairs} \sum_{rs\in[mn]} \frac{1}{2}\left[\tilde{T}_{rs}^{mn}(K_{rs}^{mn} - K_{rs}^{mn} + \tilde{R}_{rs}^{mn}) + \bar{T}_{rs}^{mn}(K_{rs}^{mn} - K_{rs}^{mn} + \bar{R}_{rs}^{mn})\right]
\end{aligned} \tag{3.33}
$$

with $f_r^m = Q_{xr}f_x^m$. Even though the summation over pairs m,n includes both occupied subspaces in order to simplify notation, the closed (i,j) and active (t,u) orbitals are to be localized separately as only then the RHF energy is invariant. PAO indices r,s are spanning both the virtual and if needed active space, and thus Pauli violating terms are assumed to be zero [21]. The residual eqs. 2.82 are now defined as

$$
\begin{aligned}
\tilde{R}_{rs}^{mn} &= [\mathbf{K}^{mn} - \mathbf{K}^{nm} + \mathbf{S}^{\text{virt}}\tilde{\mathbf{T}}^{mn}\mathbf{F}^\alpha + \mathbf{F}^\alpha\tilde{\mathbf{T}}^{mn}\mathbf{S}^{\text{virt}} \\
&\quad - f_{mm'}^\alpha \mathbf{S}^{\text{virt}}\tilde{\mathbf{T}}^{m'n}\mathbf{S}^{\text{virt}} - \mathbf{S}^{\text{virt}}\tilde{\mathbf{T}}^{mm'}\mathbf{S}^{\text{virt}} f_{m'n}^\alpha]_{rs} \\
\bar{R}_{rs}^{mn} &= [\mathbf{K}^{mn} - \mathbf{K}^{nm} + \mathbf{S}^{\text{virt}}\bar{\mathbf{T}}^{mn}\mathbf{F}^\beta + \mathbf{F}^\beta\bar{\mathbf{T}}^{mn}\mathbf{S}^{\text{virt}} \\
&\quad - f_{mi}^\beta \mathbf{S}^{\text{virt}}\bar{\mathbf{T}}^{in}\mathbf{S}^{\text{virt}} - \mathbf{S}^{\text{virt}}\bar{\mathbf{T}}^{mi}\mathbf{S}^{\text{virt}} f_{in}^\beta]_{rs} \\
\check{R}_{rs}^{mn} &= [\mathbf{K}^{mn} + \mathbf{S}^{\text{virt}}\check{\mathbf{T}}^{mn}\mathbf{F}^\beta + \mathbf{F}^\alpha\check{\mathbf{T}}^{mn}\mathbf{S}^{\text{virt}} \\
&\quad - f_{mm'}^\alpha \mathbf{S}^{\text{virt}}\check{\mathbf{T}}^{m'n}\mathbf{S}^{\text{virt}} - \mathbf{S}^{\text{virt}}\check{\mathbf{T}}^{mi}\mathbf{S}^{\text{virt}} f_{in}^\beta]_{rs} \\
\tilde{r}_r^m &= \left[(\mathbf{f}^\alpha)^m + \mathbf{F}^\alpha\tilde{\mathbf{t}}^m - f_{mn}^\alpha\mathbf{S}^{\text{virt}}\tilde{\mathbf{t}}^n\right]_r \\
\bar{r}_r^m &= \left[(\mathbf{f}^\beta)^m + \mathbf{F}^\beta\bar{\mathbf{t}}^m - f_{mi}^\beta\mathbf{S}^{\text{virt}}\bar{\mathbf{t}}^i\right]_r.
\end{aligned} \tag{3.34}
$$

Again, $\mathbf{K}^{mn}, \mathbf{F}^\alpha, \mathbf{F}^\beta$ are now PAO space quantities. Although the local approach does require more matrix operations in both the closed- and open-shell spaces than the comparable canonical methods, it requires eventually less computational effort if pair and domain approximations are introduced; one can even achieve linear scaling [35, 37].

4 Canonical Gradients

In the previous two chapters it was described how to calculate a molecular wave function and energy by approximately solving the electronic Schrödinger equation. According to the Hellman-Feynman theorem, this knowledge of the exact wave function can be used to calculate any derivative property as a simple expectation value [74, pp. 191]:

$$\frac{dE}{dq} = \langle \Psi | \frac{\partial \hat{H}}{\partial q} | \Psi \rangle \tag{4.1}$$

Depending on the type of perturbation q, different properties are available. Dipole moments μ^f are for instance the first derivative with respect to an external electrostatic field $q = \{\epsilon_f\}$ in direction $f = \{x, y, z\}$. As this work is concerned with nuclear gradients to predict equilibrium geometries, a special focus will be put on the perturbation being a deformation of the nuclear geometry $q = \{\Delta R_A\}$. Within the Born-Oppenheimer approximation, the molecule's equilibrium geometry corresponds to a minimum on the PES. It can be distinguished from other critical points such as saddle points (transition states) by calculation of the second derivative [1, 4].

One assumption made during the derivation of eq. 4.1 is that the system's exact wave function is known and used. For most approximate wave functions,

$$\Psi^q = \left. \frac{\partial \Psi}{\partial q} \right|_{q=0} \neq 0, \tag{4.2}$$

and the Hellman-Feynman theorem is incomplete [1, 6]. To simplify the upcoming expressions, a shorthand notation Ψ^q will from now on be used for all quantities differentiated with respect to q. A complete derivative of the energy with respect to an arbitrary perturbation q using an approximate wave function thus requires an extension of eq. 4.1:

$$E(q) = \frac{\langle \Psi(q) | \hat{H}(q) | \Psi(q) \rangle}{\langle \Psi(q) | \Psi(q) \rangle} \tag{4.3}$$

In (R)HF, the wave function $\Psi(q) \approx \Phi(q)$ is spanned by a linear combination of atom-centred basis functions, and both the expansion coefficients $C_{\mu p}(q)$ as well as the position of the basis functions are a function of the perturbation. Similarly, the amplitudes of the MP2 first-order

wave function, $t_\lambda(q)$ are perturbation-dependent. In general, the full analytic first derivative can be written as

$$\left.\frac{dE}{dq}\right|_{q=0} = \left(\frac{\partial E}{\partial h_{\mu\nu}}\right) h_{\mu\nu}^q + \left(\frac{\partial E}{\partial(\mu\nu|\tau\upsilon)}\right)(\mu\nu|\tau\upsilon)^q$$
$$+ \left(\frac{\partial E}{\partial S_{\mu\nu}}\right) S_{\mu\nu}^q + \left(\frac{\partial E}{\partial C_{\mu p}}\right) C_{\mu p}^q + \left(\frac{\partial E}{\partial t_\lambda}\right) t_\lambda^q + \dots \tag{4.4}$$

The atom-centred basis functions generating the one- and two-electron integrals $h_{\mu\nu}$ and $(\mu\nu|\tau\upsilon)$ change only if the nuclear positions are altered, thus rendering the derivatives of the two-electron integrals zero for many perturbations (for instance dipole moments). Similarly, the basis set's metric is uninfluenced with $S_{\mu\nu}^q = 0$. This is obviously not true for geometry optimizations: during geometry optimizations the integral and overlap matrix derivatives are usually computed on-the-fly and directly contracted with the precomputed prefactors. This way one general routine can be used for all gradient computations and no derivative integrals have to be stored on disk [1], [2, pp. 32].

The last contributions remaining are the coefficients determining the wave function. Their derivatives $C_{\mu p}^q, t_\lambda^q, \dots$ are called the system's linear response vector; this vector determines how the electronic structure changes when the system is perturbed [4]. Generally, the linear response's dependency on the perturbation is not known, making it complicated to calculate if needed. Thus at this point it makes sense to distinguish between two types of coefficients, the variational and non-variational ones, as variational coefficients fulfil the stationary conditions

$$g_\lambda(\mathbf{t}) = \frac{dE}{dt_\lambda} = 0 \tag{4.5}$$

and henceforth one does not need to calculate a linear response [1]. Examples for variational coefficients are the (R)MP2 amplitudes t_λ found by minimizing the Hylleraas functional or the MO coefficients $C_{\mu p}$ during a (R)HF calculation. The very same MO coefficients $C_{\mu p}$ are however non-variational in the context of an (R)MP2 calculation and thus require the calculation of a linear response at (R)MP2 level gradients. The derivatives of any non-variational wave function parameters, collected in a vector $\mathbf{c}^q$, are obtained by differentiation of the stationary conditions $\mathbf{g}(q, \mathbf{c}) = 0$ used to generate the parameters in the first place. There are as many equations as parameters and the stationary conditions $\mathbf{g}(q, \mathbf{c})$ need to be fulfilled independently of the perturbation q, so

$$g_p^q = g_p^{(q)} + \left(\frac{\partial g_p}{\partial c_{q'}}\right) c_{q'}^q = 0 \tag{4.6}$$

where $g_p^{(q)}$ are all terms computed with derivative integrals $h_{\mu\nu}^q$, $(\mu\nu|\tau\upsilon)^q$. This set of linear response equations is to be solved to calculate all derivatives $\mathbf{c}^q$. It should be noted that the stationary conditions are themselves the first derivatives of the energy with respect to a set of

parameters, so

$$G_{pq} = \frac{\partial g_p}{\partial c_q} = \frac{\partial^2 E}{\partial c_p \partial c_q} \tag{4.7}$$

is actually the energies Hessian matrix. As $\mathbf{G}$ tends to be a rather large matrix, the set of equations 4.6 is commonly solved iteratively instead of explicitly constructing and inverting the Hessian [1, 4].

For the set of Hartree-Fock MO coefficients, eqs. 4.6 are referred to as coupled perturbed HF equations (CPHF) and for the localization conditions in local methods they are known as coupled perturbed localization equations (CPL) [2, pp. 128]. Solving those equations for every perturbation and inserting the solutions into eq. 4.4 will then give the desired gradient. For nuclear gradients, the number of sets of response equations to solve is $3N_{at}$ for N_{at} atoms. This is computationally not satisfying, as the problem size still depends on the number of perturbations and is thus not much cheaper than brute-force numerical derivation at the cost of $2 \cdot 3N_{at}$ [1]. For the first derivatives of the energy this unfavourable scaling can be avoided by using a Lagrangian formalism, which results in just one set of equations, no matter how many atoms a system contains. This formalism is introduced in the following section. Unfortunately, it is not applicable to any higher order derivatives [9, 28, 29].

4.1 The Lagrangian Ansatz

The computational bottleneck during gradient calculations is solving a set of response equations for all non-variational parameters $\mathbf{c}$ in order to find their derivatives $\mathbf{c}^q$. To avoid this effort, the derivatives $\mathbf{c}^q$ can be removed from the gradient expression, as first demonstrated by Handy and Schaefer [1, 4, 28, 29]. This is done by constructing a Lagrangian functional $\mathcal{L}$ yielding the same energy as the original energy expression as long as the stationary conditions $\mathbf{g}(q, \mathbf{c}) = 0$ are fulfilled:

$$\mathcal{L}(q, \mathbf{c}, \mathbf{z}) = E(q, \mathbf{c}) - z_p g(q, \mathbf{c})_p \tag{4.8}$$

There is one Lagrangian multiplier z_p for every equation $g(q, \mathbf{c})_p = 0$ with $z_p \neq 0$. If the Lagrangian functional at $q = 0$ is stationary with respect to both, $\mathbf{z}$ and $\mathbf{c}$, and the energy is linear in the integral expressions and overlap matrices, $\mathcal{L}$ evaluated with derivative integrals and overlaps also represents the desired gradient expression E^q:

$$\frac{dE}{dq} = \mathcal{L}^{(q)} = E^{(q)} + z_p g_p^{(q)} \tag{4.9}$$

The functional's derivative with respect to **c** allows for the determination of the Lagrangian multipliers

$$\frac{d\mathcal{L}}{dc} = 0. \tag{4.10}$$

This additional set of equations is called z-vector equations and can be solved instead of eq. 4.6. There is now one equation for each non-variational parameter **c** instead of each perturbation. The z-vector equations determining the Hartree-Fock MO coefficients perturbed response are called zCPHF equations, the localization condition's response is collected in the zCPL equations. So in order to calculate the energy derivative using a Lagrangian ansatz, we need to insert the one- and two-electron integral derivatives as well as the derivatives of all overlap matrices into our otherwise known and stationary Lagrangian functional. Therefore, we first need to find the Lagrangian multipliers **z**.

4.2 Closed-Shell Hartree-Fock Gradients

The closed-shell HF gradient can be readily constructed from the HF energy expression eq. 2.12 as the energy is stationary with respect to small variations of the MO coefficients $\mathbf{C}(q)$ [5–7, 100]. As a second condition besides minimizing the energy, HF requires the occupied MOs to form an orthonormal set. Using the Lagrangian formalism, the HF energy thus is

$$\mathcal{L}_{HF} = E_{HF} - 2z_{ij}(C_{\mu i}S_{\mu\nu}C_{\nu j} - \delta_{ij}) \tag{4.11}$$

with the factor -2 introduced for convenience. Prior to constructing the gradient, the Lagrangian multipliers need to be determined by making the unperturbed functional $\mathcal{L}$ stationary in **U**; the change of the optimized orbitals will again be expressed as an orbital rotation, but not necessarily a unitary one [2, pp. 30]. In the basis of unperturbed MO coefficients $\mathbf{C}(0)$ and inserting eqs. 2.12 and 2.24 at $\mathbf{U} = \mathbf{1}$ yields in first-order

$$
\begin{aligned}
\mathcal{L}_{HF}(\mathbf{U}) &= 4h_{pi}U_{pi} + 2\sum_j U_{pi}\left(2(pi|jj) - (pj|ij)\right) \\
&\quad + 2\sum_i U_{pj}\left(2(ii|pj) - (ip|ij)\right) - 4z_{pi}U_{pi} + E_{nuc} \\
&= 4f_{pi}U_{pi} - 4z_{pi}U_{pi} + E_{nuc}.
\end{aligned} \tag{4.12}
$$

The multipliers are thus

$$\frac{d\mathcal{L}_{HF}}{dU_{pi}} = 4f_{pi} - 4z_{pi} = 0. \tag{4.13}$$

With $\mathbf{C}^\dagger\mathbf{S}\mathbf{C}$ being a symmetric matrix and $f_{ai} = 0$, $\mathbf{z}$ has to be symmetric as well and $z_{ia} = z_{ai} = 0$. As integral and overlap matrix derivatives are evaluated in the AO basis, transformation of eq. 2.12 into the same basis simplifies the upcoming derivative; it is

$$
\begin{aligned}
E_{HF} &= D^{(0)}_{\mu\nu} h_{\mu\nu} + \frac{1}{2} D^{(0)}_{\mu\nu} D^{(0)}_{\tau\upsilon} \left((\mu\nu|\tau\upsilon) - \frac{1}{2}(\mu\tau|\nu\upsilon) \right) + E_{nuc} \\
&= D^{(0)}_{\mu\nu} h_{\mu\nu} + \frac{1}{2} \left(D^{(0)}_{\mu\nu} D^{(0)}_{\tau\upsilon} - \frac{1}{2} D_{\mu\tau} D_{\nu\upsilon} \right) (\mu\nu|\tau\upsilon) + E_{nuc}
\end{aligned}
\tag{4.14}
$$

with $D^{(0)}_{\mu\nu} = 2C_{\mu i}C_{\nu i}$ the zeroth-order density matrix. The closed-shell HF nuclear gradient thus reads [2, pp. 55]

$$
E^q = \mathcal{L}^{(q)}_{HF} = D^{(0)}_{\mu\nu} h^q_{\mu\nu} + \frac{1}{4} \left(2D^{(0)}_{\mu\nu} D^{(0)}_{\tau\upsilon} - D^{(0)}_{\mu\tau} D^{(0)}_{\nu\upsilon} \right) (\mu\nu|\tau\upsilon)^q - 2C_{\mu i} f_{ij} C_{\nu j} S^q_{\mu\nu} + E^q_{nuc}.
\tag{4.15}
$$

Before proceeding further, the general gradient expression eq. 4.15 can be simplified in order to calculate a molecule's dipole moment. If the perturbation due to a uniform external electric field $q = \{\epsilon_f\}$ is small, we can use perturbation theory to extend the systems electronic Hamilton operator as

$$
\hat{H}_{el} = \hat{H}^{(0)}_{el} + \Lambda\hat{H}^{(1)}_{el} = \hat{H}^{(0)}_{el} - [\mu^f_{el} + \mu^f_{nuc}]\epsilon_f
\tag{4.16}
$$

with μ^f_{el} denoting the electronic dipole moment in direction f and μ^f_{nuc} its nuclear complement. As the zeroth-order Hamiltonian is independent of the electric field, the derivative reads as

$$
\frac{d\hat{H}_{el}}{d\epsilon_f} = -[\mu^f_{el} + \mu^f_{nuc}].
\tag{4.17}
$$

Using the general definition of the dipole moment of a set of particles $\{A\}$ in direction f as

$$
\mu^f = \sum_A Q_A \mathbf{r}_{A,f},
\tag{4.18}
$$

with $\mathbf{r}_{A,f}$ the position vector projected on the f-axis and Q_A the particle charge, the electronic dipole moment matrix in atomic units and AO basis is

$$
(\mu_{el})^f_{\mu\nu} = -\langle\mu|\mathbf{r}_f|\nu\rangle.
\tag{4.19}
$$

As can be seen, $\mathbf{r}_f$ is a one-particle operator. The AO basis set (or in general the nuclear positions) are assumed to be independent of ϵ_f, and thus the total molecular dipole moment is

$$
\mu^f_{HF} = \mu^f_{el} + \mu^f_{nuc} = D^{(0)}_{\mu\nu}(\mu_{el})^f_{\mu\nu} + \mu^f_{nuc},
\tag{4.20}
$$

where we have inserted ansatz 4.16 into eq. 4.15 and set $h^q_{\mu\nu} = (\mu\nu|\tau\upsilon)^q = S^q_{\mu\nu} = 0$. The nuclear dipole moment $\mu^f_{nuc} = dE_{nuc}/d\epsilon_f$ can be derived in the same manner as the electronic one [74,

pp. 407], [2, pp. 312].

4.3 Open-Shell Hartree-Fock Gradients

Similar to closed-shell HF, the restricted open-shell gradients [24, 26] are conveniently found by constructing a Lagrangian, this time using the RHF energy expression eq. 2.41, and introducing an orthonormality constraint, restraining both the closed and active space at the same time:

$$\mathcal{L}_{RHF} = E_{RHF} - \frac{1}{2}z_{mn}(C_{\mu m}S_{\mu\nu}C_{\nu n} - \delta_{mn}) \tag{4.21}$$

The perturbed MO coefficients will be expanded again in the basis of unperturbed MOs and $\mathcal{L}_{RHF}$ made stationary in $\mathbf{U}$:

$$
\begin{aligned}
\mathcal{L}_{RHF}(\mathbf{U}) &= 2d_{mm}^{(0)+}h_{pm}U_{pm} + \sum_n U_{pm}d_{mm}^{(0)+}d_{nn}^{(0)+}\left((pm|nn) - \frac{1}{2}(pn|mn)\right) \\
&+ \sum_m U_{pn}d_{mm}^{(0)+}d_{nn}^{(0)+}\left((mm|pn) - \frac{1}{2}(mp|mn)\right) - \sum_u U_{pt}\left((pu|tu)\right) \\
&- z_{pm}U_{pm} + E_{nuc} \\
&= 2d_{mm}^{(0)+}f_{pm}^{+}U_{pm} + 2f_{pt}^{-}U_{pt} - z_{pm}U_{pm} + E_{nuc}
\end{aligned}
\tag{4.22}
$$

The RHF charge densitiy in MO basis is $\mathbf{d}^{(0)+} = \mathbf{C}^{\dagger}\mathbf{S}\mathbf{D}^{(0)+}\mathbf{S}\mathbf{C}$. The derivatives are

$$\frac{d\mathcal{L}_{RHF}}{dU_{ij}} = 2d_{jj}^{(0)+}f_{ij}^{+} - z_{ij} = 4f_{ij}^{+} - z_{ij} = 0 \tag{4.23}$$

$$\frac{d\mathcal{L}_{RHF}}{dU_{tu}} = 2d_{uu}^{(0)+}f_{tu}^{+} + 2f_{tu}^{-} - z_{tu} = 2f_{tu}^{+} + 2f_{tu}^{-} - z_{tu} = 0 \tag{4.24}$$

$$\frac{d\mathcal{L}_{RHF}}{dU_{ai}} = 2d_{ii}^{(0)+}f_{ai}^{+} - z_{ai} = 4f_{ai}^{+} - z_{ai} = 0 \tag{4.25}$$

$$\frac{d\mathcal{L}_{RHF}}{dU_{at}} = 2d_{tt}^{(0)+}f_{at}^{+} + 2f_{at}^{-} - z_{at} = 2f_{at}^{+} + 2f_{at}^{-} - z_{at} = 0 \tag{4.26}$$

$$\frac{d\mathcal{L}_{RHF}}{dU_{it}} = 2d_{tt}^{(0)+}f_{it}^{+} + 2f_{it}^{-} - z_{it} = 4f_{it}^{+} - z_{it} = 0 \tag{4.27}$$

$$\frac{d\mathcal{L}_{RHF}}{dU_{ti}} = 2d_{ii}^{(0)+}f_{ti}^{+} - z_{ti} = 4f_{ti}^{+} - z_{ti} = 0. \tag{4.28}$$

Using the RHF Brillouin theorem eq. 2.44, we can immediately see that there is no contribution involving virtual orbitals in eqs. 4.25 and 4.26, as $f_{ai}^{+} = f_{at}^{+} + f_{at}^{-} = 0$. Eq. 4.27 has been simplified by the third RHF Brillouin condition $f_{it}^{+} - f_{it}^{-} = 0$ and it can be concluded that $\mathbf{z}$ is

again symmetric. With the Lagrangian multipliers established, the full RHF gradient is

$$
\begin{aligned}
E^q = \mathcal{L}^{(q)}_{RHF} = {} & D^{(0)+}_{\mu\nu} h^q_{\mu\nu} + \frac{1}{4} \left(2 D^{(0)+}_{\mu\nu} D^{(0)+}_{\tau\upsilon} - D^{(0)+}_{\mu\tau} D^{(0)+}_{\nu\upsilon} - D^{(0)-}_{\mu\tau} D^{(0)-}_{\nu\upsilon} \right) (\mu\nu|\tau\upsilon)^q \\
& - \left[2 C_{\mu i} f^+_{ij} C_{\nu j} + C_{\mu t}(f^+_{tu} + f^-_{tu}) C_{\nu t} + 4 C_{\mu i} f^+_{it} C_{\nu t} \right] S^q_{\mu\nu} + E^q_{nuc}.
\end{aligned}
\tag{4.29}
$$

Compared to the evaluation of closed-shell HF gradients, it can be seen that the increase in effort for an extension to open-shell HF gradients is very moderate. For problems without unpaired electrons, above gradient simplifies to eq. 4.15 [24], [2, pp. 71]. The molecular dipole moment can be derived analogously to the previous section to be (*cf.* [2, p. 313]):

$$
\mu^f_{RHF} = D^{(0)+}_{\mu\nu} (\mu_{el})^f_{\mu\nu} + \mu^f_{nuc}.
\tag{4.30}
$$

4.4 Closed-Shell Second-Order Møller-Plesset Perturbation Theory Gradients

As the total energy in perturbation theory is a sum, the second-order correction to the gradient, E^q_{MP2}, can simply be added to the HF gradient expression:

$$
E^q_{tot} = E^q_{HF} + E^q_{MP2} = \mathcal{L}^{(q)}_{HF} + \mathcal{L}^{(q)}_{MP2}
\tag{4.31}
$$

Hence we are left with the task of constructing a gradient expression from either the MP2 energy, eq. 2.69, or the corresponding Hylleraas functional, eq. 2.75, and then adding it to the HF gradient. As the Hylleraas functional is stationary with respect to small variations of the MP2 amplitudes $\tilde{T}^{ij}_{ab}$, it is the preferred choice with the Lagrangian ansatz as

$$
\mathcal{L}_{MP2} = E_2 - \frac{1}{2} x_{pq} (\mathbf{C}^\dagger \mathbf{S} \mathbf{C} - \mathbf{1})_{pq} + z_{ai} f_{ai}.
\tag{4.32}
$$

We have again introduced the orthonormality condition as a constraint for the MOs, but this time extended the Lagrangian multipliers $\mathbf{x} = \mathbf{x}^\dagger$ to the full space, as the first order wave function is spanned by all available orbitals, not just the occupied space as in HF. A second stationary condition is introduced, as the MP2 energy or Hylleraas functional contain the HF MO coefficients as non-variational parameters only. From previous reasoning one would expect to use the Hartree-Fock-Roothaan equations 2.27 as the governing stationary condition. A simpler but equivalent ansatz, however, is to require the HF MOs to always fulfil the Brillouin condition $f_{ai} = 0$ [1, 100].

As always, in the next step a set of Lagrangian multipliers making $\mathcal{L}_{MP2}$ stationary in $\mathbf{U}$ needs to be determined. The derivative contribution from the Hylleraas functional can be collected in

a tensor

$$A_{pi} = \frac{\partial E_2}{\partial U_{pi}} = 4K_{ab}^{pj}\tilde{T}_{ab}^{ij} + 2\left[\mathbf{f}\mathbf{d}^{(2)} + 2\mathbf{g}(\mathbf{d}^{(2)})\right]_{pi} \tag{4.33}$$

$$A_{pa} = \frac{\partial E_2}{\partial U_{pa}} = 4K_{pb}^{ij}\tilde{T}_{ab}^{ij} + 2\left[\mathbf{f}\mathbf{d}^{(2)}\right]_{pa}. \tag{4.34}$$

To simplify notation, we introduced a second-order density matrix $\mathbf{d}^{(2)}$ as

$$
\begin{aligned}
d_{ij}^{(2)} &= -2T_{ab}^{ik}\tilde{T}_{ba}^{kj} \\
d_{ab}^{(2)} &= 2T_{ac}^{ij}\tilde{T}_{cb}^{ji} \\
d_{ai}^{(2)} &= d_{ia}^{(2)} = 0
\end{aligned} \tag{4.35}
$$

and a general two-electron integral contraction $\mathbf{g}(\mathbf{M})$ as

$$
\begin{aligned}
g(\mathbf{M})_{pq} &= M_{\mu\nu}\left((pq|\mu\nu) - \frac{1}{2}(p\mu|\nu q)\right) \\
&= M_{p'q'}\left((pq|p'q') - \frac{1}{2}(pp'|q'q)\right).
\end{aligned} \tag{4.36}
$$

Similarly, the Brillouin condition's derivative is

$$\bar{A}(\bar{\mathbf{z}})_{pi} = z_{bj}\frac{\partial f_{bj}}{\partial U_{pi}} = [\mathbf{f}\bar{\mathbf{z}} + 2\mathbf{g}(\bar{\mathbf{z}})]_{pi} \tag{4.37}$$

$$\bar{A}(\bar{\mathbf{z}})_{pa} = z_{bj}\frac{\partial f_{bj}}{\partial U_{pa}} = [\mathbf{f}\bar{\mathbf{z}}]_{pa} \tag{4.38}$$

with $\bar{\mathbf{z}}$ being a symmetric tensor with $\bar{z}_{ij} = \bar{z}_{ab} = 0$ and $\bar{z}_{ai} = \bar{z}_{ia} = z_{ai}$. This leads to a set of perturbed equations called the zCPHF equations [28]:

$$\left[\mathbf{A} + \bar{\mathbf{A}}(\bar{\mathbf{z}}) + \mathbf{x}\right]_{pq} = 0 \tag{4.39}$$

Knowing that the orthonormality condition multipliers $\mathbf{x}$ form a symmetric matrix, the above set of equations can be rewritten in order to decouple the determination of $\mathbf{x}$ and $\mathbf{z}$ as

$$x_{pq} = \frac{1}{2}(1 + \tau_{pq})\left[\mathbf{A} + \bar{\mathbf{A}}(\bar{\mathbf{z}})\right]_{pq} \tag{4.40}$$

$$0 = (1 - \tau_{ai})\left[\mathbf{A} + \bar{\mathbf{A}}(\bar{\mathbf{z}})\right]_{ai}. \tag{4.41}$$

The operator τ_{pq} permutes the indices p and q. Insertion of eq. 4.37 into eq. 4.41 leaves us with a set of linear equations

$$(1 - \tau_{ai})\left[\mathbf{A} + \mathbf{f}\bar{\mathbf{z}} + \mathbf{g}(\bar{\mathbf{z}})\mathbf{d}^{(0)}\right]_{ai} = 0. \tag{4.42}$$

Assuming canonical orbitals with $f_{pq} = \delta_{pq}\epsilon_p$, the above equations can be solved iteratively:

$$z_{ai}^{(x+1)} = -\frac{A_{ai} - A_{ia} + 2g(\bar{\mathbf{z}}^{(x)})_{ai}}{\epsilon_a - \epsilon_i} \tag{4.43}$$

The contraction of $\bar{\mathbf{z}}$ with the Coulomb and exchange integrals to form $\mathbf{g}(\bar{\mathbf{z}})$ is computationally equivalent to the contraction $\mathbf{g}(\mathbf{d})$ used to solve the Hartree-Fock-Rothaan equations and can thus be done using the same infrastructure [1]. Iterative convergence can be improved by including DIIS [101–104] and by introduction of an additional level-shift s to the denominator as $\epsilon_a - \epsilon_i + s$, but as the orbital energies for closed-shell molecules are usually well separated the latter is hardly necessary. Knowing $\mathbf{z}$, the calculation of $\mathbf{x}$ via eq. 4.40 is straight forward and we can continue to build the gradient:

$$E_{tot}^q = D_{\mu\nu}h_{\mu\nu}^q + \frac{1}{2}D_{\mu\nu,\tau\upsilon}(\mu\nu|\tau\upsilon)^q + X_{\mu\nu}S_{\mu\nu}^q + E_{nuc}^q. \tag{4.44}$$

with

$$X_{\mu\nu} = -2C_{\mu i}f_{ij}C_{\nu j} - \frac{1}{2}C_{\mu p}x_{pq}C_{\nu q} \tag{4.45}$$

and the effective one- and two-particle densities

$$D_{\mu\nu} = \left[\mathbf{C}(\mathbf{d}^{(0)} + \mathbf{d}^{(2)} + \bar{\mathbf{z}})\mathbf{C}^\dagger\right]_{\mu\nu} \tag{4.46}$$

$$D_{\mu\nu,\tau\upsilon} = 4C_{\mu i}C_{\nu a}C_{\tau j}C_{\upsilon b}\tilde{T}_{ab}^{ij} + 2(D_{\mu\nu} - \frac{1}{2}D_{\mu\nu}^{(0)})D_{\tau\upsilon}^{(0)} - (D_{\mu\tau} - \frac{1}{2}D_{\mu\tau}^{(0)})D_{\nu\upsilon}^{(0)}. \tag{4.47}$$

It is worth noting that the most expensive part during a MP2 gradient evaluation is not the iterative determination of z_{ai}, but the transformation of the so-called three-external integrals form AO to MO basis. These occur in eq. 4.33 as $T_{ab}^{ij}K_{ab}^{pj} = T_{ab}^{ij}(pa|jb)$. In order to reduce the computational cost for this transformation step, the amount of contractions and their dimension can be reduced by the introduction of the pair and domain approximation as common in local methods, and furthermore by approximating the integrals K_{ab}^{pj} as described in sec. 5.6 using density fitting [9, 29, 100]. Dipole moments are available as

$$\mu_{MP2}^f = D_{\mu\nu}(\mu_{el})_{\mu\nu}^f + \mu_{nuc}^f \tag{4.48}$$

for the full MP2 dipole moment and

$$\mu_{un}^f = (\mathbf{D}^{(0)} + \mathbf{D}^{(2)})_{\mu\nu}(\mu_{el})_{\mu\nu}^f + \mu_{nuc}^f \tag{4.49}$$

for the MP2 unrelaxed dipoles.

4.5 Open-Shell Second-Order Møller-Plesset Perturbation Theory Gradients

The second-order correction to the RHF gradient is again constructed in a similar manner as the closed-shell correction, but extended by additional terms accounting for the active orbitals [25, 26]. It is based on the open-shell Hylleraas functional, eq. 2.81, which can be simplified by introducing unrelaxed second-order densities conveniently including the now-occurring single-excitations as

$$
\begin{aligned}
\tilde{d}_{mn}^{(2)} &= -\frac{1}{2}\,\mathrm{tr}\left\{ \tilde{\mathbf{T}}^{mm'}\tilde{\mathbf{T}}^{nm'\dagger} + 2\check{\mathbf{T}}^{mi}\check{\mathbf{T}}^{ni\dagger} + 2\tilde{\mathbf{t}}^{m\dagger}\tilde{\mathbf{t}}^{n} \right\} \\
\tilde{d}_{ab}^{(2)} &= \frac{1}{2}\left[\tilde{\mathbf{T}}^{mn}\tilde{\mathbf{T}}^{mn\dagger} + 2\check{\mathbf{T}}^{mi}\check{\mathbf{T}}^{mi\dagger} + 2\tilde{\mathbf{t}}^{m}\tilde{\mathbf{t}}^{m\dagger} \right]_{ab} \\
\tilde{d}_{am}^{(2)} &= \tilde{d}_{ma}^{(2)} = \tilde{t}_a^m \\
\bar{d}_{ij}^{(2)} &= -\frac{1}{2}\,\mathrm{tr}\left\{ \bar{\mathbf{T}}^{ki\dagger}\bar{\mathbf{T}}^{kj} + 2\check{\mathbf{T}}^{mi\dagger}\check{\mathbf{T}}^{mj} + 2\bar{\mathbf{t}}^{i\dagger}\bar{\mathbf{t}}^{j} \right\} \\
\bar{d}_{xy}^{(2)} &= \frac{1}{2}\left[\bar{\mathbf{T}}^{ij\dagger}\bar{\mathbf{T}}^{ij} + 2\check{\mathbf{T}}^{mi\dagger}\check{\mathbf{T}}^{mi} + 2\bar{\mathbf{t}}^{i}\bar{\mathbf{t}}^{i\dagger} \right]_{xy} \\
\bar{d}_{xi}^{(2)} &= \bar{d}_{ix}^{(2)} = \bar{t}_x^i
\end{aligned}
$$

(4.50)

(4.51)

and with their total and spin-density equivalents defined as $\mathbf{d}^{(2)+} = \tilde{\mathbf{d}}^{(2)} + \bar{\mathbf{d}}^{(2)}$ and $\mathbf{d}^{(2)-} = \tilde{\mathbf{d}}^{(2)} - \bar{\mathbf{d}}^{(2)}$. In order to avoid contracting three sets of amplitudes with the three-external integrals, unified amplitudes are generated, thereby reducing the computational effort for the generation of $K_{xy}^{pm}T_{xy}^{mn}$ to one contraction:

$$
T_{xy}^{mn} = \frac{1}{2}\left[\tilde{T}_{xy}^{mn} + \bar{T}_{xy}^{mn} + \check{T}_{xy}^{mn} + \check{T}_{xy}^{mn\dagger} \right]
$$

(4.52)

All quantities with non-matching spins of upper and lower label are zero by definition. If the integral's symmetry of $K_{xy}^{mn} = K_{yx}^{nm}$ is taken into consideration, the occurring contractions require similar effort as for a comparable closed-shell system. As a reminder: all amplitudes, Fock matrices and unrelaxed second-order densities denoted with a tilde are α-spin quantities, all denoted with a bar β-spin quantities.

With above considerations in mind, eq. 2.81 now reads

$$
E_2 = 2\,\mathrm{tr}\left\{ \mathbf{T}^{mn}\mathbf{K}^{nm} \right\} + \mathrm{tr}\left\{ \tilde{\mathbf{f}}\tilde{\mathbf{d}}^{(2)} \right\} + \mathrm{tr}\left\{ \bar{\mathbf{f}}\bar{\mathbf{d}}^{(2)} \right\}
$$

(4.53)

The Lagrangian functional is generated by using the above expression, and augmenting it with

the orthonormality and RHF Brillouin conditions (eq. 2.44) as constraints:

$$
\begin{aligned}
\mathcal{L}_{RMP2} &= E_2 - \frac{1}{2} x_{pq} (\mathbf{C}^\dagger \mathbf{S} \mathbf{C} - \mathbf{1})_{pq} + z_{ai} f^+_{ai} + z_{at}(f^+_{at} + f^-_{at}) + z_{ti}(f^+_{ti} - f^-_{ti}) \\
&= E_2 - \frac{1}{2} x_{pq} (\mathbf{C}^\dagger \mathbf{S} \mathbf{C} - \mathbf{1})_{pq} + z^+_{pq} f^+_{pq} + z^-_{pq} f^-_{pq}
\end{aligned}
\tag{4.54}
$$

The matrices of Lagrangian multipliers $\mathbf{z}^+, \mathbf{z}^-$ are zero in all blocks except

$$
\begin{aligned}
z^+_{ai} &= z^+_{ia} = z_{ai}, \\
z^+_{at} &= z^+_{ta} = z_{at}, & z^-_{at} &= z^-_{ta} = z_{at} \\
z^+_{ti} &= z^+_{it} = z_{ti}, & z^-_{ti} &= z^-_{it} = -z_{ti}.
\end{aligned}
\tag{4.55}
$$

The Hylleraas functional's unperturbed derivative with respect to the orbital rotations U_{pq} is again collected in a derivative matrix $\mathbf{A}$ with

$$
\begin{aligned}
A_{pi} &= 4K^{pm}_{xy} T^{im}_{xy} + 2 \left[\tilde{\mathbf{f}}\tilde{\mathbf{d}}^{(2)} + \bar{\mathbf{f}}\bar{\mathbf{d}}^{(2)} + 2\mathbf{g}(\mathbf{d}^{(2)+}) \right]_{pi} \\
A_{pt} &= 4K^{pm}_{xy} T^{tm}_{xy} + 4K^{mn}_{py} T^{mn}_{xy} + 2 \left[\tilde{\mathbf{f}}\tilde{\mathbf{d}}^{(2)} + \bar{\mathbf{f}}\bar{\mathbf{d}}^{(2)} + \mathbf{g}(\mathbf{d}^{(2)+}) + \mathbf{g}^-(\mathbf{d}^{(2)-}) \right]_{pt} \\
A_{pa} &= 4K^{mn}_{py} T^{mn}_{xy} + 2 \left[\tilde{\mathbf{f}}\tilde{\mathbf{d}}^{(2)} + \bar{\mathbf{f}}\bar{\mathbf{d}}^{(2)} \right]_{pa}
\end{aligned}
\tag{4.56}
$$

and similar to $\mathbf{g}(\mathbf{M})$ defined in eq. 4.36, an additional exchange-integral contribution in the open-shell space occurs as

$$
g^-(\mathbf{M})_{pq} = -\frac{1}{2} M_{\mu\nu}(p\mu|\nu q) = -\frac{1}{2} M_{p'q'}(pp'|q'q).
\tag{4.57}
$$

The now three Brillouin condition derivatives populate

$$
\begin{aligned}
\bar{A}(\mathbf{z})_{pi} &= \left[\mathbf{f}^+\mathbf{z}^+ + \mathbf{f}^-\mathbf{z}^- + 2\mathbf{g}(\mathbf{z}^+) \right]_{pi} \\
\bar{A}(\mathbf{z})_{pt} &= \left[\mathbf{f}^+\mathbf{z}^+ + \mathbf{f}^-\mathbf{z}^- + \mathbf{g}(\mathbf{z}^+) + \mathbf{g}^-(\mathbf{z}^-) \right]_{pt} \\
\bar{A}(\mathbf{z})_{pa} &= \left[\mathbf{f}^+\mathbf{z}^+ + \mathbf{f}^-\mathbf{z}^- \right]_{pa}.
\end{aligned}
\tag{4.58}
$$

The solution of eq. 4.41 is different for each subspace

$$
\begin{aligned}
(1 - \tau_{ai}) \left[\mathbf{A} + \mathbf{f}^+\mathbf{z}^+ + \mathbf{g}(\mathbf{z}^+)\mathbf{d}^{(0)+} \right]_{ai} &= 0 \\
(1 - \tau_{at}) \left[\mathbf{A} + \mathbf{f}^+\mathbf{z}^+ + \mathbf{f}^-\mathbf{z}^- + \mathbf{g}(\mathbf{z}^+)\mathbf{d}^{(0)+} + \mathbf{g}^-(\mathbf{z}^-)\mathbf{d}^{(0)-} \right]_{at} &= 0 \\
(1 - \tau_{it}) \left[\mathbf{A} + \mathbf{f}^+\mathbf{z}^+ + \mathbf{f}^-\mathbf{z}^- + \mathbf{g}(\mathbf{z}^+)\mathbf{d}^{(0)+} + \mathbf{g}^-(\mathbf{z}^-)\mathbf{d}^{(0)-} \right]_{ti} &= 0
\end{aligned}
\tag{4.59}
$$

but based on the same three contractions $(\mathbf{f}^+\mathbf{z}^+ + \mathbf{f}^-\mathbf{z}^-), \mathbf{g}(\mathbf{z}^+)$, and $\mathbf{g}^-(\mathbf{z}^-)$ that need to be computed only once for every iteration. This way, costs are kept at a minimum, roughly doubling

for each single step x:

$$
\begin{aligned}
z_{ai}^{(x+1)} &= -\frac{A_{ai} - A_{ia} + 2g(\mathbf{z}^{+(x)})_{ai}}{\tilde{\epsilon}_a - \frac{1}{2}(\tilde{\epsilon}_i + \bar{\epsilon}_i)} \\
z_{at}^{(x+1)} &= -\frac{A_{at} - A_{ta} + g(\mathbf{z}^{+(x)})_{at} + g^-(\mathbf{z}^{-(x)})_{at}}{\tilde{\epsilon}_a - \tilde{\epsilon}_t} \\
z_{ti}^{(x+1)} &= -\frac{A_{ti} - A_{it} + 2g(\mathbf{z}^{+(x)})_{ti} - g(\mathbf{z}^{+(x)})_{it} - g^-(\mathbf{z}^{-(x)})_{it}}{\tilde{\epsilon}_t - \frac{1}{2}(\tilde{\epsilon}_i + \bar{\epsilon}_i)}
\end{aligned}
\tag{4.60}
$$

Again, the infrastructure for the integral contraction from the RHF code can be reused and DIIS will improve convergence. A difficulty not occurring during the calculation of the closed-shell zCPHF equations but often present in open-shell molecules are the very small differences in orbital energies $\epsilon_t - \epsilon_i$. As the ideal shift s needed for denominator correction can neither be chosen too large nor too small for a fast and robust convergence, and can be very different for different problems, the program tries to guess the right shift for every calculation. This is done via the following algorithm:

$$
s = \sum_{m,x} \max(0;\ 0.3 - \min |\epsilon_x - \epsilon_m|) \ \forall \ x \neq m
\tag{4.61}
$$

Having found the densities relaxation contributions $\mathbf{z}^+$ and $\mathbf{z}^-$, the calculation of $\mathbf{x}$ from eq. 4.40 is straight forward and we can continue to build the gradient which is formally equivalent to the closed-shell regime with

$$
E_{tot}^q = D_{\mu\nu}^+ h_{\mu\nu}^q + \frac{1}{2} D_{\mu\nu,\tau\upsilon}(\mu\nu|\tau\upsilon)^q + X_{\mu\nu} S_{\mu\nu}^q + E_{nuc}^q.
\tag{4.62}
$$

but uses different definitions of the matrices

$$
\begin{aligned}
X_{\mu\nu} &= -\left[2C_{\mu i}f_{ij}^+ C_{\nu j} + C_{\mu t}(f_{tu}^+ + f_{tu}^-)C_{\nu t} + 4C_{\mu i}f_{it}^+ C_{\nu t}\right] - \frac{1}{2}C_{\mu p}x_{pq}C_{\nu q}
\tag{4.63} \\
D_{\mu\nu}^+ &= \left[\mathbf{C}(\mathbf{d}^{(0)+} + \mathbf{d}^{(2)+} + \mathbf{z}^+)\mathbf{C}^\dagger\right]_{\mu\nu}
\tag{4.64} \\
D_{\mu\nu}^- &= \left[\mathbf{C}(\mathbf{d}^{(0)-} + \mathbf{d}^{(2)-} + \mathbf{z}^-)\mathbf{C}^\dagger\right]_{\mu\nu}
\tag{4.65} \\
D_{\mu\nu,\tau\upsilon} &= 4C_{\mu m}C_{\nu x}C_{\tau n}C_{\upsilon y}T_{xy}^{mn} + 2(D_{\mu\nu}^+ - \frac{1}{2}D_{\mu\nu}^{(0)+})D_{\tau\upsilon}^{(0)+} - (D_{\mu\tau}^+ - \frac{1}{2}D_{\mu\tau}^{(0)+})D_{\nu\upsilon}^{(0)+} \\
&\quad -(D_{\mu\tau}^- - \frac{1}{2}D_{\mu\tau}^{(0)-})D_{\nu\upsilon}^{(0)-}.
\tag{4.66}
\end{aligned}
$$

The relaxed and unrelaxed dipole moments are

$$
\mu_{RMP2}^f = D_{\mu\nu}^+(\mu_{el})_{\mu\nu}^f + \mu_{nuc}^f
\tag{4.67}
$$

and

$$\mu_{un}^f = (\mathbf{D}^{(0)+} + \mathbf{D}^{(2)+})_{\mu\nu}(\mu_{el})_{\mu\nu}^f + \mu_{nuc}^f. \tag{4.68}$$

5 Gradients for Local Second-Order Møller-Plesset Perturbation Theory

Local (R)MP2 gradients are similar to their respective canonical counterparts, but with additional contributions due to MO localization and local approximations. For closed-shell LMP2 gradients this results in an additional Lagrangian constraint in the occupied space containing the localization stationary condition [9, 29]. For open-shell systems, two additional localization constraints occur, as doubly and singly occupied orbitals are localized separately. Hence, the local procedure requires one or two additional sets of response equations, called the z-vector coupled perturbed localization (zCPL) equations, to be solved. Also, there are further contributions to the zCPHF equations and gradient due to the projection of the amplitudes to the PAO domain being perturbation-dependent through the dependence of the projector on the LMOs (*c.f.* eq. 3.24). This PAO contribution is formally the same for IBO and PM orbitals and will be discussed together with the general form of the additional response equations in sec. 5.1. Following this general discussion, the explicit form of the zCPL equations for both localization schemes will be given and the respective full gradient expressions derived in sections 5.2 and 5.4. The last two sections of this chapter will discuss the application of density fitting to our gradient methods as well as an electrostatic method for treating solvent effects.

5.1 Coupled Perturbed Localization Equations (zCPL)

For local gradients, we can use the already known Lagrangian ansatz from chapter 4 (eq. 4.32 or 4.54) and simply extend it as

$$\mathcal{L}_{\text{LMP2}} = E_2 \underbrace{- \frac{1}{2} x_{pq} (\mathbf{C}^\dagger \mathbf{SC} - \mathbf{1})_{pq}}_{\text{orthonormality}} + \underbrace{z_{ai} f_{ai}}_{\substack{\text{variation} \\ \text{(Brillouin)}}} + \underbrace{\sum_{i<j} z_{ij}^{\text{loc}} g_{ij}}_{\text{localization}} \tag{5.1}$$

or

$$\mathcal{L}_{\text{LRMP2}} = E_2 - \underbrace{\frac{1}{2}x_{pq}(\mathbf{C}^\dagger\mathbf{S}\mathbf{C} - \mathbf{1})_{pq}}_{\text{orthonormality}} + \underbrace{z_{pq}^+ f_{pq}^+ + z_{pq}^- f_{pq}^-}_{\substack{\text{variation} \\ \text{(Brillouin)}}} + \underbrace{\sum_{m<n} z_{mn}^{\text{loc}} g_{mn}}_{\text{localization}}. \tag{5.2}$$

The additional constraints $\mathbf{g}$ introduced to keep the LMOs local are the PM or IBO stationary condition for the occupied and if applicable active space, eqs. 3.7 or 3.21. Lagrangian multipliers mixing the localization conditions are zero by definition

$$z_{it}^{\text{loc}} := 0. \tag{5.3}$$

All other changes are formally hidden in the Hylleraas functionals E_2 which are now the localized expressions eq. 3.30 or 3.31, respectively.

For the PAO contribution, the derivative matrix of the canonical Hylleraas functional, $\mathbf{A}$, is extended by an amplitude contribution

$$\tilde{A}_{pq} = \frac{\partial E_2}{\partial t_\lambda^{\text{MO}}} \left.\frac{\partial t_\lambda^{\text{MO}}}{\partial U_{pq}}\right|_{\mathbf{U}=\mathbf{0}} = 2R_\lambda^{\text{MO}} \left.\frac{\partial t_\lambda^{\text{MO}}}{\partial U_{pq}}\right|_{\mathbf{U}=\mathbf{0}}, \tag{5.4}$$

where we have used the general definition of the MP2 residuals, eq. 2.73. This way, the fact that the projection to the domain in the virtual space is perturbation dependent can be considered a constant contribution to the zCPHF equations and there is no need for solving an additional set of linear equations. In order to describe the orbital dependence of an amplitude in MO basis, we expand the change of the PAO space projector $\mathbf{Q}$ to first-order in an orbital rotation $\mathbf{U}$ as

$$\mathbf{U}\mathbf{t}_{\text{MO}}^m = \mathbf{U}\mathbf{Q}\mathbf{t}_{\text{PAO}}^m \qquad\qquad\qquad = \mathbf{U}\mathbf{C}^\dagger\mathbf{S}_1\mathbf{t}_{\text{PAO}}^m \tag{5.5}$$

$$\mathbf{U}\mathbf{T}_{\text{MO}}^{mn} + \mathbf{T}_{\text{MO}}^{mn}\mathbf{U}^\dagger = \mathbf{U}\mathbf{Q}\mathbf{T}_{\text{PAO}}^{mn}\mathbf{Q}^\dagger + \mathbf{Q}\mathbf{T}_{\text{PAO}}^{mn}\mathbf{Q}^\dagger\mathbf{U}^\dagger = \mathbf{U}\mathbf{C}^\dagger\mathbf{S}_1\mathbf{T}_{\text{PAO}}^{mn}\mathbf{Q}^\dagger + \mathbf{Q}\mathbf{T}_{\text{PAO}}^{mn}\mathbf{S}_1\mathbf{C}\mathbf{U}^\dagger.$$

As the stationary quantity in local MP2 are the amplitudes in PAO basis, there will be no direct derivative contribution from PAO space amplitudes. In canonical MP2 on the other hand, the MO amplitudes are stationary and $\tilde{\mathbf{A}}$ vanishes entirely [9]. It should be noted that, contrary to the amplitudes (*cf.* eqs. 3.25 and 3.26), the residuals cannot be simply transformed back from the PAO to the MO basis, as $\mathbf{Q}$ is not a unitary rotation operator. Thus, the residuals have to be assembled partly in the MO (right index), partly in the PAO basis (left index), denoted as $\mathbf{R}_{\text{MIX}}^{mn}$. Inserting eq. 5.5 into 5.4, for closed-shell LMP2 gradients $\tilde{\mathbf{A}}$ is

$$\tilde{\mathbf{A}} = 4\mathbf{C}^\dagger\mathbf{S}_1\tilde{\mathbf{T}}_{\text{PAO}}^{ij}\mathbf{R}_{\text{MIX}}^{ij} \tag{5.6}$$

whereas in open-shell systems it reads

$$\tilde{\mathbf{A}} = \mathbf{C}^\dagger \mathbf{S}_1 \left[\tilde{\mathbf{T}}_{\mathrm{PAO}}^{\mathrm{mn}} \tilde{\mathbf{R}}_{\mathrm{MIX}}^{\mathrm{mn}\dagger} + \bar{\mathbf{T}}_{\mathrm{PAO}}^{\mathrm{mn}} \bar{\mathbf{R}}_{\mathrm{MIX}}^{\mathrm{mn}\dagger} + 2\check{\mathbf{T}}_{\mathrm{PAO}}^{\mathrm{mn}} \check{\mathbf{R}}_{\mathrm{MIX}}^{\mathrm{mn}\dagger} + 2\check{\mathbf{T}}_{\mathrm{PAO}}^{\mathrm{mn}\dagger} \check{\mathbf{R}}_{\mathrm{MIX}}^{\mathrm{mn}} \right.$$
$$\left. + 2\tilde{\mathbf{t}}_{\mathrm{PAO}}^{\mathrm{m}} \tilde{\mathbf{r}}_{\mathrm{MO}}^{\mathrm{m}\dagger} + 2\bar{\mathbf{t}}_{\mathrm{PAO}}^{\mathrm{m}} \bar{\mathbf{r}}_{\mathrm{MO}}^{\mathrm{m}\dagger} \right]. \tag{5.7}$$

Fortunately, the quantities needed to generate the contractions of amplitudes and residuals are mostly equivalent to those needed for the generation of integral contractions $K_{py}^{mn} Q_{ys} T_{rs}^{mn}$ and second-order densities in PAO space. In our gradient code, thus, the residuals are never explicitly calculated and the additional work needed to consider the PAO contribution $\tilde{\mathbf{A}}$ is very limited. For closed-shell systems, we follow the approach of Schütz *et al.* as explained in thier 2004 publication [29] where not even $\tilde{\mathbf{A}}$ is constructed. For open-shell systems, this approach is not feasible, as there are nine instead of four different blocks to be considered in the zCPHF equations (blocks $ij, tu, ab, ti, it, ...$); we will thus explicitly calculate $\tilde{\mathbf{A}}$, which induces no significant extra computational costs though.

In general, transforming the second-order unrelaxed densities to PAO space is straight forward with

$$
\begin{aligned}
d_{ij}^{(2)} &= -2\,\mathrm{tr}\left\{ \mathbf{S}^{\mathrm{virt}} \mathbf{T}^{ik} \mathbf{S}^{\mathrm{virt}} \tilde{\mathbf{T}}^{kj} \right\} \\
d_{rs}^{(2)} &= 2[\mathbf{T}^{ij} \mathbf{S}^{\mathrm{virt}} \tilde{\mathbf{T}}^{ji}]_{rs} \\
d_{ri}^{(2)} &= d_{ir}^{(2)} = 0
\end{aligned}
\tag{5.8}
$$

for closed-shell molecules and

$$
\begin{aligned}
\tilde{d}_{mn}^{(2)} &= -\frac{1}{2}\,\mathrm{tr}\left\{ \mathbf{S}^{\mathrm{virt}} \tilde{\mathbf{T}}^{mm'} \mathbf{S}^{\mathrm{virt}} \tilde{\mathbf{T}}^{nm'\dagger} + 2\mathbf{S}^{\mathrm{virt}} \check{\mathbf{T}}^{mi} \mathbf{S}^{\mathrm{virt}} \check{\mathbf{T}}^{ni\dagger} + 2\mathbf{S}^{\mathrm{virt}} \tilde{\mathbf{t}}^{m\dagger} \tilde{\mathbf{t}}^n \right\} \\
\tilde{d}_{rs}^{(2)} &= \frac{1}{2}\left[\tilde{\mathbf{T}}^{mn} \mathbf{S}^{\mathrm{virt}} \tilde{\mathbf{T}}^{mn\dagger} + 2\check{\mathbf{T}}^{mi} \mathbf{S}^{\mathrm{virt}} \check{\mathbf{T}}^{mi\dagger} + 2\tilde{\mathbf{t}}^m \tilde{\mathbf{t}}^{m\dagger} \right]_{rs} \\
\tilde{d}_{rm}^{(2)} &= \tilde{d}_{mr}^{(2)} = \tilde{t}_r^m \\
\bar{d}_{ij}^{(2)} &= -\frac{1}{2}\,\mathrm{tr}\left\{ \mathbf{S}^{\mathrm{virt}} \bar{\mathbf{T}}^{ki\dagger} \mathbf{S}^{\mathrm{virt}} \bar{\mathbf{T}}^{kj} + 2\mathbf{S}^{\mathrm{virt}} \check{\mathbf{T}}^{mi\dagger} \mathbf{S}^{\mathrm{virt}} \check{\mathbf{T}}^{mj} + 2\mathbf{S}^{\mathrm{virt}} \bar{\mathbf{t}}^{i\dagger} \bar{\mathbf{t}}^j \right\} \\
\bar{d}_{rs}^{(2)} &= \frac{1}{2}\left[\bar{\mathbf{T}}^{ij} \mathbf{S}^{\mathrm{virt}} \bar{\mathbf{T}}^{ij\dagger} + 2\check{\mathbf{T}}^{mi\dagger} \mathbf{S}^{\mathrm{virt}} \check{\mathbf{T}}^{mi} + 2\bar{\mathbf{t}}^i \bar{\mathbf{t}}^{i\dagger} \right]_{rs} \\
\bar{d}_{ri}^{(2)} &= \bar{d}_{ir}^{(2)} = \bar{t}_r^i
\end{aligned}
$$

(5.9)

(5.10)

in open-shell systems. For the latter systems, eq. 4.53 can then be reused to calculate the systems energy within the local approximation as well. Following above considerations, the derivative within the local approximation of the first right-hand side term in eq. 4.53 is

$$\tilde{A}'_{ap} = 2[\mathbf{Q}\mathbf{K}^{nm}\mathbf{T}^{mn}\mathbf{S}\mathbf{C}]_{ap} \tag{5.11}$$

$$\tilde{A}'_{tp} = K_{tr}^{ji} \left(\bar{T}_{rs}^{ij} + \check{T}_{rs}^{ij} \right) [\mathbf{S}\mathbf{C}]_{sp}, \; s \notin t \tag{5.12}$$

with all integrals and amplitudes in PAO space. The upper contribution $\tilde{A}'_{ap}$ is a by-product of the contractions in eq. 4.56 and can thus simply be reused. For $\tilde{A}'_{tp}$, this is not true and we have to calculate this active-space contribution explicitly. The second and third terms in eq. 4.53 yield the following derivative contribution:

$$
\begin{aligned}
\tilde{\mathbf{A}}^{\mathrm{PAO}} &= \frac{1}{2}\tilde{\mathbf{T}}^{mn}\mathbf{F}^{\alpha}\tilde{\mathbf{T}}^{mn\dagger} + \frac{1}{2}\bar{\mathbf{T}}^{ij}\mathbf{F}^{\beta}\bar{\mathbf{T}}^{ij\dagger} + \check{\mathbf{T}}^{mi\dagger}\mathbf{F}^{\alpha}\check{\mathbf{T}}^{mi} + \check{\mathbf{T}}^{mi}\mathbf{F}^{\beta}\check{\mathbf{T}}^{mi\dagger} \\
&\quad - f_{mn}^{\alpha}\left[\tilde{\mathbf{t}}^{m}\tilde{\mathbf{t}}^{n\dagger} + \tilde{\mathbf{T}}^{mm'\dagger}\mathbf{S}^{\mathrm{virt}}\tilde{\mathbf{T}}^{nm'} + \check{\mathbf{T}}^{mi}\mathbf{S}^{\mathrm{virt}}\check{\mathbf{T}}^{ni\dagger} + \check{\mathbf{T}}^{mi\dagger}\mathbf{S}^{\mathrm{virt}}\check{\mathbf{T}}^{ni}\right] \\
&\quad - f_{ij}^{\beta}\left[\bar{\mathbf{t}}^{i}\bar{\mathbf{t}}^{j\dagger} + \bar{\mathbf{T}}^{ik\dagger}\mathbf{S}^{\mathrm{virt}}\tilde{\mathbf{T}}^{jk} + \check{\mathbf{T}}^{ik}\mathbf{S}^{\mathrm{virt}}\check{\mathbf{T}}^{jk\dagger} + \check{\mathbf{T}}^{ik\dagger}\mathbf{S}^{\mathrm{virt}}\check{\mathbf{T}}^{jk}\right]
\end{aligned}
\tag{5.13}
$$

In our working code, the sums above are limited to pairs $i > j$ whenever possible for best performance. Most of the contractions needed, especially those over three pair-indices as for instance $-f_{mn}^{\alpha}\tilde{\mathbf{T}}^{mm'\dagger}\mathbf{S}^{\mathrm{virt}}\tilde{\mathbf{T}}^{nm'}$ are almost equivalent to those in eqs. 5.9 and 5.10 and can be reused. Contractions including an external Fock matrix block, *e.g.* $\tilde{\mathbf{T}}^{mn}\mathbf{F}^{\alpha}\tilde{\mathbf{T}}^{mn\dagger}$, are additional work. Eq. 5.7 can thus be reformulated as

$$
\begin{aligned}
\tilde{A}_{ip} &= 0 \\
\tilde{A}_{xp} &= \tilde{A}'_{xp} + Q_{xr}\tilde{A}^{\mathrm{PAO}}_{rs}[\mathbf{SC}]_{sp} \ s \notin t.
\end{aligned}
\tag{5.14}
$$

The additional set of equations to be solved in order to find the multipliers $\mathbf{z}^{\mathrm{loc}}$ can be generated by augmenting the zCPHF equations 4.39 with $\tilde{\mathbf{A}}$ and the derivatives of the LMO stationary conditions, $\mathbf{a}(\mathbf{z}^{\mathrm{loc}})$:

$$
\left[\mathbf{A} + \tilde{\mathbf{A}} + \bar{\mathbf{A}}(\bar{\mathbf{z}}) + \mathbf{a}(\mathbf{z}^{\mathrm{loc}}) + \mathbf{x}\right]_{pq} = 0 \qquad \text{(closed)} \tag{5.15}
$$

$$
\left[\mathbf{A} + \tilde{\mathbf{A}} + \bar{\mathbf{A}}(\mathbf{z}^{\pm}) + \mathbf{a}(\mathbf{z}^{\mathrm{loc}}) + \mathbf{x}\right]_{pq} = 0 \qquad \text{(open)} \tag{5.16}
$$

Taking into account the symmetry of $\mathbf{x}$, the equations can be decoupled. The occupied space contribution in LMO basis for closed- and open-shell systems thus is

$$
0 = (1 - \tau_{ij})\left[\mathbf{A} + \mathbf{a}(\mathbf{z}^{\mathrm{loc}})\right]_{ij} \qquad \text{(closed)} \tag{5.17}
$$

$$
0 = (1 - \tau_{mn})\left[\mathbf{A} + \mathbf{a}(\mathbf{z}^{\mathrm{loc}})\right]_{mn} \qquad \text{(open)}. \tag{5.18}
$$

There is no contribution of $\bar{A}(\bar{z})_{ij}$ and $\tilde{A}_{ij}$, or $\bar{A}(z^{\pm})_{mn}$ and $\tilde{A}_{mn}$, to the zCPL equations, and $a(z^{\mathrm{loc}})_{it} = a(z^{\mathrm{loc}})_{ti} = 0$. The zCPL equations are best solved in the local basis, their result transformed to the canonical MO basis, and added as a constant contribution $\mathbf{a}(\mathbf{z}^{\mathrm{loc}})$ to the

zCPHF equations

$$0 = (1 - \tau_{ai}) \left[\mathbf{A} + \tilde{\mathbf{A}} + \bar{\mathbf{A}}(\bar{\mathbf{z}}) + \mathbf{a}(\mathbf{z}^{\mathrm{loc}}) \right]_{ai} \qquad \text{(closed)} \qquad (5.19)$$

$$0 = (1 - \tau_{xm}) \left[\mathbf{A} + \tilde{\mathbf{A}} + \bar{\mathbf{A}}(\mathbf{z}^{\pm}) + \mathbf{a}(\mathbf{z}^{\mathrm{loc}}) \right]_{xm} \qquad \text{(open)} \qquad (5.20)$$

with

$$x_{pq} = \frac{1}{2}(1 + \tau_{pq}) \left[\mathbf{A} + \tilde{\mathbf{A}} + \bar{\mathbf{A}}(\bar{\mathbf{z}}) + \mathbf{a}(\mathbf{z}^{\mathrm{loc}}) \right]_{pq} \qquad \text{(closed)} \qquad (5.21)$$

$$x_{pq} = \frac{1}{2}(1 + \tau_{pq}) \left[\mathbf{A} + \tilde{\mathbf{A}} + \bar{\mathbf{A}}(\mathbf{z}^{\pm}) + \mathbf{a}(\mathbf{z}^{\mathrm{loc}}) \right]_{pq} \qquad \text{(open)} \qquad (5.22)$$

thereby making $\mathcal{L}$ stationary in $\mathbf{U}$. The localization of the internal space, which is collected in $\mathbf{a}(\mathbf{z}^{\mathrm{loc}})$, is of course different if IBOs are used instead of PM orbitals, and has to be considered separately for closed and active orbitals. It will be explained in more detail in the following sections. For later use, we define

$$C_{ij,kl} = \left(\frac{\partial P}{\partial V_{ij} \partial V_{kl}} \right)_{\mathbf{V}=\mathbf{0}} = \left(\frac{\partial g_{ij}}{\partial V_{kl}} \right)_{\mathbf{V}=\mathbf{0}} \qquad (5.23)$$

and analogously $C_{tu,t'u'}$ should there be active orbitals present. As introduced in section 3.1, $\mathbf{V} = \mathbf{U} - \mathbf{1}$.

5.2 Pipek-Mezey zCPL

Following above considerations, the PM contribution to the zCPL equations can be found to read [9]

$$a_{ij}^{\mathrm{PM}} = \sum_{k>l} C_{ij,kl}^{\mathrm{PM}} z_{kl}^{\mathrm{loc}} \ \forall \ i > j \qquad (5.24)$$

$$C_{ij,kl}^{\mathrm{PM}} = \sum_{A}^{atoms} (1 - \tau_{ij})(1 - \tau_{kl}) \delta_{ik} [2 s_{ij}^A s_{kl}^A + \frac{1}{2} s_{jl}^A (s_{ii}^A + s_{kk}^A - s_{jj}^A - s_{ll}^A)]. \qquad (5.25)$$

As the derivatives with respect to V_{ij} and V_{kl} commute, the derivative must be symmetrized as

$$s_{ii}^A - s_{jj}^A = \frac{1}{2} [s_{ii}^A + s_{kk}^A - s_{jj}^A - s_{ll}^A]. \qquad (5.26)$$

For active orbitals, a second land independent contribution a_{tu}^{PM} has to be calculated. This is done by replacing all indices indicating doubly occupied orbitals by active space indices. Similar, the constant zCPHF contributions $a(\mathbf{z}^{\mathrm{loc}})_{pi}$ – and if applicable $a(\mathbf{z}_{\mathrm{act}}^{\mathrm{loc}})_{pt}$ – can then be computed

as

$$a_{pi} = ([\mathbf{w}\mathbf{S}^A\mathbf{b}^A\mathbf{w}^\dagger]_{pi} \tag{5.27}$$

$$a_{pt} = ([\mathbf{w}\mathbf{S}^A\mathbf{b}^A\mathbf{w}^\dagger]_{pt} \tag{5.28}$$

using the unitary rotation $\mathbf{w}$ as defined in eq. 3.5 to directly transfer the contribution to the canonical MO basis. It is convenient for the gradient expressions later on to introduce a symmetric matrix

$$b_{ii}^A = 2z_{ij}^{\mathrm{loc}} s_{ij}^A \tag{5.29}$$

$$b_{ij}^A = z_{ij}^{\mathrm{loc}} \left[s_{jj}^A - s_{ii}^A \right] \ \forall \ i \neq j, \tag{5.30}$$

and, if active orbitals are present, also its complement b_{tt}^A, b_{tu}^A defined equivalently.

5.3 Pipek-Mezey Gradient Expression

Having computed the Lagrangian multipliers $\{\mathbf{x}, \mathbf{z}, \mathbf{z}^{\mathrm{loc}}\}$, insertion of the integral and overlap matrix derivatives into eqs. 5.1 or 5.2 yields the desired gradient expression. The closed-shell gradient, as before, can be factorized as

$$E_{\mathrm{tot}}^q = D_{\mu\nu}h_{\mu\nu}^q + \frac{1}{2}D_{\mu\nu,\tau\upsilon}(\mu\nu|\tau\upsilon)^q + [\mathbf{X}_1]_{\mu\nu}[\mathbf{S}_1]_{\mu\nu}^q + E_{nuc}^q. \tag{5.31}$$

The effective one-particle density $D_{\mu\nu}$ is equivalent to its canonical pendant eq. 4.46 if the local second-order density is transformed back to the AO basis

$$D_{\mu\nu}^{(2)} = P_{\mu r}d_{rs}^{(2)}P_{\nu s} \tag{5.32}$$

and the overlap contribution and effective two-particle density are

$$[\mathbf{X}_1]_{\mu\nu} = -2C_{\mu i}f_{ij}C_{\nu j} - \frac{1}{2}C_{\mu p}x_{pq}C_{\nu q} + [\mathbf{X}_1^{\mathrm{PM}}]_{\mu\nu} + [\mathbf{C}(\tilde{\mathbf{A}} + \tilde{\mathbf{A}}^\dagger)\mathbf{C}^\dagger]_{\mu\nu} \tag{5.33}$$

$$D_{\mu\nu,\tau\upsilon} = 4C_{\mu i}C_{\tau j}P_{\nu r}P_{\upsilon s}\tilde{T}_{rs}^{ij} + 2(D_{\mu\nu} - \frac{1}{2}D_{\mu\nu}^{(0)})D_{\tau\upsilon}^{(0)} - (D_{\mu\tau} - \frac{1}{2}D_{\mu\tau}^{(0)})D_{\nu\upsilon}^{(0)}. \tag{5.34}$$

The additional contributions in $\mathbf{X}_1$ arise due to the (indirect) dependence of the stationary condition $\mathbf{g}_{\mathrm{PM}}$ and PAO projection matrix $\mathbf{P}$ on the overlap matrix $\mathbf{S}_1$. The first contribution is collected in $[\mathbf{X}_1^{\mathrm{PM}}]_{\mu\nu}$, and the latter can be found similar to eq. 5.4, using the relation $\mathbf{C}\mathbf{C}^\dagger\mathbf{S}_1 = 1$ for the second step:

$$\frac{\partial E_2}{\partial t_\lambda^{\mathrm{MO}}}\frac{\partial t_\lambda^{\mathrm{MO}}}{\partial[\mathbf{S}_1]_{\mu\nu}} = 2R_\lambda^{\mathrm{MO}}\frac{\partial t_\lambda^{\mathrm{MO}}}{\partial[\mathbf{S}_1]_{\mu\nu}} = \mathbf{C}(\tilde{\mathbf{A}} + \tilde{\mathbf{A}}^\dagger)\mathbf{C}^\dagger{}_{\mu\nu} \tag{5.35}$$

For closed-shell PM localization,

$$[\mathbf{X}_1^{\mathrm{PM}}]_{\mu\nu} = \sum_A [\mathbf{L}_0 \mathbf{b}^A \mathbf{L}_0^\dagger]_{\mu\nu} \delta_{\mu\in A}, \tag{5.36}$$

with $\delta_{\mu\in A}$ restricting the AO space index μ to basis functions at atom A only, *cf.* eqs. 3.4 or A3 [29]. Similarly, the open-shell gradient is

$$E_{\mathrm{tot}}^q = D_{\mu\nu}^+ h_{\mu\nu}^q + \frac{1}{2} D_{\mu\nu,\tau\upsilon}(\mu\nu|\tau\upsilon)^q + [\mathbf{X}_1]_{\mu\nu}[\mathbf{S}_1]_{\mu\nu}^q + E_{nuc}^q \tag{5.37}$$

using

$$\begin{aligned}
[\mathbf{X}_1]_{\mu\nu} &= -\left[2C_{\mu i}f_{ij}^+ C_{\nu j} + C_{\mu t}(f_{tu}^+ + f_{tu}^-)C_{\nu t} + 4C_{\mu i}f_{it}^+ C_{\nu t}\right] \\
&\quad - \frac{1}{2}C_{\mu p}x_{pq}C_{\nu q} + [\mathbf{X}_1^{\mathrm{PM}}]_{\mu\nu} + [\mathbf{C}(\tilde{\mathbf{A}} + \tilde{\mathbf{A}}^\dagger)\mathbf{C}^\dagger]_{\mu\nu} \tag{5.38} \\
[\mathbf{X}_1^{\mathrm{PM}}]_{\mu\nu} &= \sum_A \left(L_{\mu i}b_{ij}^A L_{\nu j} + L_{\mu t}b_{tu}^A L_{\nu u}\right)\delta_{\mu\in A} \tag{5.39} \\
D_{\mu\nu,\tau\upsilon} &= 4C_{\mu m}C_{\tau n}P_{\nu r}P_{\upsilon s}T_{rs}^{mn} + 2(D_{\mu\nu}^+ - \frac{1}{2}D_{\mu\nu}^{(0)+})D_{\tau\upsilon}^{(0)+} - (D_{\mu\tau}^+ - \frac{1}{2}D_{\mu\tau}^{(0)+})D_{\nu\upsilon}^{(0)+} \\
&\quad - (D_{\mu\tau}^- - \frac{1}{2}D_{\mu\tau}^{(0)-})D_{\nu\upsilon}^{(0)-}. \tag{5.40}
\end{aligned}$$

The one-particle effective densities $\mathbf{D}^+$ and $\mathbf{D}^-$ are defined in eqs. 4.64 and 4.65. As the one-particle effective densities for both, the closed- and open-shell local gradients are equivalent to their canonical complements, we can use the corresponding canonical expressions for the dipole moments as well.

5.4 Intrinsic Bond Orbitals zCPL

Even though IBOs can be computed efficiently, the projection steps involving two different basis sets lead to several additional terms in the theory and implementation of analytical energy gradients as compared to PM localization. The theory in this chapter thus has been adapted for best readability, with most intermediate quantities being different to those used for best performance in the actual implementation. Despite this complicated theoretical framework, the actual computation is quite fast, as all required matrix multiplications can be formulated to contain at least one index in the occupied (active) space or minimal basis B_2.

The IAO coefficient matrix $\mathbf{B}$, eq. 3.19, depends only on overlap and density matrices, thus it is invariant with respect to unitary rotations of the doubly occupied or active orbitals. Consequently, the restricted matrix product $B_{\mu\rho}B_{\nu\rho}$ $\rho \in A$ (*cf.* eq. 3.18) is stationary to any changes in the occupied or active orbitals as well – at least unless we mix subspaces or the basis

set changes. Based on this consideration, and with a related localization criterion, the IBO zCPL equations are very similar to the PM ones (eq. 5.24):

$$a_{ij}^{\text{IB}} = \sum_{k>l} C_{ij,kl}^{\text{IB}} z_{kl}^{\text{loc}} \; \forall \; i > j \tag{5.41}$$

$$C_{ij,kl}^{\text{IB}} = \sum_{A}^{atoms} (1 - \tau_{ij})(1 - \tau_{kl})\delta_{ik}[2(p-1)q_{ij}^A q_{kl}^A (q_{kk}^A)^{p-2}$$

$$+ \frac{1}{2} q_{jl}^A ((q_{ii}^A)^{p-1} + (q_{kk}^A)^{p-1} - (q_{jj}^A)^{p-1} - (q_{ll}^A)^{p-1})] \tag{5.42}$$

As before, the derivative has been symmetrized in $ij - kl$ as

$$(q_{ii}^A)^{p-1} - (q_{jj}^A)^{p-1} = \frac{1}{2}[(q_{ii}^A)^{p-1} + (q_{kk}^A)^{p-1} - (q_{jj}^A)^{p-1} - (q_{ll}^A)^{p-1}]. \tag{5.43}$$

Again, above equations are also valid for active orbitals t, u, although the partial charges q_{tu}^A have to be recomputed as $\mathbf{B}$ is different for both localization spaces. After inserting eq. 5.41 into eqs. 5.17 or 5.18 and solving the zCPL equations in the occupied space, the constant contributions to zCPHF, $a(\mathbf{z}^{\text{loc}})_{pi}$ and if needed $a(\mathbf{z}^{\text{loc}})_{pt}$, can be computed as

$$a_{pi} = [\mathbf{w}\mathbf{Q}^A\mathbf{b}^A\mathbf{w}^\dagger]_{pi} + \sum_{A}^{atoms} \sum_{\rho' \in A} [\mathbf{S}_1\mathbf{L}_0\mathbf{b}^A\mathbf{L}_0^\dagger\mathbf{S}_1\mathbf{B}]_{\mu\rho'} B_{\mu\rho'}^{pi} \tag{5.44}$$

$$a_{pt} = [\mathbf{w}\mathbf{Q}^A\mathbf{b}^A\mathbf{w}^\dagger]_{pt} + \sum_{A}^{atoms} \sum_{\rho' \in A} [\mathbf{S}_1\mathbf{L}_0\mathbf{b}^A\mathbf{L}_0^\dagger\mathbf{S}_1\mathbf{B}]_{\mu\rho'} B_{\mu\rho'}^{pt} \tag{5.45}$$

The symmetric matrix $\mathbf{b}^A$ is defined similar as for PM with

$$b_{ii}^A = 2(p-1)(q_{ii}^A)^{p-2} z_{ij}^{\text{loc}} q_{ij}^A \tag{5.46}$$

$$b_{ij}^A = z_{ij}^{\text{loc}} \left[(q_{jj}^A)^{p-1} - (q_{ii}^A)^{p-1}\right] \; \forall \; i \neq j \tag{5.47}$$

and b_{tt}, b_{tu} accordingly. For the internal-external contribution, further terms arise as now orbital spaces are mixed:

$$\sum_{A} \text{tr} \left\{ (\delta\mathbf{B}^{(A)})^\dagger \mathbf{S}_1\mathbf{L}_0\mathbf{b}^A\mathbf{L}_0^\dagger\mathbf{S}_1\mathbf{B}^{(A)} \right\} := \text{tr} \left\{ (\delta\mathbf{B})^\dagger \mathbf{G} \right\} \tag{5.48}$$

Here, δ indicates an infinitesimal first-order variation of a quantity, and $\mathbf{B}^{(A)}$ means summation over IAOs $\rho' \in A$ at atom A only.

We can expand the above contribution using non-orthonormal IAO coefficients by inserting the definition of the symmetric orthogonalization given in eq. 3.12:

$$\text{tr} \left\{ (\delta\mathbf{B})^\dagger \mathbf{G} \right\} = \text{tr} \left\{ (\delta\bar{\mathbf{B}})^\dagger \mathbf{G}\mathbf{H}' \right\} + \text{tr} \left\{ (\delta\mathbf{H}')\bar{\mathbf{B}}^\dagger \mathbf{G} \right\} \tag{5.49}$$

It is $\mathbf{H'} = [\bar{\mathbf{B}}^\dagger \mathbf{S}_1 \bar{\mathbf{B}}]^{-1/2}$. The bar used in above expression will indicate non-orthonormalized quantities in this section. The general derivative of a square matrix $\mathbf{X}^{-1/2}$ is

$$[\delta \mathbf{X}^{-\frac{1}{2}}]_{ab} = -U_{ac} \frac{(\mathbf{U}^\dagger \delta \mathbf{X} \mathbf{U})_{cd}}{\sqrt{x_c} x_d + x_c \sqrt{x_d}} U_{bd}, \tag{5.50}$$

with the associated eigenvalue problem

$$[\mathbf{U}^\dagger \mathbf{X} \mathbf{U}]_{cd} = x_c \delta_{cd}. \tag{5.51}$$

Indices $a - d$ are arbitrary. This derivative expression and the property of cyclic permutation in a trace can be used to factorize eq. 5.49 further by defining

$$H_{\rho'\sigma'} = -\frac{1}{2} W_{\rho'\rho} \frac{[\mathbf{W}^\dagger (\bar{\mathbf{B}}^\dagger \mathbf{G} + \mathbf{G}^\dagger \bar{\mathbf{B}}) \mathbf{W}]_{\rho\sigma}}{\sqrt{h'_\rho} h'_\sigma + h'_\rho \sqrt{h'_\sigma}} W_{\sigma'\sigma} \tag{5.52}$$

which results in

$$\mathrm{tr}\left\{ (\delta \mathbf{B})^\dagger \mathbf{G} \right\} = \mathrm{tr}\left\{ (\delta \bar{\mathbf{B}})^\dagger (\mathbf{G} \mathbf{H'} + 2 \mathbf{S}_1 \bar{\mathbf{B}} \mathbf{H}) \right\} = \mathrm{tr}\left\{ (\delta \bar{\mathbf{B}})^\dagger \mathbf{V} \right\}. \tag{5.53}$$

$\mathbf{W}$ is the matrix that diagonalizes $\bar{\mathbf{B}}^\dagger \mathbf{S}_1 \bar{\mathbf{B}}$ and h'_ρ are the corresponding eigenvalues. Transforming all quantities into a spectral basis and back seems like a lot of computational effort at first, however, this operation only takes place in the much smaller auxiliary basis B_2 and is only necessary once per localization subspace for every point on the PES.

The non-orthonormal IAO coefficient matrix $\bar{\mathbf{B}}$ is implicitly defined in eq. 3.19. This allows for further expansion

$$\begin{aligned}
\mathrm{tr}\left\{ (\delta \mathbf{B}^\dagger \mathbf{G} \right\} &= \mathrm{tr}\left\{ (\delta \mathbf{L})^\dagger (\mathbf{V} \mathbf{S}_{21} + \mathbf{S}_{12} \mathbf{V}^\dagger) \mathbf{L}_0 \right\} \\
&- \mathrm{tr}\left\{ (\delta \mathbf{L})^\dagger \mathbf{Z}^\dagger (\mathbf{V} \mathbf{S}_{21} + \mathbf{S}_{12} \mathbf{V}^\dagger) \bar{\mathbf{L}}_0 \mathbf{Y} \right\} \\
&+ \mathrm{tr}\left\{ (\delta \mathbf{L})^\dagger \mathbf{Z}^\dagger \mathbf{S}_1 \bar{\mathbf{L}}_0 \mathbf{Y} \bar{\mathbf{L}}_0^\dagger (\mathbf{V} \mathbf{S}_{21} + \mathbf{S}_{12} \mathbf{V}^\dagger) \bar{\mathbf{L}}_0 \mathbf{Y} \right\}
\end{aligned} \tag{5.54}$$

with $\mathbf{Y} = [\bar{\mathbf{L}}_0^\dagger \mathbf{S}_1 \bar{\mathbf{L}}_0]^{-1}$ and $\mathbf{Z} = \mathbf{S}_1^{-1} \mathbf{S}_{12} \mathbf{S}_2^{-1} \mathbf{S}_{21}$. The derivatives of $\tilde{L}_{\mu p}$ (*cf.* eq. 3.20), despite being orthonormalized as well, are more convenient to calculate, as the depolarized density matrix can be reformulated as

$$\tilde{\mathbf{D}}^{(0)} = \tilde{\mathbf{L}}_0 \tilde{\mathbf{L}}_0^\dagger = \bar{\mathbf{L}}_0 \mathbf{Y} \bar{\mathbf{L}}_0^\dagger. \tag{5.55}$$

This avoids further transformations into a spectral basis and back, as the derivative $\delta \mathbf{X}^{-1} = -\mathbf{X}^{-1}(\delta \mathbf{X})\mathbf{X}^{-1}$ is directly available. Collecting all terms, the full derivative with respect to V_{ri}

is

$$
\begin{aligned}
a_{pi} &= \sum_A^{atoms} [\mathbf{w}\mathbf{Q}^A \mathbf{b}^A \mathbf{w}^\dagger]_{pi} + [\mathbf{C}^\dagger(\mathbf{V}\mathbf{S}_{21} + \mathbf{S}_{12}\mathbf{V}^\dagger)\mathbf{C}]_{pi} \\
&\quad - [\bar{\mathbf{C}}^\dagger(\mathbf{1} - \mathbf{S}_1\tilde{\mathbf{D}}^{(0)})(\mathbf{V}\mathbf{S}_{21} + \mathbf{S}_{12}\mathbf{V}^\dagger)\bar{\mathbf{C}}_0\mathbf{Y}]_{pi}.
\end{aligned}
\tag{5.56}
$$

The active space contribution is formally equivalent, and a_{ij}, a_{tu} are symmetric.

5.5 Intrinsic Bond Orbitals Gradient Expression

Having computed the Lagrangian multipliers $\{\mathbf{x}, \mathbf{z}, \mathbf{z}^{\text{loc}}\}$, insertion of the integral and overlap matrix derivatives into eqs. 5.1 or 5.2 does not yield the desired gradient expression. Contrary to PM, IBOs are not linear in the overlap matrices $\mathbf{S}_1, \mathbf{S}_{12}, \mathbf{S}_2$, and thus

$$
E_{tot}^q \neq \mathcal{L}^{(q)}.
\tag{5.57}
$$

Instead, we have to use the chain rule

$$
E_{tot}^q = \mathcal{L}_{(R)HF}^{(q)} + \sum_I \left(\frac{\partial \mathcal{L}_{L(R)MP2}}{\partial I}\right) I^q
\tag{5.58}
$$

with I being the one- and two-electron integrals and all overlap matrices. In practical terms, this does not matter too much, as the gradient still needs to be factorized and derivatives of non-linear terms simply result in sums (product rule). Also, the linearity of the one- and two-electron integrals is not affected and subsequently, they can be treated as before. Thus, the closed-shell gradient can still be factorized as (*cf.* eq. 5.31)

$$
E_{\text{tot}}^q = D_{\mu\nu}h_{\mu\nu}^q + \frac{1}{2}D_{\mu\nu,\tau\upsilon}(\mu\nu|\tau\upsilon)^q + [\mathbf{X}_1]_{\mu\nu}[\mathbf{S}_1]_{\mu\nu}^q + [\mathbf{X}_{12}]_{\mu\rho}[\mathbf{S}_{12}]_{\mu\rho}^q + [\mathbf{X}_2]_{\rho\sigma}[\mathbf{S}_2]_{\rho\sigma}^q + E_{nuc}^q.
\tag{5.59}
$$

The effective one- and two-particle densities are equivalent to those in eqs. 4.46 and 5.34, respectively and the remaining task is thus to find the overlap contributions. As the orthonormality condition and PAO space projectors remain unchanged, we can immediately write (*cf.* eq. 5.33):

$$
[\mathbf{X}_1]_{\mu\nu} = -2C_{\mu i}f_{ij}C_{\nu j} - \frac{1}{2}C_{\mu p}x_{pq}C_{\nu q} + [\mathbf{X}_1^{\text{IBO}}]_{\mu\nu} + [\mathbf{C}(\tilde{\mathbf{A}} + \tilde{\mathbf{A}}^\dagger)\mathbf{C}^\dagger]_{\mu\nu}
\tag{5.60}
$$

In order to find $\mathbf{X}_1^{\text{IBO}}, \mathbf{X}_{12}$ and $\mathbf{X}_2$, we start with an ansatz closely related to eq. 5.48

$$
\text{tr}\left\{(\delta\mathbf{B})^\dagger\mathbf{G}\right\} + \frac{1}{2}\text{tr}\left\{(\delta\mathbf{S}_1)\mathbf{L}_0\mathbf{b}^A\mathbf{L}_0^\dagger\mathbf{S}_1\mathbf{B}\mathbf{B}^\dagger\right\} + \frac{1}{2}\text{tr}\left\{(\delta\mathbf{S}_1)\mathbf{B}\mathbf{B}^\dagger\mathbf{S}_1\mathbf{L}_0\mathbf{b}^A\mathbf{L}_0^\dagger\right\}
\tag{5.61}
$$

Without further ado, we expand

$$\text{tr}\left\{(\delta\mathbf{B})^\dagger\mathbf{G}\right\} = \text{tr}\left\{(\delta\bar{\mathbf{B}})^\dagger\mathbf{V}\right\} + \text{tr}\left\{(\delta\mathbf{S}_1)\bar{\mathbf{B}}\mathbf{H}\bar{\mathbf{B}}^\dagger\right\} \tag{5.62}$$

and

$$
\begin{aligned}
\text{tr}\left\{(\delta\bar{\mathbf{B}})^\dagger\mathbf{V}\right\} =\ & \text{tr}\left\{(\delta\mathbf{S}_1)\mathbf{S}_1^{-1}(\mathbf{V}\mathbf{S}_{21} + \mathbf{S}_{12}\mathbf{V}^\dagger)\tilde{\mathbf{D}}^{(0)}\right\} \\
&- \text{tr}\left\{(\delta\mathbf{S}_1)\mathbf{S}_1^{-1}\mathbf{V}\mathbf{S}_{21}\mathbf{S}_1^{-1}\right\} \\
&- \text{tr}\left\{(\delta\mathbf{S}_1)\tilde{\mathbf{D}}^{(0)}\mathbf{V}\mathbf{S}_{21}\tilde{\mathbf{D}}^{(0)}\right\} \\
&+ \text{tr}\left\{(\delta\mathbf{S}_2)\mathbf{S}_2^{-1}\mathbf{S}_{21}(\mathbf{S}_1^{-1}-\tilde{\mathbf{D}}^{(0)})(\mathbf{V}\mathbf{S}_{21} + \mathbf{S}_{12}\mathbf{V}^\dagger)\bar{\mathbf{L}}_0\mathbf{Y}\mathbf{L}_0^\dagger\mathbf{S}_{12}\mathbf{S}_2^{-1}\right\} \\
&+ \text{tr}\left\{(\delta\mathbf{S}_{21})(\mathbf{S}_1^{-1}+\mathbf{D}^{(0)} - \tilde{\mathbf{D}}^{(0)})\mathbf{V}\right\} \\
&- \text{tr}\left\{(\delta\mathbf{S}_{21})(\mathbf{S}_1^{-1}-\tilde{\mathbf{D}}^{(0)})(\mathbf{V}\mathbf{S}_{21} + \mathbf{S}_{12}\mathbf{V}^\dagger)\bar{\mathbf{L}}_0\mathbf{Y}\mathbf{L}_0^\dagger\mathbf{S}_{12}\mathbf{S}_2^{-1}\right\} \\
&- \text{tr}\left\{(\delta\mathbf{S}_{21})\mathbf{L}_0\mathbf{Y}\bar{\mathbf{L}}_0^\dagger(\mathbf{V}\mathbf{S}_{21} + \mathbf{S}_{12}\mathbf{V}^\dagger)(\mathbf{S}_1^{-1}-\tilde{\mathbf{D}}^{(0)})\mathbf{S}_{12}\mathbf{S}_2^{-1}\right\}.
\end{aligned} \tag{5.63}
$$

Collecting all terms and replacing $\delta\mathbf{S}$ by the respective derivatives $\mathbf{S}^q$, the overlap contributions are

$$
\begin{aligned}
\mathbf{X}_1^{\text{IBO}} =\ & \frac{1}{2}(\mathbf{L}_0\mathbf{b}^A\mathbf{L}_0^\dagger\mathbf{S}_1\mathbf{B}\mathbf{B}^\dagger + \mathbf{B}\mathbf{B}^\dagger\mathbf{S}_1\mathbf{L}_0\mathbf{b}^A\mathbf{L}_0^\dagger) + \bar{\mathbf{B}}\mathbf{H}\bar{\mathbf{B}}^\dagger + \mathbf{S}_1^{-1}(\mathbf{V}\mathbf{S}_{21} + \mathbf{S}_{12}\mathbf{V}^\dagger)\tilde{\mathbf{D}}^{(0)} \\
&- \frac{1}{2}\mathbf{S}_1^{-1}(\mathbf{V}\mathbf{S}_{21} + \mathbf{S}_{12}\mathbf{V}^\dagger)\mathbf{S}_1^{-1} - \frac{1}{2}\tilde{\mathbf{D}}^{(0)}(\mathbf{V}\mathbf{S}_{21} + \mathbf{S}_{12}\mathbf{V}^\dagger)\tilde{\mathbf{D}}^{(0)}
\end{aligned} \tag{5.64}
$$

$$
\begin{aligned}
\mathbf{X}_{12} =\ & (\mathbf{S}_1^{-1}+\mathbf{D}^{(0)} - \tilde{\mathbf{D}}^{(0)})\mathbf{V} - (\mathbf{S}_1^{-1}-\tilde{\mathbf{D}}^{(0)})(\mathbf{V}\mathbf{S}_{21} + \mathbf{S}_{12}\mathbf{V}^\dagger)\bar{\mathbf{L}}_0\mathbf{Y}\mathbf{L}_0^\dagger\mathbf{S}_{12}\mathbf{S}_2^{-1} \\
&- \mathbf{L}_0\mathbf{Y}\bar{\mathbf{L}}_0^\dagger(\mathbf{V}\mathbf{S}_{21} + \mathbf{S}_{12}\mathbf{V}^\dagger)(\mathbf{S}_1^{-1}-\tilde{\mathbf{D}}^{(0)})\mathbf{S}_{12}\mathbf{S}_2^{-1}
\end{aligned} \tag{5.65}
$$

$$
\mathbf{X}_2 = \mathbf{S}_2^{-1}\mathbf{S}_{21}(\mathbf{S}_1^{-1}-\tilde{\mathbf{D}}^{(0)})(\mathbf{V}\mathbf{S}_{21} + \mathbf{S}_{12}\mathbf{V}^\dagger)\bar{\mathbf{L}}_0\mathbf{Y}\mathbf{L}_0^\dagger\mathbf{S}_{12}\mathbf{S}_2^{-1}. \tag{5.66}
$$

The derivatives of $\mathbf{S}_1$ and $\mathbf{S}_2$ form symmetric matrices, and thus the contributions $\mathbf{X}_1$ and $\mathbf{X}_2$ are required to be symmetric as well.

The open-shell IBO gradient is very similar to PM, with the one- and two particle densities formally corresponding to those in eqs. 4.64, 4.65, and 5.40 respectively; the overlap contributions are introduced the same way as for the closed-shell IBO gradient:

$$
\begin{aligned}
E_{\text{tot}}^q =\ & D_{\mu\nu}^+ h_{\mu\nu}^q + \frac{1}{2}D_{\mu\nu,\tau\upsilon}(\mu\nu|\tau\upsilon)^q + [\mathbf{X}_1]_{\mu\nu}[\mathbf{S}_1]_{\mu\nu}^q + [\mathbf{X}_{12}]_{\mu\rho}[\mathbf{S}_{12}]_{\mu\rho}^q + [\mathbf{X}_2]_{\rho\sigma}[\mathbf{S}_2]_{\rho\sigma}^q \\
&+ E_{nuc}^q
\end{aligned} \tag{5.67}
$$

The contributions to the main basis overlap are (*cf.* eq. 5.38)

$$
\begin{aligned}
[\mathbf{X}_1]_{\mu\nu} =\ & -\left[2C_{\mu i}f_{ij}^+C_{\nu j} + C_{\mu t}(f_{tu}^+ + f_{tu}^-)C_{\nu t} + 4C_{\mu i}f_{it}^+C_{\nu t}\right] \\
&- \frac{1}{2}C_{\mu p}x_{pq}C_{\nu q} + [\mathbf{X}_1^{\text{IBO}}]_{\mu\nu} + [\mathbf{C}(\tilde{\mathbf{A}} + \tilde{\mathbf{A}}^\dagger)\mathbf{C}^\dagger]_{\mu\nu}.
\end{aligned} \tag{5.68}
$$

As the IAOs are different for both localization spaces, the contractions $\mathbf{X}_1^{\text{IBO}}, \mathbf{X}_{12}$ and $\mathbf{X}_2$ need to be augmented by active-space contributions and are thus expressed as a sum:

$$\mathbf{X}_1^{\text{IBO}} = \mathbf{X}_1^{\text{IBO,cl}} + \mathbf{X}_1^{\text{IBO,ac}} \tag{5.69}$$

$$\mathbf{X}_{12} = \mathbf{X}_{12}^{\text{cl}} + \mathbf{X}_{12}^{\text{ac}} \tag{5.70}$$

$$\mathbf{X}_2 = \mathbf{X}_2^{\text{cl}} + \mathbf{X}_2^{\text{ac}} \tag{5.71}$$

Here, all quantities with superscript 'cl' are evaluated using closed-shell orbital indices and IAOs, those with superscript 'ac' the respective active space quantities. IBO (R)LMP2 Dipole moments are available via eqs. 4.48 and 4.67.

5.6 The Density Fitting Approximation

One of the rate determining steps for iterative MP2 energy calculations is the transformation of the four-index, two-electron exchange integrals $(\mu\nu|\tau\upsilon)$ to the integrals $(ai|bj)$ in MO basis prior to contraction with amplitudes T_{ab}^{ij} in every iteration step, as can be seen for instance in eq. 2.75. The RMP2 energy and Hylleraas functional, eqs. 2.80 and 2.81, contain even three contractions per iteration. Property calculations require such a type of contraction only once, but in turn over an extended index space with three external indices, see for instance eq. 4.33. Such contractions during gradient calculations are expensive since the transformation of the integrals from AO to MO basis as well as the contraction $(pa|bj)T_{ab}^{ij}$ scale as $\mathcal{O}(N^5)$. The resolution of the identity approximation, also called density fitting (DF) approximation, is a convenient way to replace those four-index integrals with products of two- and three-index integrals [29, 60, 61, 105, 106]. Replacing the integrals may not alter the formal scaling, but by using density fitting, the computational time can still be reduced significantly for both energy and gradient calculations in larger basis sets while sacrificing almost none of the method's accuracy [36, 62, 107].

Density fitting approximations can be introduced at both, the HF and (L,R)MP2 level energy calculations; we will first examine the influence of a density fitted MP2 reference on the gradients, assuming everything is based on a non-density fitted HF calculation; then in a second step we will consider a DF-HF reference as well. For a non-fitted HF reference, the Fock matrix contributions to the gradient remain unchanged, and only the contractions of amplitudes and exchange integrals in the zCPHF calculations and two-particle densities, for example eqs. 4.33, 4.34 and 4.47, or 4.56 and 4.66, need to be adapted. The exact exchange integrals in AO basis (*cf.* eq. 2.68) can be approximated as

$$K_{\nu\upsilon}^{\mu\tau} = (\mu\nu|\tau\upsilon) \approx (\mu\nu|A)[\mathbf{J}^{-1}]_{AB}(B|\tau\upsilon) = J_A^{\mu\nu}[\mathbf{J}^{-1}]_{AB}J_B^{\tau\upsilon} \tag{5.72}$$

by expanding the orbital product densities $(\mu\nu|$ in an auxiliary basis set with indices A, B. For infinitely large auxiliary basis sets, this operation corresponds to an identity operation and is exact. As basis sets of infinite size are not available, one typically uses Gaussian sets or bases specifically designed for density fitting [108–110]. The three-index, two-electron Coulomb integrals are defined as

$$J_A^{\mu\nu} = (\mu\nu|A) = \int d\mathbf{r}_1 \int d\mathbf{r}_2 \frac{\chi_\mu(\mathbf{r}_1)\chi_\nu(\mathbf{r}_1)\chi_A(\mathbf{r}_2)}{|\mathbf{r}_1 - \mathbf{r}_2|} \tag{5.73}$$

and

$$J_{AB} = \int d\mathbf{r}_1 \int d\mathbf{r}_2 \frac{\chi_A(\mathbf{r}_1)\chi_B(\mathbf{r}_2)}{|\mathbf{r}_1 - \mathbf{r}_2|} \tag{5.74}$$

is the Coulomb-kernel matrix represented in the auxiliary basis. Here, $\chi_\mu(\mathbf{r}_1)$ are the functions of the AO, and $\chi_A(\mathbf{r}_1)$ of the auxiliary density fitting basis. The derivatives of the two-electron integrals thus are approximated by

$$(\mu\nu|\tau\upsilon)^q \approx [J_A^{\mu\nu}]^q c_{\tau\upsilon}^A + c_{\mu\nu}^A [J_A^{\tau\upsilon}]^q - c_{\mu\nu}^A J_{AB}^q c_{\tau\upsilon}^B \tag{5.75}$$

with the DF coefficients $c_{\mu\nu}^A = [\mathbf{J}^{-1}]_{AB} J_B^{\mu\nu}$; eq. 5.75 is the derivative of eq. 5.72 using the lemma $[\mathbf{J}^{-1}]^q = -\mathbf{J}^{-1}\mathbf{J}^q\mathbf{J}^{-1}$. Defining

$$V_{ia}^A = \tilde{T}_{ab}^{ij} c_{jb}^A, \tag{5.76}$$

$$V_{\mu\nu}^A = c_{\mu i}^A V_{ia}^A c_{\nu a}^A, \tag{5.77}$$

the two-particle densities first term in a closed-shell system (*cf.* eq. 4.47) reads

$$4C_{\mu i} C_{\tau j} C_{\nu a} C_{\upsilon b} \tilde{T}_{ab}^{ij} (\mu\nu|\tau\upsilon)^q \approx 8[J_A^{\mu\nu}]^q V_{\mu\nu}^A - 4J_{AB}^q V_{ia}^A c_{ia}^B. \tag{5.78}$$

For open-shell gradients, the amplitudes $\tilde{T}$ are to be replaced by unified amplitudes T, eq. 4.52, and indices i, a with m, x respectively in order to adapt eq. 4.66. The computationally most efficient way to generate the above contribution is to first transform the integrals $J_{\mu\nu}^A$ to the MO basis as J_{ia}^A (via $J_{i\nu}^A$), then calculate c_{ia}^A, and subsequently contract the latter coefficients with the MP2 amplitudes to form V_{ia}^A. The intermediates V_{ia}^A are then back-transformed via $V_{i\nu}^A$ to an AO representation $V_{\mu\nu}^A$. As a by-product, the half-transformed quantities $V_{i\nu}^A$ and $J_{i\nu}^A$ can be used to generate the zCPHF contributions at only minimal additional cost as

$$K_{ab}^{pj} \tilde{T}_{ab}^{ij} \approx C_{\mu p} J_{\mu\nu}^A V_{i\nu}^A \tag{5.79}$$

$$K_{pb}^{ij} \tilde{T}_{ab}^{ij} \approx C_{\nu p} J_{i\nu}^A V_{ia}^A. \tag{5.80}$$

The open-shell equivalents are again obtained by extending the summations over the active orbitals, rendering them only moderately more expensive.

For use in local gradients, we can extend the DF formalism to the LMO and PAO spaces: the derivatives of the approximated two-electron integrals, eq. 5.75, remain formally unchanged, but the intermediates $\mathbf{V}^A$ now contain amplitudes in the PAO basis:

$$V_{ir}^A = \sum_j \sum_{s \in [ij]} \tilde{T}_{rs}^{ij} c_{js}^A \tag{5.81}$$

During back-transformation, united amplitudes $[i]_U$ are formed by summation over all other indices j in a domain $[ij]$ yielding

$$V_{i\nu}^A = \sum_{r \in [i]_U} V_{ir}^A P_{\nu r}. \tag{5.82}$$

Taking into account the sparsity of the PAO matrices, both above steps and all below scale with $\mathcal{O}(N^2)$. The zCPHF contributions are

$$K_{rs}^{pj} \tilde{T}_{rs}^{ij} \approx C_{\mu p} J_{\mu\nu}^A V_{i\nu}^A \tag{5.83}$$

$$K_{ps}^{ij} \tilde{T}_{rs}^{ij} \approx C_{\nu p} J_{i\nu}^A V_{ir}^A \tag{5.84}$$

and the two-particle density contribution is

$$4 C_{\mu i} C_{\tau j} P_{\nu r} P_{\upsilon s} \tilde{T}_{rs}^{ij} (\mu\nu|\tau\upsilon)^q \approx 8 [J_A^{\mu\nu}]^q V_{\mu\nu}^A - 4 J_{AB}^q V_{ir}^A c_{ir}^B. \tag{5.85}$$

We will now in a second step discuss the changes introduced if DF-(L,R)MP2 gradients are based on a density-fitted (R)HF reference. It is important to know that the density fitting bases used on both, the HF and MP2 level, are different. Thus there are two different sets of three-index integrals $J_A^{\mu\nu}$ and Coulomb-kernels J_{AB} used in our gradient method, and the equations following below cannot be simply combined with the DF-MP2 contributions introduced above. Consequentially, if $J_A^{\mu\nu}$ and J_{AB} are different on different levels of theory, there are also different derivatives to be computed during gradient calculations. Despite these additional steps – in comparison to gradients without any density-fitting –, the fully density-fitted gradients are significantly faster [29].

The DF-(R)HF programs available in MOLPRO use local fitting domains to reduce the exchange contributions scaling to $\mathcal{O}(N)$ [36]. Although the energy seems to be very sensitive towards the choice and size of the local fitting domains, the orbitals are more robust and will tolerate smaller fitting domains. Thus, smaller domains are used during orbital optimization and the final energy is subsequently calculated as

$$E_{HF} = \operatorname{tr}\left\{\mathbf{d}^{(0)}\mathbf{h}\right\} + \frac{1}{2}[\mathbf{c}(\mathbf{D}^{(0)})]_A J_{AB}^{-1}[\mathbf{c}(\mathbf{D}^{(0)})]_B - J_A^{ij} J_{AB}^{-1} J_B^{ij} \tag{5.86}$$

with vectors

$$c(\mathbf{D}^{(0)})_A = D_{\mu\nu}^{(0)} J_A^{\mu\nu} \tag{5.87}$$

and $J_A^{ij} = C_{\mu i} J_A^{\mu\nu} C_{\nu j}$ the three-index integrals in MO-basis. Above energy expression avoids the explicit construction of a Fock matrix and is evaluated without local approximations. We will use it as starting point for deriving the gradient expression, ignoring it's implicit dependence on the local fitting domains. Also, the indirect dependence of the subsequent LMP2 calculation on the HF fitting domains will be neglected. According to Schütz *et al.* both approximations acoount only for a few microhartree of error relative to the DF-HF energy without local fitting [29]. Additionally, the Fock matrix obtained with local fitting domains is sufficiently precise for subsequent LMP2 and gradient calculations and is thus not rebuild.

Looking at the L(R)MP2 gradient expressions, the two-particle densities, eqs. 4.47 and 4.66, which are to be contracted with the two-electron integrals, have to be partly modified. The first term in both expressions, involving the MP2 amplitudes, is subject to the MP2 density fitting and has been discussed above. Remaining are the second to last terms, and using the derivative approximation eq. 5.75 the contribution in closed-shell systems is

$$
\begin{aligned}
(\mu\nu|\tau\upsilon)^q \left(2\check{D}_{\mu\nu} D_{\tau\upsilon}^{(0)} - \check{D}_{\mu\tau} D_{\nu\upsilon}^{(0)} \right) &\approx (J_A^{\mu\nu})^q \left(\check{D}_{\mu\nu}[\mathbf{c}(\mathbf{D}^{(0)})]_A + D_{\mu\nu}^{(0)}[\mathbf{c}(\check{\mathbf{D}})]_A - 2\check{D}_{\mu\tau} c_{\tau i}^A L_{\nu i} \right) \\
&+ J_{AB}^q \left(c_{i\mu}^A \check{D}_{\mu\nu} c_{\nu i}^B - [\mathbf{c}(\check{\mathbf{D}})]_A [\mathbf{c}(\mathbf{D}^{(0)})]_B \right).
\end{aligned}
\tag{5.88}
$$

with $\check{D}_{\mu\nu} = D_{\mu\nu} - \frac{1}{2} D_{\mu\nu}^{(0)}$. The open-shell expression is similar:

$$
\begin{aligned}
(\mu\nu|\tau\upsilon)^q &\left(2\check{D}_{\mu\nu}^+ D_{\tau\upsilon}^{(0)+} - \check{D}_{\mu\tau}^+ D_{\nu\upsilon}^{(0)+} - \check{D}_{\mu\tau}^- D_{\nu\upsilon}^{(0)-} \right) \\
\approx (J_A^{\mu\nu})^q &\left(\check{D}_{\mu\nu}^+[\mathbf{c}(\mathbf{D}^{(0)+})]_A + D_{\mu\nu}^{(0)+}[\mathbf{c}(\check{\mathbf{D}}^+)]_A - n_m \check{D}_{\mu\tau}^+ c_{\tau m}^A L_{\nu m} - \check{D}_{\mu\tau}^- c_{\tau t}^A L_{\nu t} \right) \\
+ J_{AB}^q &\left(\tfrac{1}{2} n_m c_{m\mu}^A \check{D}_{\mu\nu}^+ c_{\nu m}^B + \tfrac{1}{2} c_{t\mu}^A \check{D}_{\mu\nu}^- c_{\nu t}^B - [\mathbf{c}(\check{\mathbf{D}}^+)]_A [\mathbf{c}(\mathbf{D}^{(0)+})]_B \right)
\end{aligned}
\tag{5.89}
$$

It is $\check{D}_{\mu\nu}^+ = D_{\mu\nu}^+ - \frac{1}{2} D_{\mu\nu}^{(0)+}$, $\check{D}_{\mu\nu}^- = D_{\mu\nu}^- - \frac{1}{2} D_{\mu\nu}^{(0)-}$, and n_m the occupation number of orbital m. Apart from contributions to the final gradient, there are also changes in the zCPHF equations, as those contain quantities such as $\mathbf{g}(\mathbf{D}^{(2)})$ and $\mathbf{g}(\bar{\mathbf{z}})$, *cf.* eqs. 4.33, 4.37, 4.56, and 4.58. The required quantities are based on the contraction of two-electron integrals with matrices such as $\mathbf{D}^{(2)}$ and $\bar{\mathbf{z}}$. For closed-shell systems, the contractions can be approximated as

$$[\mathbf{g}(\mathbf{D}^{(2)})]_{pi} \approx \left([\mathbf{c}(\mathbf{D}^{(2)})]_A J_A^{\mu\nu} L_{\mu i} - \frac{1}{2} c_{i\tau}^A D_{\tau\upsilon}^{(2)} J_A^{\nu\upsilon} \right) L_{\nu p} \tag{5.90}$$

whereas in open-shell systems they are

$$[\mathbf{g}(\mathbf{D}^{(2)+})]_{pm} \approx \left([\mathbf{c}(\mathbf{D}^{(2)+})]_A J_A^{\mu\nu} L_{\mu m} - \frac{1}{2} c_{m\tau}^A D_{\tau\upsilon}^{(2)+} J_A^{\upsilon\nu} \right) L_{\nu p} \tag{5.91}$$

$$[\mathbf{g}^-(\mathbf{D}^{(2)-})]_{pt} \approx -\frac{1}{2} c_{t\tau}^A D_{\tau\upsilon}^{(2)-} J_A^{\upsilon\nu} L_{\nu p}. \tag{5.92}$$

For $[\mathbf{g}(\mathbf{D}^{(2)})]_{pi}$ and $[\mathbf{g}(\mathbf{D}^{(2)+})]_{pm}$, the Coulomb part is a contraction of the three-index integrals with a precomputed vector $[\mathbf{c}(\mathbf{D}^{(2)})]_A$, with the result subsequently transformed to MO basis. There is no Coulomb contribution for $[\mathbf{g}^-(\mathbf{D}^{(2)-})]_{pt}$. For calculation of the exchange parts, the half-transformed fitting coefficients $c_{i\tau}^A$ are weighted using the appropriate density matrix prior to contraction with the three-index integrals; in open-shell systems, $\mathbf{D}^{(2)+}$ and $\mathbf{D}^{(2)-}$ are contracted at same time to avoid reading the integrals twice. By exploiting the sparsity of both fitting coefficients and densities, the compuational cost can be reduced from $\mathcal{O}(N^4)$ to $\mathcal{O}(N^2)$ [29].

The contractions $\mathbf{g}(\bar{\mathbf{z}})$, $\mathbf{g}(\mathbf{z}^+)$, and $\mathbf{g}^-(\mathbf{z}^-)$ can in principle be found in the same manner as above. As those contractions are needed for every zCPHF iteration, however, it is sensible to exploit the fact that $\bar{\mathbf{z}}, \mathbf{z}^+, \mathbf{z}^-$ are symmetric in some off-diagonal blocks and zero everywhere else. Thus the exchange contribution is computed in a mixed AO/LMO basis as

$$[\mathbf{g}(\bar{\mathbf{z}})]_{pi} \approx \left([\mathbf{c}(\bar{\mathbf{z}})]_A J_A^{\mu\nu} L_{\mu i} - \frac{1}{2} c_{\nu j}^A z_{\tau j} J_A^{\mu\tau} L_{\mu i} - \frac{1}{2} c_{ij}^A z_{\tau j} J_A^{\nu\tau} \right) L_{\nu p} \tag{5.93}$$

using $z_{\mu j} = C_{\mu a} z_{aj}$ or

$$[\mathbf{g}(\mathbf{z}^+)]_{pm} \approx \left([\mathbf{c}(\mathbf{z}^+)]_A J_A^{\mu\nu} L_{\mu m} - \frac{1}{2} c_{\nu n}^A z_{\tau n}^+ J_A^{\mu\tau} L_{\mu m} - \frac{1}{2} c_{mn}^A z_{\tau n}^+ J_A^{\nu\tau} \right) L_{\nu p} \tag{5.94}$$

$$[\mathbf{g}^-(\mathbf{z}^-)]_{pt} \approx -\frac{1}{2} \left(c_{\nu u}^A z_{\tau u}^- J_A^{\mu\tau} L_{\mu t} + c_{tu}^A z_{\tau u}^- J_A^{\nu\tau} \right) L_{\nu p} \tag{5.95}$$

with $z_{\mu n}^{\pm} = C_{\mu x} z_{xn}^{\pm}$ and $z_{tu}^{\pm} = z_{ai}^- = 0$. The three-index integrals in AO basis, $J_A^{\mu\tau}$, are transformed using first $z_{\mu k}$ for one index and subsequently $L_{\mu i}$ for the second one. All half- and fully transformed fitting coefficients $c_{\nu j}^A$ and c_{ij}^A can be precomputed outside the zCPHF loop and stored on disk, and the computational effort is again $\mathcal{O}(N^2)$ [29].

5.7 Description of Solvent Effects using the Conductor-like Screening Model

Up until now, it was implicitly assumed that the systems investigated in this work are single molecules in the gas phase with negligible chemical environment, which is of course not true for

most chemical systems. As chemistry often happens in solution, a cheap and robust way to treat solvents during a geometry optimization would be desirable. The straight-forward approach of including a solvent into the quantum mechanical calculation might be precise, however, it is very expensive to do so; on the other hand, using cheap multipole expansions might not work for non-spherical systems. Thus, a general approach being both reasonably precise and affordable at the same time is to describe the electrostatic solvent-solute interaction using the conductor-like screening model (COSMO) [63]. In this ansatz, the investigated molecule is placed inside a cavity within a dielectric continuum representing the solvent. The cavity can be constructed by drawing spheres around the atoms of the solute molecule using atom-specific radii. According to the original publication, van der Waals radii increased by up to 20% are a reasonable choice; the current MOLPRO implementation has a database of optimized radii [111]. In a second step, grid points are placed on the cavity surface and subsequently the surface can be approximated by numerous small segments spanned between those points.

The interactions between the different segments S_γ on the cavity surface can be collected in a matrix $\mathbf{A}$, those between the solute nuclei and all surface segments in $\mathbf{B}$, and those between the solute electrons and surface segments in a vector $\mathbf{c}$ [63, 112]:

$$A_{\gamma\gamma} = 3.8 \frac{1}{|S_\gamma|^{1/2}} \tag{5.96}$$

$$A_{\gamma\theta} = \frac{1}{|\mathbf{t}_\gamma - \mathbf{t}_\theta|} \ \forall \ \gamma \neq \theta \tag{5.97}$$

$$B_{\gamma A} = \frac{1}{|\mathbf{t}_\gamma - \mathbf{R}_A|} \tag{5.98}$$

$$c_\gamma = -D_{\mu\nu}^{(0)} \langle \mu(1)| \frac{1}{|\mathbf{r}_1 - \mathbf{t}_\gamma|} |\nu(1)\rangle = D_{\mu\nu}^{(0)} L_{\mu\nu}^\gamma \tag{5.99}$$

The nuclear coordinates of atom A are collected in $\mathbf{R}_A$ and $\mathbf{t}_\gamma$ points at the center of a surface segment S_γ with surface area $|S_\gamma|$. For an ideal dielectric, the potential on the cavity surface, which is generated by the solutes charge distribution, vanishes due to the continuums response. Therefore, the continuum screening charge vector $\mathbf{q}^*$ reads

$$\mathbf{q}^* = -\mathbf{A}^{-1}(\mathbf{BZ} + \mathbf{c}). \tag{5.100}$$

with the nucleic charges Z_A collected in $\mathbf{Z}$. For finite dielectrics, this continuum charge can be scaled in good approximation to be

$$\mathbf{q} \approx f(\epsilon)\mathbf{q}^* \tag{5.101}$$

with

$$f(\epsilon) = \frac{\epsilon - 1}{\epsilon + x} < 1. \tag{5.102}$$

Here, ϵ is the relative dielectric permittivity of the solvent and x an empiric parameter recommended to be $x = 0.5$ for neutral molecules [63]; for $x = 0$ Gauss law is recovered [113].

During a HF calculation the screening charges are generated in every iteration from the current (charge) density matrix and added as external point charges $h_{\mu\nu}^{\text{diel}}, g_{\mu\nu}^{\text{diel}}$ to the Fock operators one- and two-electron contributions [112]:

$$h_{\mu\nu}^{\text{diel}} = -f(\epsilon)[\mathbf{Z}^\dagger \mathbf{B}^\dagger \mathbf{A}^{-1}]_\gamma L_{\mu\nu}^\gamma \tag{5.103}$$

$$g_{\mu\nu}^{\text{diel}} = -f(\epsilon)[\mathbf{c}^\dagger \mathbf{A}^{-1}]_\gamma L_{\mu\nu}^\gamma \tag{5.104}$$

with $L_{\mu\nu}^\gamma$ implicitly defined in eq. 5.99. After convergence, the dielectric contribution to the systems energy is

$$E_{\text{diel}} = D_{\mu\nu}^{(0)}(h_{\mu\nu} + \frac{1}{2}g_{\mu\nu}) - \frac{1}{2}f(\epsilon)\mathbf{Z}^\dagger \mathbf{B}^\dagger \mathbf{A}^{-1}\mathbf{B}\mathbf{Z} \tag{5.105}$$

and subsequently, the nuclear gradient contribution reads

$$E_{\text{diel}}^q = \mathbf{Z}^\dagger (\mathbf{B}^q)^\dagger \mathbf{q} + (\mathbf{c}^q)^\dagger \mathbf{q} + \frac{1}{2f(\epsilon)}\mathbf{q}^\dagger \mathbf{A}^q \mathbf{q}. \tag{5.106}$$

Both contributions can be added directly after the HF energy or gradient calculation, prior to further correlation energy treatment. As a convenient effect, the derivatives of the screening charges cancel and need thus not to be calculated [112]. The derivatives of $\mathbf{A}, \mathbf{B}$ and $\mathbf{c}$ with respect to an arbitrary perturbation q are

$$A_{\gamma\gamma}^q = 0 \tag{5.107}$$

$$A_{\gamma\theta}^q = -\frac{\mathbf{t}_\gamma - \mathbf{t}_\theta}{|\mathbf{t}_\gamma - \mathbf{t}_\theta|^3}(\Delta_{\gamma A} - \Delta_{\theta A}) \tag{5.108}$$

$$B_{\gamma A}^q = -\frac{\mathbf{t}_\gamma - \mathbf{R}_B}{|\mathbf{t}_\gamma - \mathbf{R}_B|^3}(\Delta_{\gamma A} - \delta_{AB}) \tag{5.109}$$

$$c_\gamma^q = -D_{\mu\nu}^{(0)}\langle\mu(1)|\frac{\mathbf{r}_1 - \mathbf{t}_\gamma}{|\mathbf{r}_1 - \mathbf{t}_\gamma|^3}|\nu(1)\rangle\Delta_{\gamma A} \tag{5.110}$$

where $\Delta_{\gamma A} = 1$ if S_γ is located at atom A, else $\Delta_{\gamma A} = 0$. Due to the neglect of the segment areas geometry dependence, the PES generated during a gradient calculation might not be smooth and numerical gradients can lead to slightly divergent results [63]. There are several different approaches available for subsequent COSMO-(L,R)MP2 calculations [111, 114]. Theoretically well justified and simple to implement, is a perturbation treatment based on the COSMO-HF

MO coefficients and Fock matrix. This way, the (L,R)MP2 procedure remains unchanged and the screening charges can be updated once at the end of the perturbation calculation, based on the second-order unrelaxed – or if available relaxed – charge density, and new energy and gradient contributions can be calculated from eqs. 5.105 and 5.106. This is called the PTE ansatz, and the solvent effects are consequentially considered only indirectly in the perturbation treatment.

6 Benchmark Calculations

In this chapter we will present selected calculations in order to demonstrate the gradient's precision and scope of applicability. In the first section, the newly developed closed-shell IBO gradients are tested against a test set of over one hundred small to medium-sized molecules as published by Friedrich and Hähnchen [64], referred to as the FH-set from now on. Further, we have augmented the FH-set by three molecules from the ISOL24 test set [65] as molecules with more than 30 atoms else would have been underrepresented. For the canonical open-shell gradients, we took on the task of computing the ionization potentials (IPs) of 24 molecules as reported by Sherrill and co-workers [66]; we will refer to this set as IP24. For some members of IP24 the NIST database available in reference [67] contains experimental values for comparison. Some of the IP24 ionization energies were additionally obtained using the implemented LRMP2 gradient scheme to assess errors introduced by the local approximations. Additionally, radical stabilization energies for a set of 30 reactions as discussed by Liu [21] have been obtained using LRMP2-gradients. Finally, we investigated the ground state of an iron complex discussed in [68] and [69] in order to demonstrate the gradient's overall applicability to larger molecules – in this case containing 175 atoms and five unpaired electrons.

In the following sections, most bond lengths, and bond and dihedral angles will be discussed using statistical quantities, with MAE denoting the mean absolute error defined as

$$\text{MAE} = \frac{\sum_{i=1}^{n} |q_i - r_i|}{n}, \tag{6.1}$$

where q_i and r_i are the results of a method and the respective reference, and n is the number of values to be compared in total. The root-mean-square deviation (RMS) is defined similarly as

$$\text{RMS} = \sqrt{\frac{\sum_{i=1}^{n} (q_i - r_i)^2}{n}}, \tag{6.2}$$

and MAX is simply the largest value of the n absolute differences $|q_i - r_i|$.

6.1 Closed-Shell Gradients

In order to investigate the influence of the new IBO-LMP2 gradients on molecules of different sizes, the 104 closed-shell systems included in our extended FH-set were divided into four groups depending on their number of atoms, as shown in tab. 6.1. We excluded H_2, originally contained

	N_{at}	Systems
Group 1	$2 - 9$	15
Group 2	$10 - 19$	65
Group 3	$20 - 29$	21
Group 4	$30 - 39$	5
Total	$2 - 39$	106

Table 6.1: Subgroups of the extended FH-set divided depending on the molecule's number of atoms N_{at}, and the number of systems per group.

in the FH-set [64], from group 1, and group 4 was augmented by the educts of reactions $9 - 11$ of the ISOL24 benchmark database [65]. Tab. 6.2 shows the overall performance of the Pipek-Mezey (PM) and Intrinsic Bond Orbital (IBO) localization schemes on DF-LMP2 level relative to a canonical DF-MP2 reference. We have performed calculations for both possible IBO localization

	Length (bohr)			Angle (deg)		
Iext	0	1	2	0	1	2
IBO exponent $p = 4$						
MAE	0.0029	0.0007	0.0002	0.054	0.020	0.013
RMS	0.0046	0.0012	0.0004	0.086	0.033	0.022
MAX	0.0246	0.0068	0.0033	1.048	0.287	0.184
IBO exponent $p = 2$						
MAE	0.0030	0.0007	0.0002	0.054	0.020	0.013
RMS	0.0048	0.0012	0.0004	0.085	0.033	0.022
MAX	0.0236	0.0067	0.0033	1.018	0.288	0.184
PM						
MAE	0.0031	0.0007	0.0002	0.062	0.020	0.013
RMS	0.0049	0.0013	0.0004	0.099	0.034	0.023
MAX	0.0244	0.0072	0.0032	0.992	0.285	0.183

Table 6.2: DF-LMP2/AVTZ' errors relative to DF-MP2/AVTZ' in the full extended FH-set. Shown: bond lengths and bond and dihedral angles.

exponents, $p = 2$ and $p = 4$, and all quantities are either given in Bohr (bohr) for bond lengths or degrees (deg) for bond and dihedral angles. Primary domains were generated based on IAO partial charges with $q_{ii}^A \geq 0.15$. As discussed earlier, subsequent pair domains can then be

extended using a connectivity criterion; the parameter Iext counts the number of neighbouring shells included, with Iext=1 being all atoms adjacent to the primary domain, Iext=2 all atoms adjacent to atoms within to the Iext=1 domain, and so on. Iext=0 indicates no extension. All calculations were performed in a correlation-consistent augmented triple-zeta Dunning orbital basis (AVTZ), using its non-augmented triple-zeta pendant VTZ for H-atoms; we will use AVnZ' as shorthand notation for AVnZ, H=VnZ from now on. VTZ was additionally used as fitting basis for DF-HF and DF-(L)MP2 calculations. Energy thresholds were tightened to 10^{-10} a.u., CPL accuracy required to be 10^{-8} a.u., and gradients considered converged below a norm of 10^{-5} a.u.. Core correlation effects were neglected.

Figs. 6.1 to 6.3 show the same data as tab. 6.2, but in relation to the four different size-groups. It can be seen that all three methods perform rather well, with only minor differences for different localization schemes. At first, this seems to be contradictory as PM is based on mathematically ill defined Mulliken gross charges and should thus experience difficulties in a diffuse basis set such as AVTZ'. In order to keep domain sizes equivalent across different methods, however, all PM calculations presented here use IAO partial charges for domain generation. This is necessary to ensure comparable results, as the domain size strongly influences a local method's accuracy, as can be seen from the results for different values of Iext. Yet, employing IAO partial charges for domain generation partly compensates the drawbacks of the PM localization scheme making it look more robust than it actually is. If based on Mulliken charges and for approximately similar average domain sizes, in our experience PM geometry optimization is less stable for diffuse basis sets or basis set changes – an observation consistent with those made for LMP2 single point calculations. In general, the larger the domain size, the closer the results to the canonical MP2 solution with Iext=1 being a suitable trade-off between precision and computational cost, even for larger systems as contained in group 4. The results for bond and dihedral angles follow the same general trends as those for bond lengths and are thus not plotted separately. A full set of statistical data for the four different groups, including bond and dihedral angles, is available in appendix 1.

There are two systems that deserve a closer look: Fig. 6.3 shows an unexpected large MAX error for PM Iext=0 in group 2. The molecule responsible for this deviation is a linear system:

$$HC^{(1)}{\equiv}C^{(3)}{-}C^{(4)}{\equiv}C^{(5)}{-}C^{(6)}{\equiv}C^{(7)}{-}C^{(8)}H_3$$
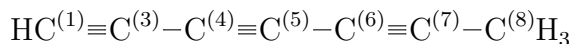
Tab 6.3 lists the signed errors of DF-LMP2 relative to DF-MP2 for the individual $C{-}C$ bond lengths and supplementary statistical data, with a negative number indicating the bond length being underestimated. The C-atoms are enumerated (1) and (3)-(8); this enumeration is consistent with MOLPROs internal labels for the system in question. One can see that both localization schemes tend to underestimate triple- and overestimate single-bonds for Iext=0.
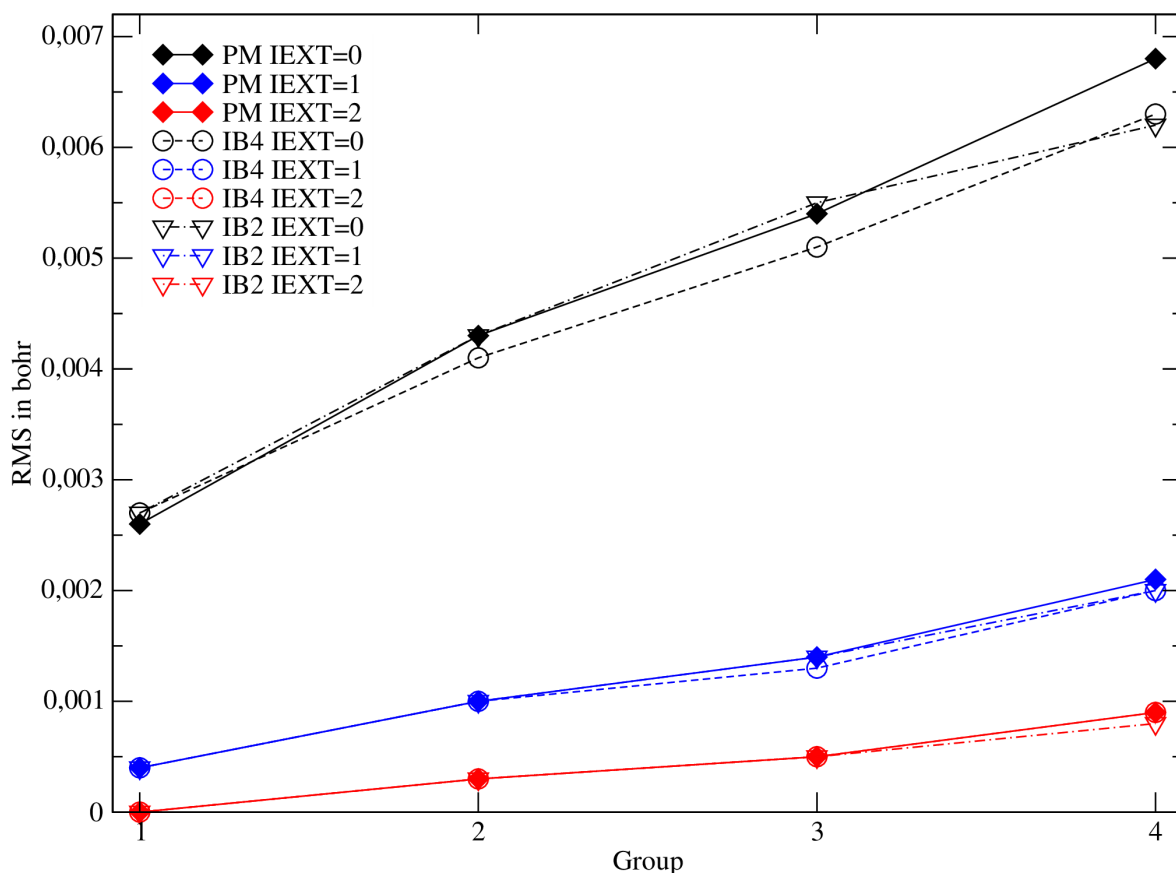
Figure 6.1: RMS of bond lengths for groups $1-4$, DF-LMP2/AVTZ' errors relative to a canonical DF-MP2/AVTZ' reference for Pipek-Mezey (PM), IBO exponent $p = 4$ (IB4), and IBO exponent $p = 2$ (IB2).

Bond	PM	IBO $p = 2$	IBO $p = 4$
1-3	-0.0027	-0.0019	-0.0020
3-4	0.0115	0.0112	0.0112
4-5	-0.0168	-0.0055	-0.0056
5-6	0.0231	0.0133	0.0135
6-7	-0.0167	-0.0030	-0.0031
7-8	0.0066	0.0097	0.0097
Sum	0.0050	0.0237	0.0238
Statistics			
RMS	0.0114	0.0066	0.0067
MAE	0.0084	0.0045	0.0046

Table 6.3: Signed errors of DF-LMP2 relative to DF-MP2 for the individual $C-C$ bond lengths in $HC \equiv C - C \equiv C - C \equiv C - CH_3$ (negative is under-estimation), and supplementary statistical data. Sum is the total error along the $C-C$-axis; all data are given in bohr.
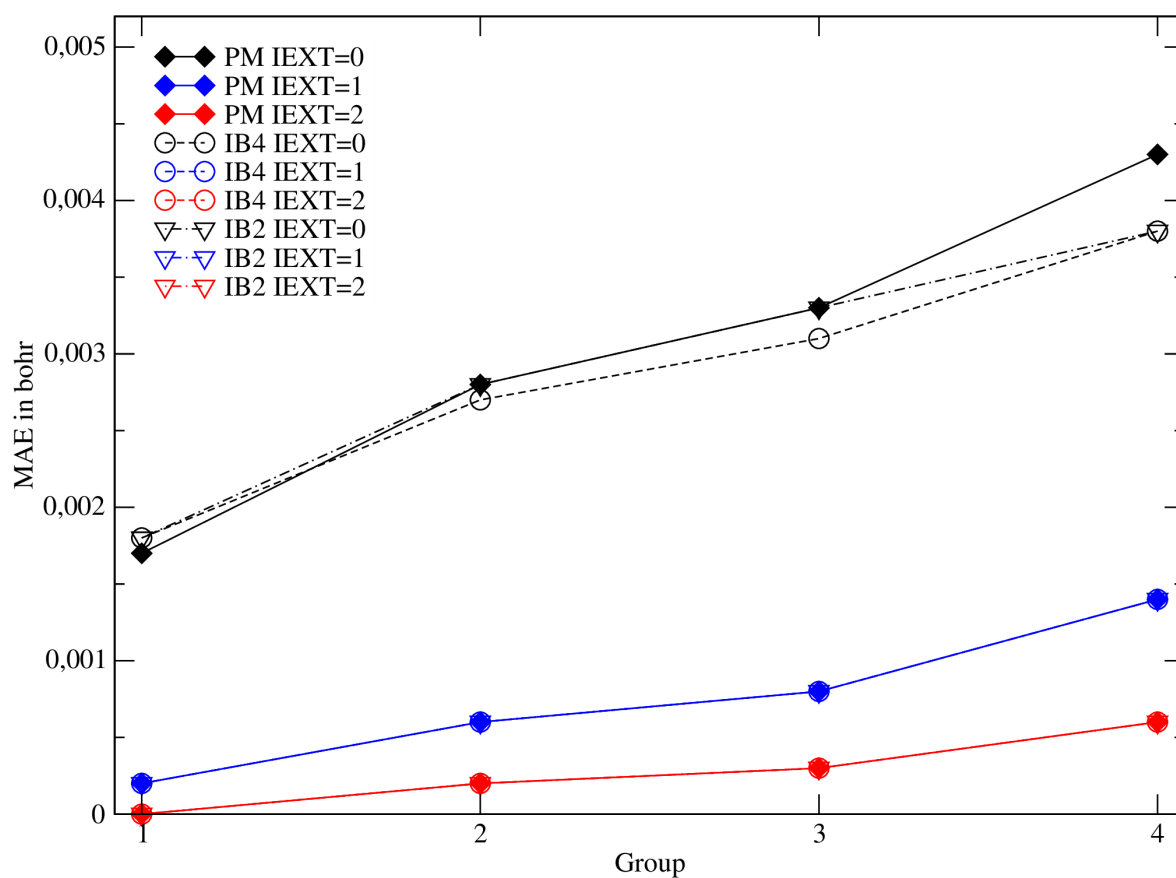
Figure 6.2: MAE of bond lengths for groups $1-4$, DF-LMP2/AVTZ' errors relative to a canonical DF-MP2/AVTZ' reference for Pipek-Mezey (PM), IBO exponent $p = 4$ (IB4), and IBO exponent $p = 2$ (IB2).
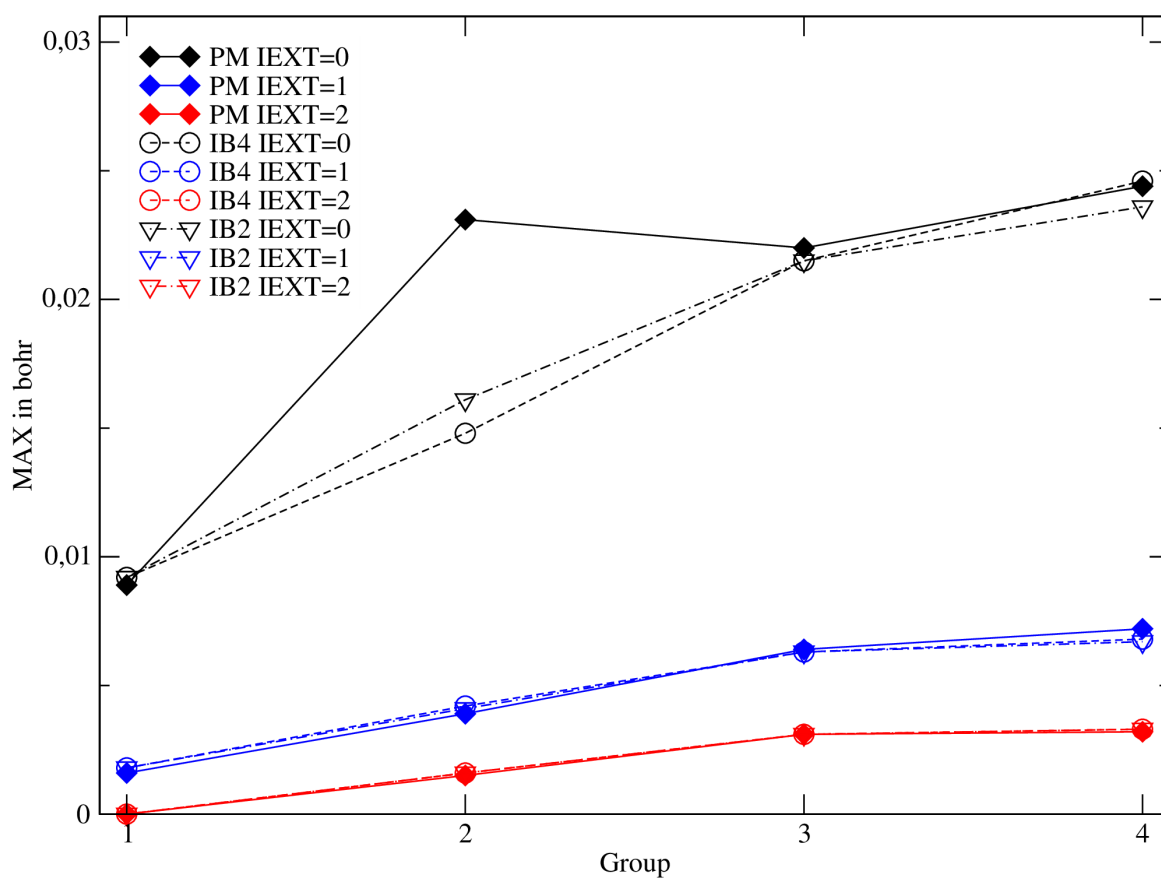
Figure 6.3: MAX of bond lengths for groups $1 - 4$, DF-LMP2/AVTZ' errors relative to a canonical DF-MP2/AVTZ' reference for Pipek-Mezey (PM), IBO exponent $p = 4$ (IB4), and IBO exponent $p = 2$ (IB2).

Yet, using IBOs the σ-bond between atoms (5) and (6) is correctly described by a single orbital with a partial charge of 1.990 at those two centres, and there are two separate, degenerate π-orbitals extending over atoms (4)-(7). This is true for both localization exponents. Contrary to this, PM localizes the σ-orbital with significant contributions not just from atoms (5) and (6) – combined partial charge 1.793 –, but also atoms (4), (7), and (8) – combined partial charge 0.174 –; the generated π-orbitals are similar to their IBO pendants. Thus, the primary domain generated from the PM σ-orbital is noticeably larger, leading to an over-proportional recovery of correlation energy for this particular orbital. This surplus in correlation energy results in the bond-length of atoms (5)-(6) being increased, whereas neighbouring bonds are shortened. Furthermore, due to the localization tails present in most PM σ-orbitals domain changes occur during geometry optimization, leading to an unstable convergence, whereas for IBOs convergence is smooth. The final LMO composition for all three schemes can be found in appendix 1. As soon as the PM primary domains are extended using at least Iext=1, the recovery of correlation energy in different parts of the molecule will be more balanced and the problem vanishes. Despite these issues with PM localization we decided to keep the system in our benchmark as the generated geometry is still intact, with the system's main features such as linearity of the C-chain and $C^{(8)}-H$ bond length symmetry being correctly recovered. The total extent of the system along the axis of C-atoms is even closer to the RMP2 reference for PM than it is for IBOs, as the larger PM errors cancel more favourably. Still, we would like to recommend IBOs as means of localization for this particular system, as they deliver better overall result on a more profound theoretical basis.

The other system to be discussed is anthracene (*cf.* fig 6.4), a member of group 3, which was excluded from the analysis above, as there was no convergence reached for Iext=0 using IBO $p = 4$. Initially, all local optimizations for anthracene were found to be difficult, as the structure supplied in the original test set was not symmetry adapted; this leads to a mixing of σ- and π-orbitals. After improving the initial geometry, PM and IBO $p = 2$ would formally converge, but even if full π-domains were used, dipole moments would be predicted and the quality of the resulting structures was dissatisfying. This behaviour is due to the localized π-orbitals breaking the molecule's symmetry, reducing it from D_{2h} to C_{2v}. Even with π-domains symmetrized, the π-orbitals 'above' and 'below' the aromatic plane would still not be symmetry-adapted, with two orbitals localized on one side of the middle ring, and just one LMO on the other. Furthermore, extending the middle ring's domains manually over all six atoms to enforce symmetrization
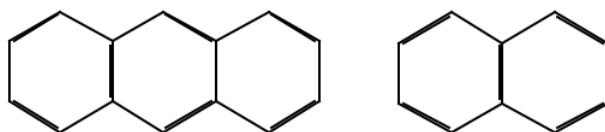
Figure 6.4: Anthracene (left) and naphthalene (right).

	Length (bohr)			Angle (deg)		
Iext	0	1	2	0	1	2
	IBO exponent $p = 4$					
MAE	$0.0082^{(1)}$	0.0011	0.0002	$0.090^{(1)}$	0.010	0.006
RMS	$0.0119^{(1)}$	0.0015	0.0004	$0.112^{(1)}$	0.012	0.008
MAX	$0.0242^{(1)}$	0.0035	0.0006	$0.223^{(1)}$	0.030	0.019
	IBO exponent $p = 2$					
MAE	0.0067	0.0010	0.0002	0.074	0.010	0.007
RMS	0.0098	0.0014	0.0003	0.088	0.012	0.008
MAX	0.0196	0.0031	0.0006	0.216	0.030	0.019
	PM					
MAE	0.0075	0.0010	0.0002	0.074	0.013	0.007
RMS	0.0106	0.0014	0.0004	0.099	0.017	0.009
MAX	0.0225	0.0031	0.0006	0.243	0.038	0.019

Table 6.4: Errors of DF-LMP2/AVTZ' geometry optimizations relative to DF-MP2/AVTZ' for anthracene. [1]Structure not converged.

resulted in the outer orbitals being slightly non-symmetric, and dipole moments remaining present in x-direction. From this investigation, we can now understand why IBO $p = 4$ would fail entirely: A higher exponent on the localization functional enforces a stronger localization by punishing localization tails (*cf.* section 3.2), and with orbitals already over-localized, this behaviour is not helpful in finding a physically meaningful description of the system. A similar molecule included to the original FH-set is naphthalene, which did not pose a problem and is thus included into our analysis. Benzene and other related aromatic systems are not members of the FH-set; tabs. 6.4 and 6.5 show the results for anthracene, and for comparison, naphthalene. In general, localization of delocalized electrons as encountered in aromatic systems can be difficult in local correlation methods.

To classify the significance of the local errors reported above, we repeated the calculations for group 2 using a quadruple-zeta orbital basis (AVQZ') to quantify the basis set error. We also performed geometry optimizations using non-density fitted MP2/AVTZ' and DF-CCSD(T)/AVTZ' gradients to investigate density-fitting and method errors. Due to the cost of coupled-cluster singles and doubles with perturbative triples correction (CCSD(T)) gradients, only a subset of 12 molecules from group 2 as listed in tab. 6.6 was used to estimate the method's error. Additionally, numerical optimizations using a four-point formula were performed for DF-LMP2/AVTZ' ($p = 4$, Iext=0) to ensure proper implementation of the presented analytic gradients. Tab. 6.7 contains the aggregated results. From those results, we can conclude that density fitting only induces very minor errors and that the localization errors even for Iext=0 are small compared to the method's intrinsic error. Basis set incompleteness errors are in the same

Iext	Length (bohr)			Angle (deg)		
	0	1	2	0	1	2
IBO exponent $p = 4$						
MAE	0.0028	0.0006	0.0001	0.035	0.006	0.003
RMS	0.0043	0.0010	0.0002	0.043	0.008	0.004
MAX	0.0081	0.0020	0.0005	0.085	0.020	0.009
IBO exponent $p = 2$						
MAE	0.0071	0.0007	0.0002	0.067	0.005	0.003
RMS	0.0099	0.0012	0.0002	0.077	0.007	0.004
MAX	0.0161	0.0023	0.0005	0.155	0.019	0.011
PM						
MAE	0.0073	0.0007	0.0002	0.090	0.005	0.004
RMS	0.0100	0.0012	0.0002	0.119	0.007	0.004
MAX	0.0173	0.0023	0.0005	0.212	0.019	0.011

Table 6.5: Errors of DF-LMP2/AVTZ' geometry optimizations relative to DF-MP2/AVTZ' for naphthalene.

Number	Name
1	Pentadiene
2	Methylfurane
3	Methylpyrrole
4	Methylpyrazole
5	Methylimidazole
6	2-Pentyne
7	$C_2H_5CONH_2$
8	$C_2H_5CO_2H$
9	$C_2H_5NH_2$
10	1-Pentyne
11	1-Pentene
12	C_3H_7CN

Table 6.6: Subset of 12 molecules from group 2 used for DF-CCSD(T)/AVTZ' gradient optimization. Names consistent with supporting information of [64].

	Length (bohr)	Angle (deg)
Method[2]		
MAE	0.0076	0.140
RMS	0.0090	0.201
MAX	0.0274	0.991
Basis set[1]		
MAE	0.0034	0.035
RMS	0.0042	0.060
MAX	0.0274	0.645
Density fitting[1]		
MAE	0.0001	0.002
RMS	0.0001	0.005
MAX	0.0006	0.107
Numerical[1]		
MAE	0.0000	0.001
RMS	0.0000	0.002
MAX	0.0001	0.027

Table 6.7: Method, basis set, and density fitting errors relative to DF-MP2/AVTZ', as well as numerical relative to analytic DF-LMP2/AVTZ' gradient performance. Calculations performed either (1) on all molecules in group 2 or (2) a subset of 12 systems as listed in tab. 6.6.

order of magnitude as localization errors for Iext=0, but the latter become negligible for Iext=1 or higher, where the local errors are smaller by at least a factor of two. With all the discussions above in mind (*cf.* HC≡C−C≡C−C≡C−CH$_3$), we thus recommend using at least Iext=1 for reliable results. Further extension to Iext=2 will again improve results by at least another factor of two towards the canonical reference, if an even higher level of precision is needed. Numerical results show that the newly developed gradient theory and its implementation seem to be without any errors.

As all statistical data discussed so far was generated from absolute (unsigned) differences, we do not know yet if, for instance, the error due to local approximations and the method error of MP2 are additive or if there is a form of error compensation. Fig 6.5 thus shows the performance of DF-MP2 and DF-LMP2 (IBO, $p = 4$) calculations relative to DF-CCSD(T) for the 12 selected molecules from group 2; all calculations were performed in an AVTZ' basis. In general, HF has a known tendency to underestimate bond lengths due to the absence of electron correlation. As can be seen, DF-MP2 overcompensates this tendency, whereas DF-LMP2, limiting correlation correction due to local approximations, produces rather reasonable results based on error compensation. All data used for this plot can be found in appendix 1.
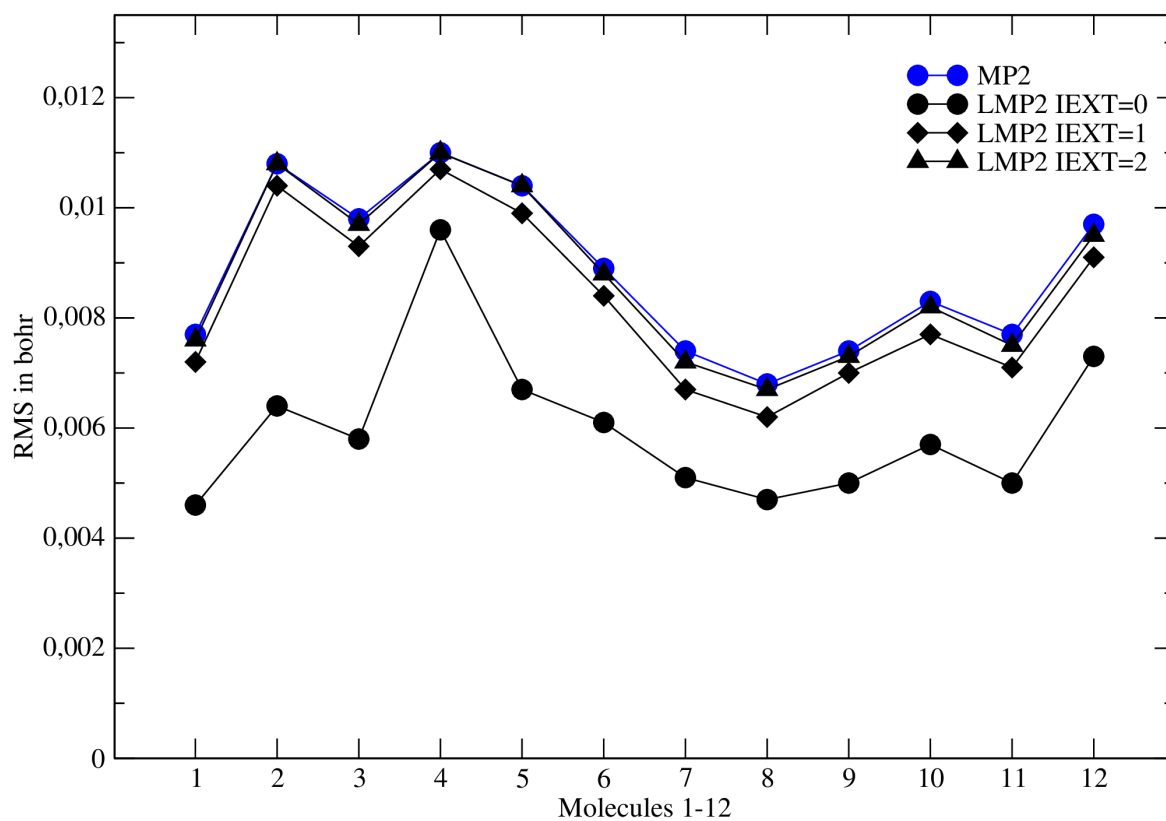
Figure 6.5: Performance of DF-MP2 and DF-LMP2 (IBO, $p = 4$) gradients relative to DF-CCSD(T) gradients; all calculations performed in AVTZ'. Molecules enumerated consistent with tab. 6.6.

6.2 Ionization Potentials

Recently, Sherrill and co-workers published a benchmark set of 24 molecules used for organic photovoltaics and other applications in organic electronics design [66]. Fig. 6.6 depicts all 24 systems, which will be called the IP24 set from now on. In the original work, all molecular
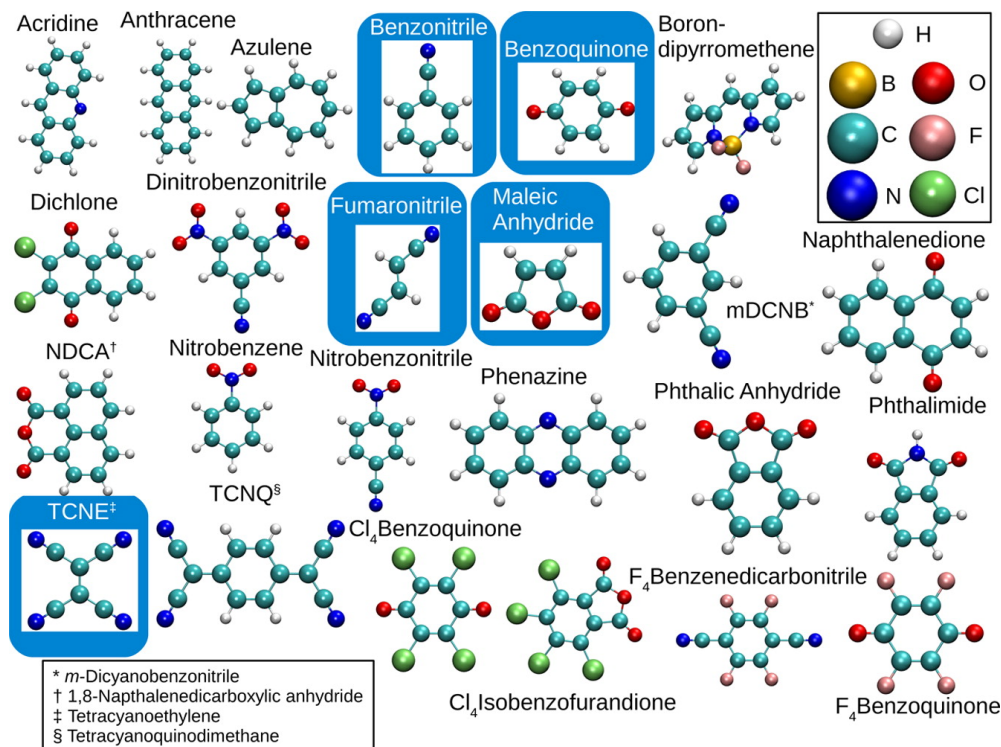
Figure 6.6: Molecules of the IP24 test set [66]. Molecules in blue boxes were treated at higher levels of theory in the original publication.

structures were optimized at the DFT(B3LYP)/6-311G** level, with the geometry constrained to the molecule's highest available point group symmetry. Except for one system, only closed-shell structures were optimized, and there was no attempt made to calculate any relaxed cation geometries. Single point energies were subsequently obtained using basis-set extrapolated RMP2 energies corrected by a δ-RCCSD(T) contribution, as suggested by the theoretical framework of focal point analysis. The coupled-cluster level δ-correction is thereby defined as the difference between an RMP2 and RCCSD(T) calculation in a given small to medium sized basis set. It is assumed to be mostly basis set independent, as higher-order correlation effects are expected to converge faster to the complete basis-set limit.

From the resulting energies, IPs can be calculated as

$$\text{IP} = E_c - E_n, \tag{6.3}$$

where E_c is the cation's energy, and E_n the energy of the neutral species. If both, E_c and E_n,

are obtained at the same molecular geometry, the IP is called a vertical IP. If the cation's geometry is optimized separately prior to calculation of E_c (we call this 'relaxation' of the cation's geometry), the IP is referred to as adiabatic IP. The authors used the vertical IPs obtained in subsequent publications for calibration of different empirical methods in order to predict IPs in different donor-acceptor systems [115–117]. Having not optimized the cation structures separately, no adiabatic IPs are given in the original publication.

In order to improve the reported results, we used our newly developed canonical RMP2 gradients, along with closed-shell MP2 gradients, to optimize the reported geometries in a correlation-consistent augmented triple-zeta Dunning basis set for all atoms except hydrogen, where we used a non-augmented correlation-consistent triple-zeta Dunning basis (abbreviated as AVTZ'). Subsequently, adiabatic and vertical IPs were calculated based on CCSD(T)/AVTZ' single point energies for neutral systems, and RHF-UCCSD(T)/AVTZ' energies for cations; we did this for all systems except borondipyrromethene. In case of borondipyrromethene, due to the large system size single points were calculated using DF-LCCSD(T)/AVTZ' and DF-RHF-DF-LUCCSD(T)/AVTZ' with VTZ fitting basis and PM Iext=1 localization. Energy thresholds were tightened to 10^{-10} a.u. in all calculations, gradients considered converged below a norm of $3 \cdot 10^{-4}$ a.u., and core correlation effects neglected. As in the original work, we restricted the molecules to the highest available point group. Molecular orientation was preserved during our geometry optimizations to keep irreducible representations (irreps) comparable to the reference. Cation geometries and single point energies were calculated not only for the irrep of the HF-level highest occupied molecular orbital (HOMO) of the neutral species, but for every irrep of the molecule's point group. This additional work is necessary, as the smallest adiabatic IP is not guaranteed to be the difference between the neutral species and the relaxed cation matching the HF HOMO's irrep. Whenever multi-reference states hindered application of our single-determinant methods, the state in question would be excluded from further considerations. The full set of coupled-cluster level adiabatic IPs for every irrep can be found in appendix 2.

Tab. 6.8 lists the smallest of the obtained adiabatic IPs for every molecule, along with the irrep of the cation. Vertical IPs were calculated using the same symmetry. Whenever the HF HOMO's irrep or the irrep from the original publication was different to ours, results for both states were given. Additionally, the vertical IPs as reported by Sherrill and co-workers, and experimental data [67] are listed for comparison. Despite being not extrapolated to the basis set limit, on the one hand, the overall precision of our calculations seems to be slightly more in agreement with experiment. In case of the vertical IPs, this might be mainly due to the fact that basis set extrapolations and focal point analysis are arbitrary concepts with empirical character and, especially for open-shell systems, not always well defined. Moreover, the underlying geometries may not be as accurate. On the other hand, the authors argue that the experimental IPs are imprecise as well, and can be off by up to 1 eV, depending on experiment and quality of data

Molecule	PG	Irrep	EXP	A/CC	V/CC	V/REF
Acridine	C_{2v}	B_1	7.8	7.86	7.91	8.04
Anthracene	D_{2h}	B_{1g}	7.44	7.36	7.40	7.52
Azulene	C_{2v}	A_2	7.42	7.32	7.45	7.55
Benzonitrile	C_{2v}	B_1	9.73	9.72	9.84	9.93
Benzoquinone	D_{2h}	$B_{2g}/B_{3g}^{(1,2)}$	10.0	10.14(10.97)	10.19(11.11)	10.27
Borondipyrromethene	C_s	A''	-	6.68*	7.23*	8.07
Dichlone	C_{2v}	$B_1/A_2^{(1,2)}$	9.5	9.62(9.81)	9.75(10.00)	9.99
Dinitrobenzonitrile	C_{2v}	B_1	-	10.87	11.02	11.15
Fumaronitrile	C_{2h}	A_u	11.3^v	11.19	11.30	11.48
Maleic Anhydride	C_{2v}	$B_2/B_1^{(2)}$	11.07^v	11.13(11.83)	11.19(11.99)	11.33
mDCNB	C_{2v}	A_2	10.20	10.22	10.33	10.45
Naphthalenedione	C_{2v}	A_2	9.5	9.63	9.82	9.88
NDCA	C_{2v}	A_2	8.92	8.94	9.04	9.14
Nitrobenzene	C_{2v}	$A_2/A_1^{(2)}$	9.94	9.94(11.07)	10.12(11.26)	10.19
Nitrobenzonitrile	C_{2v}	B_1	10.59	10.38	10.50	10.62
Phenazine	D_{2h}	B_{3g}	8.44	8.29	8.34	8.47
Phthalic Anhydride	C_{2v}	A_2	10.1^a	10.28	10.47	10.55
Phthalimide	C_{2v}	$B_1/A_2^{(2)}$	9.9^v	9.84(9.91)	10.00(10.10)	10.08
TCNE	D_{2h}	B_{1u}	11.79^a	11.71	11.77	11.99
TCNQ	D_{2h}	B_{1u}	-	9.38	9.39	9.57
Cl$_4$-Benzoquinone	D_{2h}	B_{3g}	9.74^a	9.89	9.99	10.25
Cl$_4$-Isobenzofurandione	C_{2v}	A_2	10.8	9.71	9.87	10.05
F$_4$-Benzenedicarbonitrile	D_{2h}	B_{3g}	10.65^v	10.30	10.61	10.76
F$_4$-Benzoquinone	D_{2h}	B_{3g}	10.7^a	10.70	10.97	11.14

Table 6.8: IPs in eV for 24 different molecules with experimental values (EXP) labelled as adiabatic ([a]) or vertical ([v]) if known. V/REF are the vertical IPs as given in [66], V/CC and A/CC the respective vertical and adiabatic IPs on RHF-UCCSD(T) level, based on RMP2 gradients (all AVTZ'). Irreps default to the relaxed cations smallest IP, alternatives listed if different in reference[1] or HF HOMO[2]. Alternative IPs in brackets, (*) calculated using DF-LUCCSD(T). Molecular orientation as in reference [66].

available. Thus it would be dubious to claim that our method is the overall better solution – it is, however, resting on a more profound theoretical basis. As in the original publication, we have neglected core correlation, zero-point vibrations, and relativistic effects, which as stated, seems to cause only insignificant errors. There are, however, two important lessons to be learned from our adiabatic calculations: Firstly, the effect of cationic geometry relaxation is significant, and a test set for training other methods should take such relaxation into account. And secondly, adiabatic IPs do help to identify the right state for calculating vertical IPs, as can be seen for instance for benzoquinone or dichlone. As expected, adiabatic IPs are always smaller than vertical IPs due to the adiabatic E_c contribution being calculated at the minimum of the cationic PES, whereas the vertical E_c energies are not.

To further investigate the remaining errors in our data, we repeated our coupled-cluster calculations using the explicitly correlated CCSD(T)-F12/AVTZ' and RHF-UCCSD(T)-F12/AVTZ' methods. Explicitly correlated methods yield results close to the basis set limit of the underlying method [118, 119]. Tab. 6.9 lists the results obtained using the F12b approximation for coupled-cluster single point energies, based on our (R)MP2 geometries, in comparison to the experimental values discussed previously. As borondipyrromethene was to expensive for canonical RHF-UCCSD(T) treatment and has no known experimental value, it was omitted in the F12 calculations. In appendix 2 additional data using the F12a ansatz is listed, although the results differ only slightly. As can be seen, taking correlation into account explicitly increases both, the vertical and adiabatic IPs. As the effect for both types of IP is of similar extent, we do not believe the increase to be related to the underlying geometries, but to a better description of the unpaired electrons' correlation energy in F12 methods. This leads to a stronger increase of E_c as compared to E_n, resulting to slightly larger IPs.

In order to additionally demonstrate the LRMP2/AVTZ' gradient's precision, a subset of 12 molecules from IP24 was re-optimized using PM and IBO $p = 4$ localization schemes with IAO partial charges $q_{ii}^A \geq 0.15$ and pair domains extended by Iext=1. Starting geometry for cations was the RMP2/AVTZ' geometry which yielded the lowest adiabatic IP in a given molecule and there was no symmetry restriction, as symmetry is only available for canonical RMP2 gradients. Energy thresholds were tightened to 10^{-10} a.u., CPL accuracy required to be 10^{-8} a.u, and gradients considered converged below a norm of 10^{-5} a.u. Tab. 6.10 contains the bond lengths and angles aggregated statistical data for the cations, relative to the structures obtained using canonical RMP2 gradients. We have additionally calculated the mean errors of LRMP2/AVTZ' adiabatic IPs relative to RMP2/AVTZ' IPs. LRMP2 IPs were thereby based on the respective LRMP2 optimized structures, and canonical IPs on RMP2 structures. As can be seen, the effect on the optimized geometries is of similar extent as for local closed-shell gradients, and the deviation of adiabatic is IPs negligible. The latter might be partly due to the fact that the investigated molecules are only of medium size, and partly due to error

Molecule	EXP	A/CC-F12	V/CC-F12
Acridine	7.8	7.91	7.95
Anthracene	7.44	7.40	7.44
Azulene	7.42	7.37	7.50
Benzonitrile	9.73	9.78	9.90
Benzoquinone	10.0	10.22	10.27
Dichlone	9.5	9.66	9.82
Dinitrobenzonitrile	-	10.94	11.09
Fumaronitrile	11.3^v	11.26	11.36
Maleic Anhydride	11.07^v	11.22	11.29
mDCNB	10.20	10.29	10.39
Naphthalenedione	9.5	9.68	9.86
NDCA	8.92	9.01	9.10
Nitrobenzene	9.94	10.00	10.16
Nitrobenzonitrile	10.59	10.45	10.56
Phenazine	8.44	8.34	8.38
Phthalic Anhydride	10.1^a	10.34	10.53
Phthalimide	9.9^v	9.90	10.05
TCNE	11.79^a	11.80	11.85
TCNQ	-	9.45	9.46
Cl_4-Benzoquinone	9.74^a	9.93	10.07
Cl_4-Isobenzofurandione	10.8	9.77	9.95
F_4-Benzenedicarbonitrile	10.65^v	10.37	10.70
F_4-Benzoquinone	10.7^a	10.76	11.05

Table 6.9: IPs in eV for 23 different molecules with experimental values (EXP) labelled as adiabatic (^{a}) or vertical (^{v}) if known. V/CC-F12 and A/CC-F12 are the respective vertical and adiabatic IPs on RHF-UCCSD(T)-F12b/AVTZ' level. Irreps default to the relaxed cations smallest IP, tab. 6.8. Molecular orientation as in reference.

	Length (bohr)	Angle (deg)	IP (eV)
	IBO exponent $p = 4$		
MAE	0.0008	0.015	0.01
RMS	0.0013	0.020	0.01
MAX	0.0048	0.068	0.02
	PM		
MAE	0.0008	0.018	0.01
RMS	0.0013	0.022	0.01
MAX	0.0047	0.072	0.03

Table 6.10: Localization errors relative to (R)MP2/AVTZ'. Calculations performed on molecules listed in tab. 6.11.

cancellation: Assuming almost equivalent domain sizes in the neutral species and in the cation, the correlation energy missing due to local approximations is roughly equivalent for both systems and will cancel when calculating the IP. To put the localization errors further into perspective, tab. 6.11 lists all (L)MP2-level adiabatic IPs additionally to our best theoretical estimate, the RHF-UCCSD(T)-F12b/AVTZ' adiabatic IPs reported in tab 6.9. Here we can see that despite

Molecule	A/CC-F12	Canon	IB	PM
Anthracene	7.40	7.29	7.28	7.27
Azulene	7.37	7.43	7.42	7.41
Benzonitrile	9.78	9.81	9.80	9.80
Dinitrobenzonitrile	10.94	11.00	10.98	10.98
Fumaronitrile	11.26	11.29	11.29	11.29
Maleic Anhydride	11.22	12.00	12.00	12.00
mDCNB	10.29	10.28	10.27	10.27
Naphthalenedione	9.68	9.76	9.75	9.73
Nitrobenzene	10.00	10.07	10.06	10.06
Nitrobenzonitrile	10.45	10.42	10.41	10.41
Phthalimide	9.90	10.03	10.02	10.01
TCNE	11.80	11.76	11.74	11.74

Table 6.11: Adiabatic IPs on RMP2/AVTZ' level in eV for 12 different molecules using canonical (Canon) and LRMP2 gradients with IBO $p = 4$ (IB4) and Pipek-Mezey (PM) localization. RHF-UCCSD(T)-F12b values for comparison.

the methods error being relatively small, the local error is even smaller. One has to keep in mind that the LRMP2 IPs are in turn based on local gradient optimized structures, whereas coupled-cluster level and RMP2 IPs are based on canonical RMP2 structures. Thus local single points in above comparison are influenced twice by local approximations: Once directly due to local approximations in the energy calculation, and once indirectly due to local approximations embedded in the geometry. Furthermore, most of the molecules above contain aromatic systems difficult to localize. Even for anthracene, as discussed earlier, and naphthalenedione, where convergence of the geometry optimization was not perfectly smooth either, the resulting IPs are very close to the canonical reference without additional domain extension, and the overall precession of local IPs is excellent. In our opinion, this demonstrates that local methods are a justified replacement for both, single points and gradients and can be applied with confidence to molecules being too large for treatment with canonical methods.

6.3 Radical Stabilization Energies

This test set, referred to as R30, was taken from a dissertation written at our institute in 2011 [21]. Its radical stabilization energy is defined as

$$R-H + CH_3 \cdot \longrightarrow R \cdot + CH_4,$$

with 30 different R-groups used in the original work. The original structures were optimized using DFT(B3LYP)/cc-pv(T+d)Z, and energies subsequently calculated on DF-RMP2/cc-pv(T+d)Z and DF-LUCCSD(T)/cc-pv(T+d)Z level. We have reoptimized the structures for this work using our newly developed RMP2 and DF-LRMP2 gradients, as well as numerical RCCSD(T) gradients for comparison. The radical stabilization energies of the original work as well as our results on (L)RMP2 level can be found in tab. 6.12. For consistency, we continued to use the cc-pv(T+d)Z basis set in our calculations. Energy thresholds were tightened to 10^{-10} a.u. in all calculations, gradients were considered converged below a norm of $3 \cdot 10^{-4}$ a.u., and core correlation effects neglected. In local calculations, CPL accuracy was required to be at least 10^{-8} a.u., and, with no aromatic systems present, IAO partial charges were set to $q_{ii}^A \geq 0.2$. PM domain selection was again based on IAO charges.

Compared to the original DF-RMP2 energies calculated on top of DFT(B3LYP) optimized structures, our DF-RMP2 results based on DF-RMP2 level geometries are very similar, deviating by less than 2 kJ/mol. We have additionally listed DF-LRMP2 radical stabilization energies calculated using DF-LRMP2 optimized structures. Due to the rather small systems in the test set, we have limited the domain extension in local calculations to Iext=0 and 1 only. For Iext=1, both localization schemes deviate less than 1 kJ/mol from the respective canonical results, and even for Iext=0 the errors due to the local approximation are completely negligible for almost any chemical application. Furthermore, density fitting can be applied without noticeably changing the results. Statistical data on bond lengths, and bond and dihedral angles of the local geometries relative to the canonical reference can be found in tab. 6.13, with results being similar to those of closed-shell DF-LMP2 gradients. For the $\cdot CH_2CH=CH_2$ radical, we were initially not able to converge the RMP2 level geometry. This was probably due to RMP2 breaking the molecule's C_{2v} symmetry, and thus complete active-space SCF with second-order multi-reference Rayleigh-Schrödinger perturbation theory (CASSCF-RS2) gradients were necessary for initial convergence. After this pre-optimization, all subsequent geometry optimizations using (DF-,L)RMP2 gradients were successful. To put the localization errors into perspective, we have additionally conducted geometry optimizations on RCCSD(T)/cc-pv(T+d)Z level for 21 reactions. Closed-shell systems were optimized using analytic gradients, open-shell systems with two-point numerical gradients. Due to the very high computational cost of numerical

Radical (R·)	RCC	RMP2	DF-MP2	IB1	IB0	PM1	PM0	REF
·CH_2CF_3	-	7.84	7.88	7.48	7.73	7.46	7.71	7.82
·CH_2CH_2Cl	-12.63	-10.17	-10.16	-10.65	-10.35	-10.65	-10.35	-8.91
·CH_2CH_2F	-5.54	-4.52	-4.51	-4.79	-4.59	-4.79	-4.57	-4.51
·CH_2CH_2OH	-7.02	-5.80	-5.77	-5.96	-5.36	-5.97	-5.38	-5.71
·$CH_2CH=CH_2$	-70.60	-81.00	-80.96	-81.73	-82.51	-81.73	-82.57	-81.09
·CH_2CHO	-39.27	-37.77	-37.76	-37.99	-37.63	-38.01	-37.68	-38.04
·CH_2CN	-32.87	-32.66	-32.62	-32.87	-32.21	-32.85	-32.22	-32.80
·CH_2CONH_2	-25.25	-23.72	-23.68	-23.85	-23.46	-24.26	-26.38	-23.88
·$CH_2CONH-CH_3$	-	-23.67	-23.64	-23.83	-23.32	-23.85	-23.32	-23.78
·$CH_2COO-CH_3$	-	-24.62	-24.59	-24.67	-24.06	-24.70	-24.33	-24.78
·CH_2COOH	-25.25	-24.00	-23.97	-24.10	-23.64	-24.12	-23.83	-24.15
·$CH_2CH(CH_2)_2$	-	-23.17	-23.13	-23.38	-22.24	-23.38	-22.28	-23.24
·CH_2F	-13.99	-14.23	-14.18	-14.36	-13.49	-14.36	-13.57	-14.26
·CH_2NH_2	-49.08	-49.78	-49.75	-50.13	-50.61	-50.13	-50.34	-49.66
·$CH_2NH_3^+$	20.19	20.08	20.13	20.02	20.68	20.02	20.67	20.02
·CH_2NHCH_3	-51.22	-51.30	-51.27	-51.91	-52.08	-51.90	-51.79	-51.34
·CH_2NHCHO	-44.10	-43.97	-43.92	-44.11	-42.08	-44.12	-42.36	-43.96
·$CH_2N(CH_3)_2$	-	-50.26	-50.23	-50.99	-51.09	-50.97	-50.78	-50.66
·CH_2NO_2	-12.10	-12.59	-12.55	-12.76	-11.80	-12.80	-11.87	-13.25
·CH_2OCF_3	-	-13.88	-13.81	-14.33	-12.95	-14.35	-13.04	-13.88
·CH_2OCH_3	-35.71	-34.61	-34.57	-35.16	-35.63	-35.16	-35.53	-34.62
·CH_2OCHO	-17.56	-16.74	-16.71	-17.20	-15.98	-17.20	-16.15	-16.71
·CH_2COOCH_3	-	-18.57	-18.54	-18.98	-17.65	-18.98	-17.83	-18.55
·CH_2OH	-35.71	-35.62	-35.58	-36.03	-36.59	-36.03	-36.53	-35.62
·$CH_2PH_3^+$	4.07	6.35	6.40	6.18	6.12	6.17	6.13	6.32
·$CH_2SH_2^+$	12.09	13.58	13.65	13.42	13.42	13.43	13.43	13.60
·CH_2SH	-37.91	-37.11	-37.04	-37.74	-38.95	-37.74	-38.87	-37.15
·CH_2SOOCH_3	-	4.38	4.43	4.21	4.71	4.16	4.41	4.98
·CH_2SOCH_3	-	-5.38	-5.29	-5.63	-4.47	-5.64	-4.70	-4.67
·$CH_2C≡CH$	-51.74	-51.60	-51.55	-52.05	-51.30	-52.07	-50.79	-51.58

Table 6.12: Radical stabilization energies in kJ/mol for the R30 test set. DF-LRMP2/cc-pv(T+d)Z using PM localization with Iext= 0, 1 denoted as PM0 and PM1 respectively. IBO $p = 4$ localization equivalently denoted as IB0 and IB1, and RCCSD(T)/cc-pv(T+d)Z values as RCC. RMP2 refers to the non-fitted method, and REF denotes RMP2 results from the original publication [21].

Iext	Length (bohr)		Angle (deg)	
	0	1	0	1
IBO exponent $p = 4$				
MAE	0.0024	0.0004	0.052	0.020
RMS	0.0035	0.0007	0.070	0.030
MAX	0.0133	0.0039	0.415	0.189
PM				
MAE	0.0024	0.0004	0.053	0.018
RMS	0.0034	0.0007	0.069	0.029
MAX	0.0134	0.0037	0.361	0.188

Table 6.13: DF-LRMP2/cc-pv(T+d)Z errors relative to DF-MP2/cc-pv(T+d)Z in the R30-set. Shown: bond lengths and bond and dihedral angles.

RCCSD(T) gradients, nine systems have been omitted. As can be seen in tab. 6.12, the method's intrinsic error – despite being below 4 kJ/mol – is again larger than the error due to local approximations. Nevertheless, the overall quality of the (L)RMP2 results relative to coupled cluster has a precision which is generally accepted as chemically accurate. As for the FH-set, LRMP2 Iext=1 profits from error compensation as compared to RMP2, yielding results that are slightly closer to the coupled-cluster reference.

As the original work not only lists DF-RMP2 but also DF-LUCCSD(T) radical stabilization energies, we recomputed those energies using our newly optimized DF-LRMP2, IBO $p = 4$ Iext=1 structures. The results can be found in tab. 6.14. Apart from $\cdot CH_2CN$ and $\cdot CH_2NO_2$, all systems are within 4 kJ/mol of the RCCSD(T) reference. This is an acceptable accuracy considering unrestricted local coupled-cluster single points are compared to a restricted reference. Additional errors between our DF-LUCCSD(T) results and those of the original work arise due to different localization schemes (PM vs. IBO $p = 4$), and domain sizes being slightly smaller in our local calculations. There are three possible reasons for the larger deviation of $\cdot CH_2CN$ and $\cdot CH_2NO_2$: Apart from differences between restricted and unrestricted calculations, or localization errors, the underlying geometry could be erroneous. We thus calculated RCCSD(T) single points for both systems on top of our DF-LRMP2, IBO $p = 4$ Iext=1 structures. With those results being within 1 kJ/mol of the fully optimized RCCSD(T) reference values, this source of error can be excluded. Localization errors are unlikely as well, as the LRMP2 energy printed during DF-LUCCSD(T) calculations matches the one of the preceding geometry optimization. We are thus left with a surprisingly large intrinsic error between restricted and unrestricted coupled cluster.

Radical (R$\cdot$)	RCC	LUCC/LRMP2	LUCC/REF	RCC/LRMP2
$\cdot CH_2CH_2Cl$	-12.63	-10.11	-10.58	-
$\cdot CH_2CH_2F$	-5.54	-5.14	-4.73	-
$\cdot CH_2CH_2OH$	-7.02	-4.85	-5.69	-
$\cdot CH_2CH=CH_2$	-70.60	-68.73	-69.50	-
$\cdot CH_2CHO$	-39.27	-43.84	-38.53	-
$\cdot CH_2CN$	-32.87	-39.18	-30.38	-32.67
$\cdot CH_2CONH_2$	-25.25	-25.66	-25.06	-
$\cdot CH_2COOH$	-25.25	-26.58	-25.27	-
$\cdot CH_2F$	-13.99	-14.54	-13.51	-
$\cdot CH_2NH_2$	-49.08	-51.82	-46.74	-
$\cdot CH_2NH_3{}^+$	20.19	21.48	22.05	-
$\cdot CH_2NHCH_3$	-51.22	-50.20	-49.33	-
$\cdot CH_2NHCHO$	-44.10	-42.98	-41.97	-
$\cdot CH_2NO_2$	-12.10	-19.90	-10.33	-12.14
$\cdot CH_2OCH_3$	-35.71	-36.52	-35.90	-
$\cdot CH_2OCHO$	-17.56	-17.82	-15.94	-
$\cdot CH_2OH$	-35.71	-37.13	-33.43	-
$\cdot CH_2PH_3{}^+$	4.07	5.88	2.47	-
$\cdot CH_2SH_2{}^+$	12.09	14.36	11.25	-
$\cdot CH_2SH$	-37.91	-35.76	-41.09	-
$\cdot CH_2C\equiv CH$	-51.74	-49.19	-47.86	-

Table 6.14: Radical stabilization energies in kJ/mol for 21 systems of the R30 test set. RCCSD(T)/cc-pv(T+d)Z values as denoted as RCC, DF-LUCCSD(T)/cc-pv(T+d)Z results as LUCC/LRMP2 if using DF-LRMP2 geometries with IBO $p = 4$ Iext=1 localization and LUCC/REF if taken from [21]. RCC/LRMP2 are RCCSD(T)/cc-pv(T+d)Z single points calculated on DF-LRMP2 geometries generated with IBO $p = 4$ Iext=1 localization.

6.4 Ground State of an Iron Complex

Fig. 6.7 shows the structure of $FeC_{72}N_2H_{100}$ as given in reference [68]. This system is used in literature mainly as real-life example in order to benchmark low-order scaling methods for calculating single-point energies, such as second-order N-electron valence state perturbation theory (NEVPT2) or local complete active space second-order perturbation theory with pair natural orbitals (PNO-CASPT2) [69].

There are several spin states known, with the quintett state discussed here being the single-reference ground state. We have taken on the challenge to optimize the structure on DF-LRMP2/SVP level, using Iext=0 and IBO $p = 4$ as defining parameters for the local calculation. Calculations were performed on a single computer node with two Intel Xeon E5-2680 v2 CPUs, 256 GB of memory, and four 500GB SSD drives. Using a mixed algorithm with a non-density fitted CPHF solver in an otherwise density fitted calculation, a single optimization step for the molecule with 83 core orbitals, 402 valence orbitals, and 5939 basis functions took about 44090 seconds. About 42% of the overall CPU time (18320 s) was spend in the CPHF solver, as compared to 47% (20850 s) in the MP2 solver. The overall RHF run took 2.9% (1300 s) of CPU time during each geometry optimization step. Preliminary timings for the fully density-fitted CPHF solver, conducted using a series of diradicals $[(C_4SH_3)-(CH_2)_n-(C_4SH_3)]^{2+}$ with n= 0, 10, 20 and up to 76 atoms [68, 69] show CPU time for each iterative CPHF step decreasing to about four times the cost of a single HF iteration step. For our large system this would shorten runtime for a single geometry optimization step from over 12 to about 8.6 hours as soon as the full algorithm is available. A optimized structure with both energy changes and the gradient's RMS below 10^{-5} a.u., as well as gradient norm below 10^{-3} a.u., can be found in appendix 3.
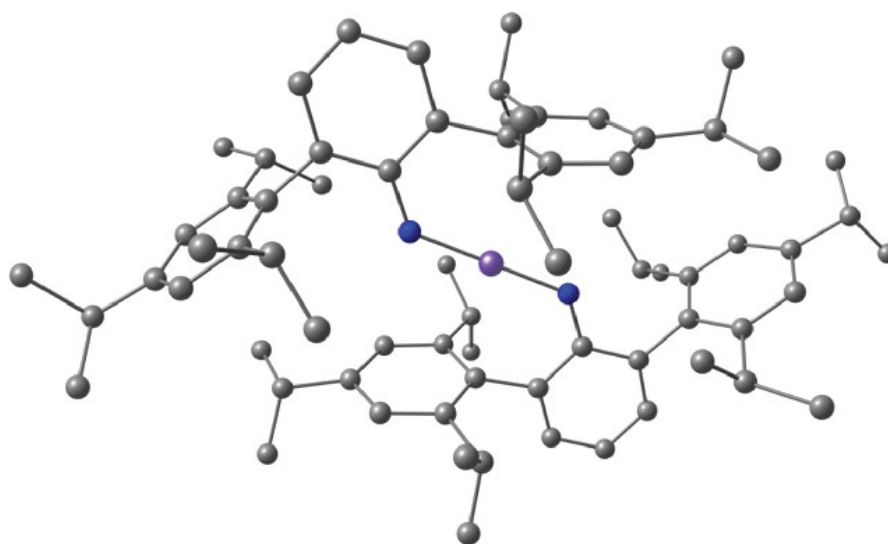
Figure 6.7: FeC$_{72}$N$_2$H$_{100}$, Fe is purple, N blue and C gray. H not shown. *Cf.* [68]; image cropped.

7 Noncovalent Interactions

Intermolecular interactions play an important role in many chemical systems, as for instance in DNA base pairs, the folding of proteins, or function materials in material science. For theoretical investigations these interactions are challenging, as they are often strongly influenced by correlation effects, making it necessary to use higher-order wave function methods in order to describe them accurately. In 2006, Hobza and co-workers thus published a benchmark database of accurate interaction energies of selected model complexes, including a subset called S22 [120]. The S22 interaction energies were calculated at the DF-MP2 level complete basis set limit (CBS limit), using a two-point extrapolation scheme as proposed by Helgaker *et al.* [121, 122] for separate basis set extrapolation of HF and correlation energy. Subsequently, coupled-cluster level energies were estimated using focal point analysis (*cf.* sec. 6.2). As the δ-CCSD(T) correction was not of satisfying quality, several revisions of the original benchmark database have since been published [123, 124]. Most important to the current work is a publication by Marchetti and Werner [119], in which for 11 of the 22 complexes CCSD(T)/CBS level energies were reported, based on CCSD(T)/AVTZ' and CCSD(T)/AVQZ' extrapolated correlation energies on top of HF/AVQZ' references. The authors additionally demonstrated the precision and affordability of explicitly correlated methods by reporting CCSD(T)-F12/AVTZ' energies, thereby showing that explicitly correlated methods in medium sized basis sets already yield results close to the CBS limit.

Already at that time it was discussed how the quality of the underlying geometries, mostly calculated at the counterpoise-corrected DF-MP2/cc-pVTZ level, would influence the resulting single point energies. In general, MP2 has a tendency to underestimate intermolecular distances for the same reason bond distances are underestimated. The latter was being discussed earlier in sec. 6.1. This in turn leads to the effect of binding energies being overestimated [119, 125]. Additionally, due to the limited basis set size, there is a significant basis-set superposition error (BSSE) present in the non-CBS-extrapolated dimer energies and geometries. This error arises due to the extended correlation space in the dimers description, with excitations occurring from monomer A into the virtual space of monomer B and vice versa. As a result, the dimer is described in an improved basis set, yielding a higher recovery of correlation energy as compared to the isolated monomers. This can, according to theory, be compensated by employing a counterpoise (CP) correction [126].

The CP corrected interaction energy is obtained as the difference of the dimer energy and the monomer energies computed in the full dimer basis at the dimer structure, i.e. with basis functions at 'ghost atoms' without charge for the other monomer. The CP correction for each monomer is the difference of its energies computed in the dimer basis and the monomer basis. The larger the basis set of a calculation, the smaller will be the BSSE and thus CP correction. Methods yielding results close to the basis set limit, such as extrapolation schemes and explicitly correlated methods, should suffer from BSSEs much less. CP corrections cannot only be applied to energies, but to forces as well, enabling CP corrected geometry optimizations.

We will investigate the influence of the BSSE, and CP correction used to compensate for it, on the geometries of noncovalent bound complexes in this section. Instead of using the original S22 set or one of its extensions [127, 128], we will discuss six complexes taken from its more recent successor, S66x8 [129]. The main differences between the two sets are: S66x8 is more balanced with respect to the different types of molecular interaction, all equilibrium geometries were calculated on the same level of theory, and additionally to the equilibrium geometries reported for S22, S66x8 has been augmented by eight further points. These points are situated along the main noncovalent interaction coordinate, allowing us to explore the PES along that path. In the original work, full geometries were optimized for the single points at equilibrium distance, and the main interaction coordinate subsequently scaled for the other seven geometries of each complex. Using HF/AV5Z, MP2/CBS(AVTZ,AVQZ) and a δ-CCSD(T)/AVDZ correction, coupled-cluster energies were approximated for every point and subsequently a fourth-order polynomial was fitted around the five points closest to the equilibrium geometry. The thus generated minimum was used as intermolecular distance in the final benchmark S66 set. We followed the same procedure, with single points generated by the methods discussed below, as full geometry optimizations for the amount of methods investigated are prohibitively expensive, especially for those methods using explicit correlation or methods without analytic gradients available [130]. The S66x8 set provides single points at a factor of $0.90, 0.95, 1.00, 1.05,$ and 1.10 relative to the reported CP DF-MP2/cc-pVTZ equilibrium geometry, and we added another one at 500 times the equilibrium distance; the additional point was used for calculating CP corrections. Augmented dunning basis sets (AVnZ') were employed for all our calculations in order to accurately describe the noncovalent interactions.

The S66 test set can be divided into three types of interaction: electrostatic interactions such as hydrogen bonds, dispersion interactions such as the $\pi - \pi$ interactions of stacked aromatic systems, and complexes with mixed electrostatic and dispersion interaction. We have chosen six systems in total, two for each type of interaction: a water dimer and an acetic acid dimer (AcOH) containing one and two hydrogen bonds, respectively, for the electrostatic interactions, as well as a stacked benzene dimer and an ethene-pentane complex as representatives of dispersion bound systems. Mixed interactions were investigated using two T-shaped complexes, an ethyne-ethyne

system and another benzene dimer. Thus each of the different interactions is represented by one small and one large system, with details listed in tab. 7.1 and equilibrium geometries supplied in appendix 4. Fig. 7.1 depicts our initial results, using DF-MP2 and CP-DF-MP2 single point energies. Basis set extrapolation was performed via a two-point formula as proposed by Karton and Martin for the HF reference and the L2 functional for the correlation energy [131, 132], in both cases using AVQZ' and AV5Z' level fitting values. The reason for the separated extrapolation is the fact that the HF interaction energy converges faster with respect to the one-electron basis set, whereas the correlation interaction energy has a slower convergence behaviour. A two-point extrapolation scheme is preferable, as the inclusion of an additional lower quality basis set often results in a lower quality of the fit. In addition, DF-MP2-F12 and CP-DF-MP2-F12 results are shown. With explicitly correlated method yielding results close to the CBS limit those values were not extrapolated. As can be seen, except for the hydrogen bonded systems, MP2 tends to underestimate bond lengths in smaller basis sets as compared to the CBS limit – whereas CP correction on the other hand systematically over-estimates intermolecular distances. This is probably due to the CP correction removing intermolecular excitations from the calculation; these excitations have an attractive effect. Yet, both methods show a smooth convergence towards the basis set limit. The explicitly correlated methods in turn are almost fully converged at the triple-zeta level, with small to almost no differences between CP corrected and uncorrected values at triple-zeta or higher cardinal numbers. Except for the overshooting CP correction, all of the above observations are complementary to our previous theoretical considerations concerning the BSSE decreasing for increasing basis set sizes.

In order to investigate the difference between the CP corrected and uncorrected MP2 equilibrium geometries, calculations were repeated using DF-LMP2 with IBO $p = 4$ localization and Iext=0 and 1 domain extension, see fig. 7.2 and appendix 4. We expected the local results to be similar to those of CP-DF-MP2, as excitations in local methods are restricted to the orbitals' respective domain and a connectivity criterion such as Iext ensures no intermolecular domains are generated. Starting a triple-zeta accuracy, our expectation is fully met for Iext=1, where such calculations

Dimer	No	Type	Comment
AcOH-AcOH	20	E	
Benzene-Benzene $\pi\pi$	24	D	
Benzene-Benzene TS	47	M	Mixed interaction according to [120]
Ethene-Pentane	44	D	
Ethyne-Ethyne TS	51	M	
Water-Water	1	E	

Table 7.1: Dimers used in this chapter. No is enumeration as in [129], and type of interaction can be (E)lectrostatic, (D)ispersion, or (M)ixed.
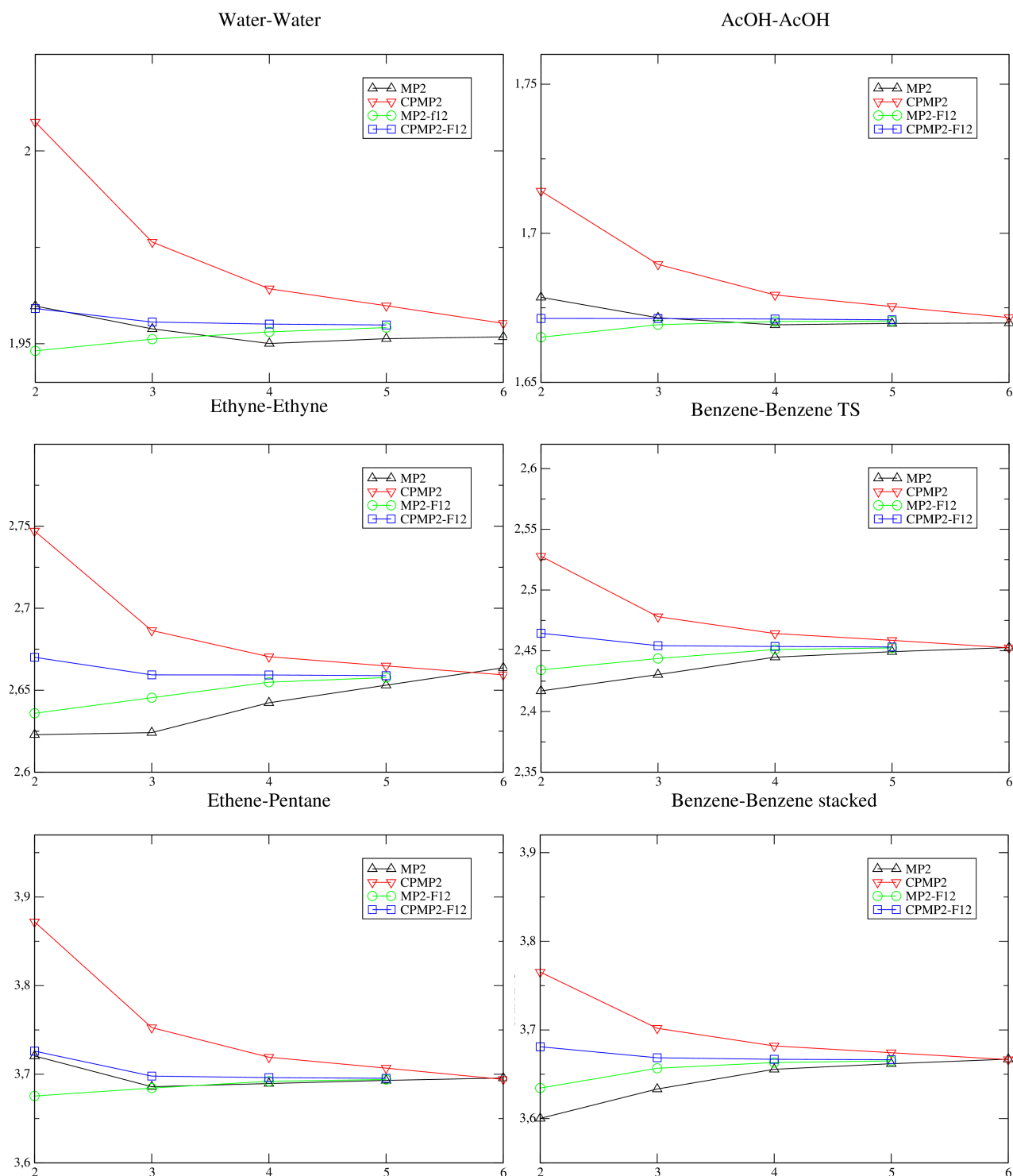
Figure 7.1: Convergence of the intermolecular equilibrium distance (Angstrom) as a function of the basis set size. x-axis: numbers $n = 1 - 5$ are cardinal numbers in AVnZ', 6 is extrapolation to the CBS limit. Depicted: MP2 (black), CP-MP2 (red), MP2-F12 (green), and CP-MP2-F12 (blue). All methods density-fitted.
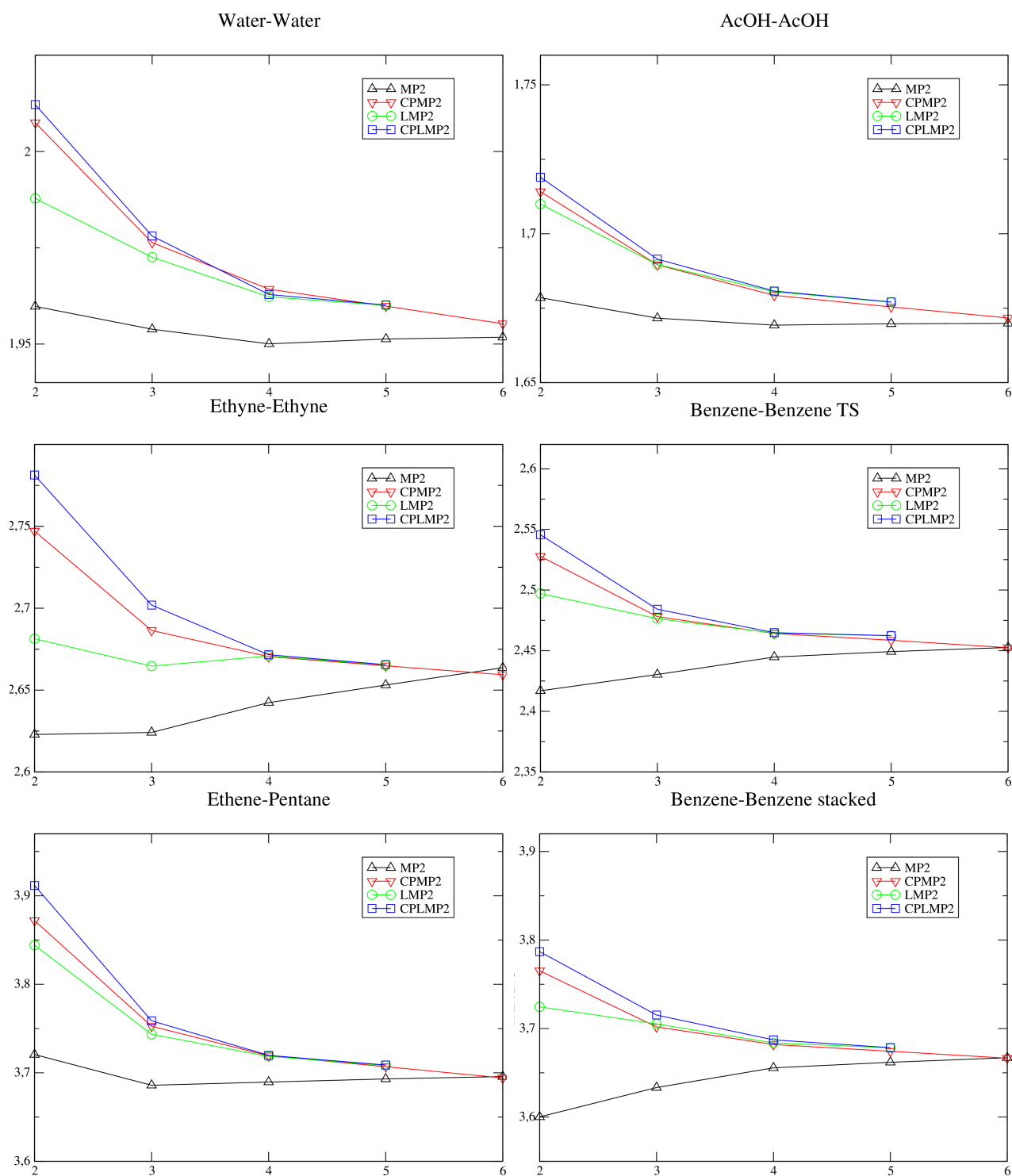
Figure 7.2: Convergence of the intermolecular equilibrium distance (Angstrom) as a function of the basis set size. x-axis: numbers $n = 1 - 5$ are cardinal numbers in AVnZ', 6 is extrapolation to the CBS limit. Depicted: MP2 (black), CP-MP2 (red), LMP2 (green), and CP-LMP2 (blue). All methods density-fitted using IBO $p = 4$, Iext=1 localization.

approximate canonical calculations within each monomer, but with limited intermolecular excitations. Thus, CP correction has only minor influence, as most intermolecular excitations are already removed by the local approximation. The only exception is the ethyne-ethyne dimer, which across all methods, seems to be described improperly in AVDZ' and AVTZ' basis sets, and we can see the discussed effects starting from the AVQZ' basis. In order to avoid being mislead by localization artefacts, we manually verified that there is no intermolecular domain generated in between the ethyne monomers. The results of local calculations without extension of the primary domains (Iext=0) are always situated above the CP-MP2 results, corresponding to an overestimation of intermolecular distance and exhibit an even worse convergence behaviour; the corresponding figures can be found in appendix 4. This might be due to too small domains for a physically meaningful description, not only of the dimer, but also at least of the larger monomers. As discussed earlier, the usage of Iext=0 is discouraged, as Iext=1 is a well balanced compromise between cost and accuracy.

The last set of plots, fig. 7.3, is concerned with the basis set convergence of DF-LMP2-F12 methods; parameters for the explicitly correlated local calculations were chosen equivalent to those of the previous DF-LMP2 calculations. As can be seen, the convergence behaviour for Iext=1 is very good, sometimes even starting at double-zeta basis sets. With the exception of the water dimer in AVDZ', there are only minor effects due to the CP correction. We have not printed the results for Iext=0, as basis set limits are systematically overestimated indicating a too severe neglect of dynamic electron correlation. Yet, as all data used in this chapter, the numbers can be found in appendix 4. Thus we can conclude, that simply performing a CP correction on a small to medium size basis set such as AVDZ' or AVTZ' is not guaranteed to generate valid results and one should be careful, especially if the correction is rather large. Additionally, if applied correctly, local approximations are yielding very similar results to CP corrected canonical values at a fraction of the computational cost. Nevertheless, explicitly correlated theories in combination with augmented triple-zeta or comparable basis sets are the more profound method to calculate intermolecular interactions, being almost free of basis set errors. Finally, a combination of both, local approximations and explicit correlation carries the advantages of both methods, yielding reliably precise results across all types of molecular interaction already in rather small basis sets at only moderate computational cost.

As a last notion: We refrain from recommending our MP2 level results over those of the original work, as we are aware of the fact that MP2 as a method does not perform equally well for all types of intermolecular interactions. For stacked $\pi - \pi$ interactions, for example, spin-scaled (SCS) MP2 [133] yields far better results, and methods such as dispersion-weighted MP2 [119], MP2.5 [134], or explicitly correlated coupled-cluster are capable of delivering excellent accuracy across all kinds of interactions. Nevertheless, our conclusion above seems to be valid in a general manner, as we have additionally evaluated all calculations on the SCS-MP2 level with
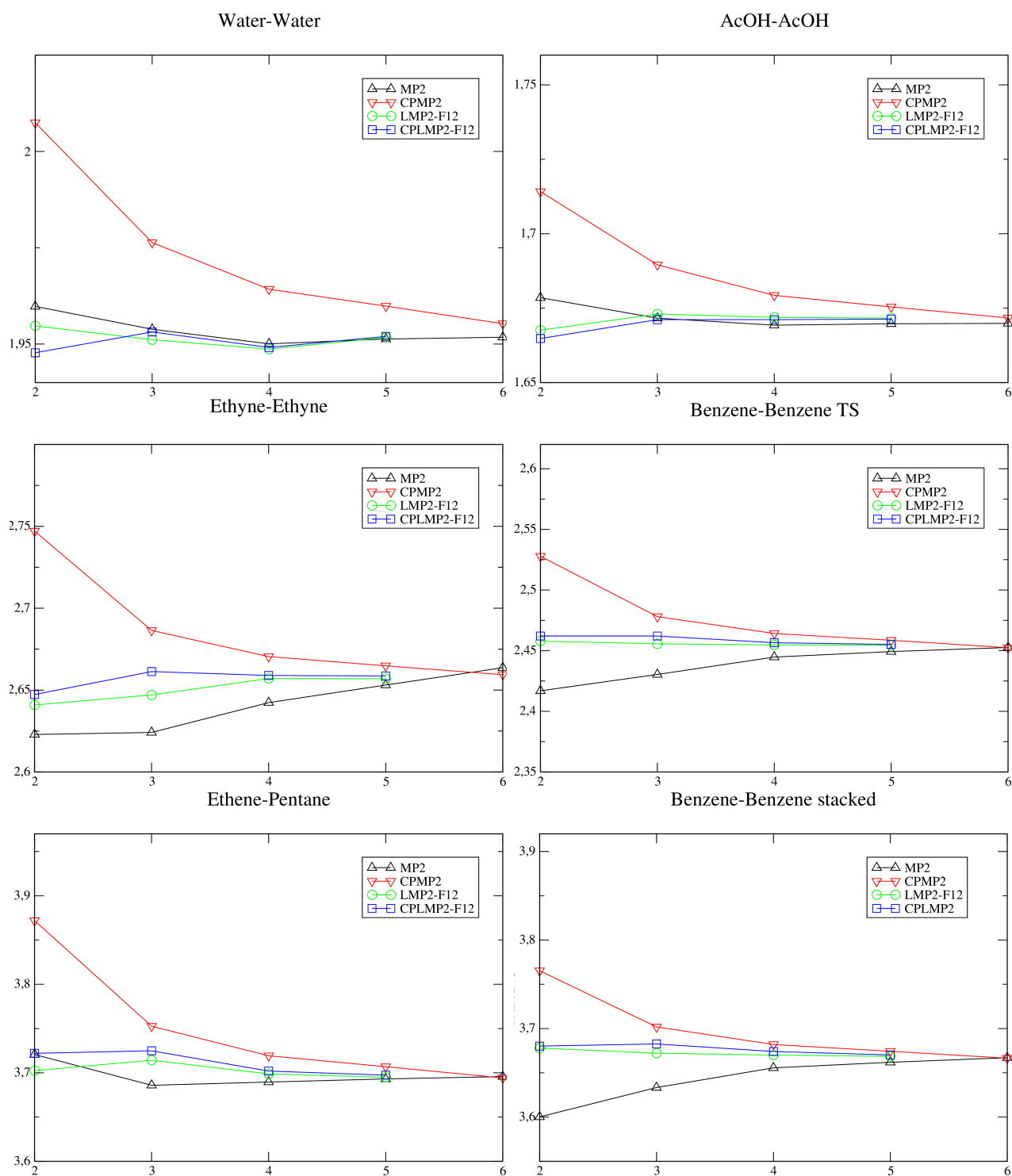
Figure 7.3: Convergence of the intermolecular equilibrium distance (Angstrom) as a function of the basis set size. x-axis: numbers $n = 1 - 5$ are cardinal numbers in AVnZ', 6 is extrapolation to the CBS limit. Depicted: MP2 (black), CP-MP2 (red), LMP2-F12 (green), and CP-LMP2-F12 (blue). All methods density-fitted using IBO $p = 4$, Iext=1 localization.

results being equivalent except for a small systematic shift towards increased CBS equilibrium distances.

8 Conclusion

One objective of this work was to extend the already existing closed-shell LMP2 nuclear gradients for use with the IBO localization scheme as an alternative to PM localization. The other aspect was to derive and implement a new family of open-shell gradients. The latter includes the canonical RMP2 gradients with symmetry, as well as density-fitted LRMP2 gradients for both PM and IBOs. Moreover, COSMO was made available for the open-shell gradients. As discussed in chapter 6, thorough testing revealed that all of the above objectives were fully met. The new IBO localization scheme was found to perform at least as good as PM localization, while at the same time not being based on mathematically ill-defined Mulliken charges. High-level coupled-cluster optimizations for 12 systems showed that the LMP2 gradients can profit from error-compensation, thus yielding results closer to the CCSD(T) level geometry than the underlying canonical MP2 gradients. It was argued that this might be due to MP2 overestimating dynamic correlation, thereby increasing bond lengths. In local methods the correlation energy is truncated, and thus fewer overshooting can be observed.

The canonical open-shell RMP2 gradients, in combination with unrestricted coupled-cluster single-point energies, were used to predict the ionization potentials of 24 molecules used in organic photovoltaic and electronic applications. Comparison with experimental data revealed very good agreement for both, vertical and adiabatic ionization potentials. Selected structures of the test set were additionally optimized using local approximations with errors comparable to those in closed-shell gradients. Open-shell LRMP2 gradients were further benchmarked against a set of 30 radical stabilization energies and compared to high-precision coupled-cluster level geometries. It was thereby confirmed that chemical accuracy within 1 kcal/mol can be reached even for MP2-level energies using our new gradients. Finally and in order to demonstrate the applicability of our new local open-shell gradients to larger systems, the geometry of the quintett state of $FeC_{72}N_2H_{100}$ was optimized.

In the last part of this work, we discussed the influence of BSSE errors on noncovalent interactions by investigating the equilibrium distances of six dimers from the S66x8 test set relative to different basis set sizes. We employed different MP2 level methods such as canonical MP2, LMP2, MP2-F12, LMP2-F12 and their counterpoise corrected pendants in order to reach the following conclusions: Firstly, CP corrected MP2 has a tendency to overestimate intermolecular

equilibrium distances, a behaviour due to the removal of attractive intermolecular excitations. Thus, it can be replaced by cheaper local correlations methods such as LMP2, where the local approximation has a similar effect if domains are chosen accordingly. Secondly, explicitly correlated methods usually recover the converged CBS equilibrium distance already at AVTZ' basis set sizes and do not necessitate a CP correction. They are thus the preferred alternative over expensive CP corrected CBS extrapolation schemes. Combining advantages of both, local approximations and explicit correlation, will yield results close to the basis set limit at very moderate computational costs.

During application of local methods in all the different investigations in this work, we found that local errors strongly depend on the right choice of domain sizes. An approach working reasonably well across all the different chemical problems discussed is a primary domain generation based on IAO partial charges being either $q_{ii}^A \geq 0.15$ for aromatic or $q_{ii}^A \geq 0.2$ for most other systems; if in doubt, $q_{ii}^A \geq 0.15$ is recommended. Additionally, primary domains should be extended using a connectivity criterion such as Iext=1 and IBO localization is preferred over the PM scheme for better convergence during geometry optimizations. Following this procedure, local errors are significantly smaller as the intrinsic error of (R)MP2 relative to high-level coupled-cluster calculations. Also, local errors are small compared to AVTZ' basis set errors and if needed, local precision can be systematically increased by using Iext=2 or higher. Density-fitting errors for the gradients are negligible as well.

In general, the gradients presented in this dissertation can be seen as an intermediate step towards density-fitted local restricted open-shell gradients on coupled-cluster level. They also lay the foundation for implementation of other properties such as for instance harmonic vibrational frequencies. But even today, the open-shell RMP2 gradients already present a theoretically profound alternative to the commonly used density functional methods for finding equilibrium structures.

Bibliography

(1)   J. Gauss, in *Modern Methods and Algorithms of Quantum Chemistry*, ed. J. Grotendorst, NIC-John von Neumann Institute for Computing, Juelich, 2000, vol. 3, pp. 541–592.

(2)   Y. Yamaguchi, J. D. Goddard, Y. Osamura and H. F. Schaefer III, *A New Dimension to Quantum Chemistry*, Oxford University Press, 1994.

(3)   F. Jensen, *Introduction to Computational Chemistry*, JOHN WILEY & SONS INC, 2007.

(4)   J. Toulouse, *Introduction to the calculation of molecular properties by response theory*, 2017, `www.lct.jussieu.fr/pagesperso/toulouse/enseignement/`.

(5)   J. Gerratt and I. M. Mills, *J. Chem. Phys.*, 1968, **49**, 1719–1729, DOI: `10.1063/1.1670299`.

(6)   P. Pulay, *Mol. Phys.*, 1969, **17**, 197–204, DOI: `10.1080/00268976900100941`.

(7)   H. F. Schaefer III and Y. Yamaguchi, *J. Mol. Struct. THEOCHEM*, 1986, **135**, 369–390, DOI: `10.1016/0166-1280(86)80070-7`.

(8)   O. Christiansen, H. Koch and P. Jørgensen, *Chem. Phys. Lett.*, 1995, **243**, 409, DOI: `10.1016/0009-2614(95)00841-q`.

(9)   A. El Azhary, G. Rauhut, P. Pulay and H.-J. Werner, *J. Chem. Phys.*, 1998, **108**, 5185–5193, DOI: `10.1063/1.475955`.

(10)   G. Rauhut and H.-J. Werner, *Phys. Chem. Chem. Phys.*, 2001, **3**, 4853–4862, DOI: `10.1039/B105126C`.

(11)   J. Friedrich, S. Coriani, T. Helgaker and M. Dolg, *J. Chem. Phys.*, 2009, **131**, 154102, DOI: `10.1063/1.3243864`.

(12)   D. Datta, S. Kossmann and F. Neese, *J. Chem. Phys.*, 2016, **145**, 114101, DOI: `10.1063/1.4962369`.

(13)   T. Helgaker, P. Jorgensen and J. Olsen, *Molecular Electronic-Structure Theory*, JOHN WILEY & SONS INC, 2000.

(14)   J. A. Pople and R. K. Nesbet, *J. Chem. Phys.*, 1954, **22**, 571–572, DOI: `10.1063/1.1740120`.

(15) G. Berthier, *Comptes rendus hebdomadaires des séances de l'Académie des sciences*, 1954, **238**, 91–93.

(16) C. C. J. Roothaan, *Rev. Mod. Phys.*, 1960, **32**, 179–185, DOI: `10.1103/RevModPhys.32.179`.

(17) R. D. Amos, J. S. Andrews, N. C. Handy and P. J. Knowles, *Chem. Phys. Lett.*, 1991, **185**, 256–264, DOI: `10.1016/s0009-2614(91)85057-4`.

(18) P. J. Knowles, J. S. Andrews, R. D. Amos, N. C. Handy and J. A. Pople, *Chem. Phys. Lett.*, 1991, **186**, 130–136, DOI: `10.1016/S0009-2614(91)85118-G`.

(19) W. J. Lauderdale, J. F. Stanton, J. Gauss, J. D. Watts and R. J. Bartlett, *Chem. Phys. Lett.*, 1991, **187**, 21–28, DOI: `10.1016/0009-2614(91)90478-R`.

(20) P. J. Knowles, C. Hampel and H.-J. Werner, *J. Chem. Phys.*, 1993, **99**, 5219–5227, DOI: `10.1063/1.465990`.

(21) Y. Liu, *Linear Scaling High-spin Open-shell Local Correlation Methods*, PhD Thesis, University of Stuttgart, 2011.

(22) M. Saitow, U. Becker, C. Riplinger, E. F. Valeev and F. Neese, *J. Chem. Phys.*, 2017, **146**, 164105, DOI: `10.1063/1.4981521`.

(23) P. Botschwina, *Chem. Phys. Lett.*, 1974, **29**, 98–101, DOI: `10.1016/0009-2614(74)80141-7`.

(24) J. D. Goddard, N. C. Handy and H. F. Schaefer III, *J. Chem. Phys.*, 1979, **71**, 1525–1530, DOI: `10.1063/1.438494`.

(25) W. J. Lauderdale, J. F. Stanton, J. Gauss, J. D. Watts and R. J. Bartlett, *J. Chem. Phys.*, 1992, **97**, 6606–6620, DOI: `10.1063/1.463664`.

(26) J. Gauss, J. F. Stanton and R. J. Bartlett, *J. Chem. Phys.*, 1992, **97**, 7825–7828, DOI: `10.1063/1.463452`.

(27) J. D. Watts, J. Gauss and R. J. Bartlett, *J. Chem. Phys.*, 1993, **98**, 8718–8733, DOI: `10.1063/1.464480`.

(28) N. C. Handy and H. F. Schaefer III, *J. Chem. Phys.*, 1984, **81**, 5031–5033, DOI: `10.1063/1.447489`.

(29) M. Schütz, H.-J. Werner, R. Lindh and F. R. Manby, *J. Chem. Phys.*, 2004, **121**, 737–50, DOI: `10.1063/1.1760747`.

(30) P. Pulay, *Chem. Phys. Lett.*, 1983, **100**, 151–154, DOI: `10.1016/0009-2614(83)80703-9`.

(31) P. J. Knowles, H.-J. Werner and M. Schütz, in *Modern Methods and Algorithms of Quantum Chemistry*, ed. J. Grotendorst, NIC-John von Neumann Institute for Computing, Juelich, 2000, vol. 3, pp. 97–179.

(32) S. Saebø and P. Pulay, *Chem. Phys. Lett.*, 1985, **113**, 13–18, DOI: `10.1016/0009-2614(85)85003-x`.

(33) S. Saebo and P. Pulay, *Annu. Rev. Phys. Chem.*, 1993, **44**, 213–236, DOI: `10.1146/annurev.pc.44.100193.001241`.

(34) P. E. Maslen and M. Head-Gordon, *Chem. Phys. Lett.*, 1998, **283**, 102–108, DOI: `10.1016/s0009-2614(97)01333-x`.

(35) M. Schütz, G. Hetzer and H.-J. Werner, *J. Chem. Phys.*, 1999, **111**, 5691–5705, DOI: `10.1063/1.479957`.

(36) H.-J. Werner, F. R. Manby and P. J. Knowles, *J. Chem. Phys.*, 2003, **118**, 8149–8160, DOI: `10.1063/1.1564816`.

(37) C. Riplinger and F. Neese, *J. Chem. Phys.*, 2013, **138**, 034106, DOI: `10.1063/1.4773581`.

(38) H.-J. Werner, G. Knizia, C. Krause, M. Schwilk and M. Dornbach, *J. Chem. Theory Comput.*, 2015, **11**, 484–507, DOI: `10.1021/ct500725e`.

(39) Q. Ma and H.-J. Werner, *J. Chem. Theory Comput.*, 2015, **11**, 5291–5304, DOI: `10.1021/acs.jctc.5b00843`.

(40) M. Schwilk, Q. Ma, C. Köppl and H.-J. Werner, *J. Chem. Theory Comput.*, 2017, **13**, 3650–3675, DOI: `10.1021/acs.jctc.7b00554`.

(41) F. Pavošević, C. Peng, P. Pinski, C. Riplinger, F. Neese and E. F. Valeev, *J. Chem. Phys.*, 2017, **146**, 174108, DOI: `10.1063/1.4979993`.

(42) D. G. Fedorov and K. Kitaura, *J. Chem. Phys.*, 2005, **123**, 134103, DOI: `10.1063/1.2007588`.

(43) P. Baudin, P. Ettenhuber, S. Reine, K. Kristensen and T. Kjærgaard, *J. Chem. Phys.*, 2016, **144**, 054102, DOI: `10.1063/1.4940732`.

(44) K. Kristensen, P. Jørgensen, B. Jansík, T. Kjærgaard and S. Reine, *J. Chem. Phys.*, 2012, **137**, 114102, DOI: `10.1063/1.4752432`.

(45) D. Bykov, K. Kristensen and T. Kjærgaard, *J. Chem. Phys.*, 2016, **145**, 024106, DOI: `10.1063/1.4956454`.

(46) P. Pulay and S. Saebø, *Theor. Chim. Acta*, 1986, **69**, 357–368, DOI: `10.1007/BF00526697`.

(47) G. Rauhut, A. El Azhary, F. Eckert, U. Schumann and H.-J. Werner, *Spectrochim. Acta*, 1999, **A 55**, 647–658, DOI: `10.1016/s1386-1425(98)00268-6`.

(48) N. J. Russ and T. D. Crawford, *Chem. Phys. Lett.*, 2004, **400**, 104–111, DOI: `10.1016/j.cplett.2004.10.083`.

(49) P. Pinski and F. Neese, *J. Chem. Phys.*, 2018, **148**, 031101, DOI: `10.1063/1.5011204`.

(50) N. J. Russ and T. D. Crawford, *J. Chem. Phys.*, 2004, **121**, 691–696, DOI: `10.1063/1.1759322`.

(51) J. E. Subotnik and M. Head-Gordon, *J. Chem. Phys.*, 2005, **123**, 64108, DOI: `10.1063/1.2000252`.

(52) R. A. Mata and H.-J. Werner, *J. Chem. Phys.*, 2006, **125**, 184110, DOI: `10.1063/1.2364487`.

(53) G. Knizia, *J. Chem. Theory Comput.*, 2013, **9**, 4834–4843, DOI: `10.1021/ct400687b`.

(54) J. Pipek and P. G. Mezey, *J. Chem. Phys.*, 1989, **90**, 4916–4926, DOI: `10.1063/1.456588`.

(55) W. C. Lu, C. Z. Wang, M. W. Schmidt, L. Bytautas, K. M. Ho and K. Ruedenberg, *J. Chem. Phys.*, 2004, **120**, 2629–2637, DOI: `10.1063/1.1638731`.

(56) T. Janowski, *J. Chem. Theory Comput.*, 2014, **10**, 3085–3091, DOI: `10.1021/ct500245f`.

(57) H.-J. Werner, P. J. Knowles, G. Knizia, F. R. Manby, M. Schütz, P. Celani, W. Györffy, D. Kats, T. Korona, R. Lindh, A. Mitrushenkov, G. Rauhut, K. R. Shamasundar, T. B. Adler, R. D. Amos, A. Bernhardsson, A. Berning, D. L. Cooper, M. J. O. Deegan, A. J. Dobbyn, F. Eckert, E. Goll, C. Hampel, A. Hesselmann, G. Hetzer, T. Hrenar, G. Jansen, C. Köppl, Y. Liu, A. W. Lloyd, R. A. Mata, A. J. May, S. J. McNicholas, W. Meyer, M. E. Mura, A. Nicklass, D. P. O'Neill, P. Palmieri, D. Peng, K. Pflüger, R. Pitzer, M. Reiher, T. Shiozaki, H. Stoll, A. J. Stone, R. Tarroni, T. Thorsteinsson and M. Wang, *MOLPRO, version 2015.1, a package of ab initio programs*, 2015, `www.molpro.net`.

(58) V. Fock, *Z. Phys.*, 1930, **61**, 126–148, DOI: `10.1007/BF01340294`.

(59) C. Møller and M. S. Plesset, *Phys. Rev.*, 1934, **46**, 618–622, DOI: `10.1103/PhysRev.46.618`.

(60) E. Baerends, D. Ellis and P. Ros, *Chem. Phys.*, 1973, **2**, 41–51, DOI: `10.1016/0301-0104(73)80059-X`.

(61) J. L. Whitten, *J. Chem. Phys.*, 1973, **58**, 4496–4501, DOI: `10.1063/1.1679012`.

(62) M. Feyereisen, G. Fitzgerald and A. Komornicki, *Chem. Phys. Lett.*, 1993, **208**, 359–363, DOI: `10.1016/0009-2614(93)87156-W`.

(63) A. Klamt and G. Schuurmann, *J. Chem. Soc., Perkin Trans. 2*, 1993, **0**, 799–805, DOI: `10.1039/P29930000799`.

(64) J. Friedrich and J. Hänchen, *J. Chem. Theory Comput.*, 2013, **9**, 5381–5394, DOI: `10.1021/ct4008074`.

(65) R. Huenerbein, B. Schirmer, J. Moellmann and S. Grimme, *Phys. Chem. Chem. Phys.*, 2010, **12**, 6940–6948, DOI: `10.1039/C003951A`.

(66)   R. M. Richard, M. S. Marshall, O. Dolgounitcheva, J. V. Ortiz, J.-L. Brédas, N. Marom and C. D. Sherrill, *J. Chem. Theory Comput.*, 2016, **12**, 595–604, DOI: `10.1021/acs.jctc.5b00875`.

(67)   S. G. Lias and J. E. Bartmess, *Gas-Phase Ion Thermochemistry*, 2018, `webbook.nist.gov/chemistry/ion/`.

(68)   Y. Guo, K. Sivalingam, E. F. Valeev and F. Neese, *J. Chem. Phys.*, 2016, **144**, 094111, DOI: `10.1063/1.4942769`.

(69)   F. Menezes, D. Kats and H.-J. Werner, *J. Chem. Phys.*, 2016, **145**, 124115, DOI: `10.1063/1.4963019`.

(70)   C. C. J. Roothan, *Rev. Mod. Phys.*, 1951, **23**, 69, DOI: `10.1103/revmodphys.23.69`.

(71)   E. Schroedinger, *Ann. Phys.*, 1926, **385**, 437–490, DOI: `10.1002/andp.19263851302`.

(72)   M. Born and R. Oppenheimer, *Ann. Phys.*, 1927, **389**, 457–484, DOI: `10.1002/andp.19273892002`.

(73)   A. Szabo and N. S. Ostlund, *Modern Quantum Chemistry: Introduction to Advanced Electronic Structure Theory*, McGraw-Hill, 1989.

(74)   P. W. Atkins and R. S. Friedman, *Molecular Quantum Mechanics*, Oxford University Press, 2010.

(75)   J. C. Slater, *Phys. Rev.*, 1929, **34**, 1293–1322, DOI: `10.1103/PhysRev.34.1293`.

(76)   G. G. Hall, *Proceedings of the Royal Society of London A: Mathematical, Physical and Engineering Sciences*, 1951, **205**, 541–552, DOI: `10.1098/rspa.1951.0048`.

(77)   J. S. Andrews, D. Jayatilaka, R. G. Bone, N. C. Handy and R. D. Amos, *Chem. Phys. Lett.*, 1991, **183**, 423–431, DOI: `10.1016/0009-2614(91)90405-X`.

(78)   T. Tsuchimochi and G. E. Scuseria, *J. Chem. Phys.*, 2010, **133**, 141102, DOI: `10.1063/1.3503173`.

(79)   A. Köhn and H.-J. Werner, *Advanced Methods in Quantum Chemistry*, 2015, `ilias3.uni-stuttgart.de/goto_Uni_Stuttgart_crs_1333710.html`.

(80)   H.-J. Werner, C. Köppl, Q. Ma and M. Schwilk, in *Fragmentation: Toward Accurate Calculations on Complex Molecular Systems*, ed. M. S. Gordon, Wiley, 2017.

(81)   T. D. Crawford, H. F. Schaefer III and T. J. Lee, *J. Chem. Phys.*, 1996, **105**, 1060–1069, DOI: `10.1063/1.471951`.

(82)   G. Knizia and H.-J. Werner, *J. Chem. Phys.*, 2008, **128**, 154103, DOI: `10.1063/1.2889388`.

(83)   J. Lennard-Jones and J. A. Pople, *Proceedings of the Royal Society of London A: Mathematical, Physical and Engineering Sciences*, 1950, **202**, 166–180, DOI: `10.1098/rspa.1950.0092`.

(84) J. M. Foster and S. F. Boys, *Rev. Mod. Phys.*, 1960, **32**, 300–302, DOI: `10.1103/RevModPhys.32.300`.

(85) S. F. Boys, in *Quantum Theory of Atoms, Molecules, and the Solid State*, ed. P. O. Löwdin, Academic Press, New York, 1966, pp. 253–262.

(86) J. W. Boughton and P. Pulay, *J. Comput. Chem.*, 1993, **14**, 736–740, DOI: `10.1002/jcc.540140615`.

(87) C. Edmiston and K. Ruedenberg, *Rev. Mod. Phys.*, 1963, **35**, 457–464, DOI: `10.1103/RevModPhys.35.457`.

(88) A. E. Reed, R. B. Weinstock and F. Weinhold, *J. Chem. Phys.*, 1985, **83**, 735–746, DOI: `10.1063/1.449486`.

(89) S. Lehtola and H. Jónsson, *J. Chem. Theory Comput.*, 2013, **9**, 5365–5372, DOI: `10.1021/ct400793q`.

(90) S. Lehtola and H. Jónsson, *J. Chem. Theory Comput.*, 2014, **10**, 642–649, DOI: `10.1021/ct401016x`.

(91) I.-M. Høyvik, B. Jansik and P. Jørgensen, *J. Chem. Phys.*, 2012, **137**, 224114, DOI: `10.1063/1.4769866`.

(92) C. Krause and H.-J. Werner, *Phys. Chem. Chem. Phys.*, 2012, **14**, 7591–604, DOI: `10.1039/c2cp40231a`.

(93) Q. Ma, M. Schwilk, C. Köppl and H.-J. Werner, *J. Chem. Theory Comput.*, 2017, **13**, 4871–4896, DOI: `10.1021/acs.jctc.7b00799`.

(94) Q. Ma and H.-J. Werner, *J. Chem. Theory Comput.*, 2018, **14**, 198–215, DOI: `10.1021/acs.jctc.7b01141`.

(95) G. Schmitz and C. Hättig, *J. Chem. Theory Comput.*, 2017, **13**, 2623–2633, DOI: `10.1021/acs.jctc.7b00180`.

(96) M. S. Frank, G. Schmitz and C. Hättig, *Mol. Phys.*, 2017, **115**, 343–356, DOI: `10.1080/00268976.2016.1263762`.

(97) H.-J. Werner and K. Pflüger, *Annu. Rep. Comput. Chem.*, 2006, **2**, 53–80, DOI: `10.1016/S1574-1400(06)02004-4`.

(98) S. Saebø and P. Pulay, *J. Chem. Phys.*, 1987, **86**, 914–922, DOI: `10.1063/1.452293`.

(99) S. Saebø and P. Pulay, *J. Chem. Phys.*, 1988, **88**, 1884–1890, DOI: `10.1063/1.454111`.

(100) J. A. Pople, R. Krishnan, H. B. Schlegel and J. S. Binkley, *Int. J. Quantum Chem.*, 1979, **16**, 225–241, DOI: `10.1002/qua.560160825`.

(101) P. Pulay, *Chem. Phys. Lett.*, 1980, **73**, 393–398, DOI: `10.1016/0009-2614(80)80396-4`.

(102) P. Pulay, *J. Comput. Chem.*, 1982, **3**, 556–560, DOI: `10.1002/jcc.540030413`.

(103)   R. Shepard and M. Minkoff, *Mol. Phys.*, 2007, **105**, 2839–2848, DOI: `10.1080/00268970701691611`.

(104)   A. J. Garza and G. E. Scuseria, *J. Chem. Phys.*, 2012, **137**, 054110, DOI: `10.1063/1.4740249`.

(105)   H.-J. Werner and F. R. Manby, *J. Chem. Phys.*, 2006, **124**, 054114, DOI: `10.1063/1.2150817`.

(106)   O. Vahtras, J. Almlöf and M. Feyereisen, *Chem. Phys. Lett.*, 1993, **213**, 514–518, DOI: `https://doi.org/10.1016/0009-2614(93)89151-7`.

(107)   R. Polly, H.-J. Werner, F. R. Manby and P. J. Knowles, *Mol. Phys.*, 2004, **102**, 2311–2321, DOI: `10.1080/0026897042000274801`.

(108)   K. Eichkorn, F. Weigend, O. Treutler and R. Ahlrichs, *Theor. Chem. Acc.*, 1997, **97**, 119–124, DOI: `10.1007/s002140050244`.

(109)   F. R. Manby, P. J. Knowles and A. W. Lloyd, *J. Chem. Phys.*, 2001, **115**, 9144–9148, DOI: `10.1063/1.1414370`.

(110)   F. Weigend, A. Köhn and C. Hättig, *J. Chem. Phys.*, 2002, **116**, 3175–3183, DOI: `10.1063/1.1445115`.

(111)   J. C. A. Oliveira, J. Feldt, N. Galamba and R. A. Mata, *J. Phys. Chem. A*, 2012, **116**, 5464–5471, DOI: `10.1021/jp301516b`.

(112)   T. N. Truong and E. V. Stefanovich, *J. Chem. Phys.*, 1995, **103**, 3709–3717, DOI: `10.1063/1.470048`.

(113)   V. Barone and M. Cossi, *J. Phys. Chem. A*, 1998, **102**, 1995–2001, DOI: `10.1021/jp9716997`.

(114)   J. G. Ángyán, *Chem. Phys. Lett.*, 1995, **241**, 51–56, DOI: `10.1016/0009-2614(95)00602-Z`.

(115)   J. W. Knight, X. Wang, L. Gallandi, O. Dolgounitcheva, X. Ren, J. V. Ortiz, P. Rinke, T. Körzdörfer and N. Marom, *J. Chem. Theory Comput.*, 2016, **12**, 615–626, DOI: `10.1021/acs.jctc.5b00871`.

(116)   L. Gallandi, N. Marom, P. Rinke and T. Körzdörfer, *J. Chem. Theory Comput.*, 2016, **12**, 605–614, DOI: `10.1021/acs.jctc.5b00873`.

(117)   O. Dolgounitcheva, M. Díaz-Tinoco, V. G. Zakrzewski, R. M. Richard, N. Marom, C. D. Sherrill and J. V. Ortiz, *J. Chem. Theory Comput.*, 2016, **12**, 627–637, DOI: `10.1021/acs.jctc.5b00872`.

(118)   O. Marchetti and H.-J. Werner, *Phys. Chem. Chem. Phys.*, 2008, **10**, 3400–3409, DOI: `10.1039/B804334E`.

(119) O. Marchetti and H.-J. Werner, *J. Phys. Chem. A*, 2009, **113**, 11580–11585, DOI: `10.1021/jp9059467`.

(120) P. Jurecka, J. Sponer, J. Cerny and P. Hobza, *Phys. Chem. Chem. Phys.*, 2006, **8**, 1985–1993, DOI: `10.1039/B600027D`.

(121) A. Halkier, T. Helgaker, P. Jørgensen, W. Klopper, H. Koch, J. Olsen and A. K. Wilson, *Chem. Phys. Lett.*, 1998, **286**, 243–252, DOI: `10.1016/S0009-2614(98)00111-0`.

(122) A. Halkier, T. Helgaker, P. Jørgensen, W. Klopper and J. Olsen, *Chem. Phys. Lett.*, 1999, **302**, 437–446, DOI: `10.1016/S0009-2614(99)00179-7`.

(123) T. Takatani, E. G. Hohenstein, M. Malagoli, M. S. Marshall and C. D. Sherrill, *J. Chem. Phys.*, 2010, **132**, 144104, DOI: `10.1063/1.3378024`.

(124) R. Podeszwa, K. Patkowski and K. Szalewicz, *Phys. Chem. Chem. Phys.*, 2010, **12**, 5974–5979, DOI: `10.1039/B926808A`.

(125) M. O. Sinnokrot and C. D. Sherrill, *J. Phys. Chem. A*, 2004, **108**, 10200–10207, DOI: `10.1021/jp0469517`.

(126) S. Boys and F. Bernardi, *Mol. Phys.*, 1970, **19**, 553–566, DOI: `10.1080/00268977000101561`.

(127) L. Gráfová, M. Pitoňák, J. Řezáč and P. Hobza, *J. Chem. Theory Comput.*, 2010, **6**, 2365–2376, DOI: `10.1021/ct1002253`.

(128) L. F. Molnar, X. He, B. Wang and K. M. Merz, *J. Chem. Phys.*, 2009, **131**, 065102, DOI: `10.1063/1.3173809`.

(129) J. Řezáč, K. E. Riley and P. Hobza, *J. Chem. Theory Comput.*, 2011, **7**, 2427–2438, DOI: `10.1021/ct2002946`.

(130) W. Győrffy, G. Knizia and H.-J. Werner, *J. Chem. Phys.*, 2017, **147**, 214101, DOI: `10.1063/1.5003065`.

(131) A. Karton and J. M. L. Martin, *Theor. Chem. Acc.*, 2006, **115**, 330–333, DOI: `10.1007/s00214-005-0028-6`.

(132) T. Helgaker, W. Klopper, H. Koch and J. Noga, *J. Chem. Phys.*, 1997, **106**, 9639–9646, DOI: `10.1063/1.473863`.

(133) S. Grimme, *J. Chem. Phys.*, 2003, **118**, 9095–9102, DOI: `10.1063/1.1569242`.

(134) P. Michal, N. Pavel, Č. Jiří, G. Stefan and H. Pavel, *ChemPhysChem*, 2009, **10**, 282–289, DOI: `10.1002/cphc.200800718`.

(135) I. Waldner, *Declaration of Authorship*, 2018, `http://www.uni-stuttgart.de/chemie/studium/promotion/Erkl._zur_Eigenstaendigkeit_der_Diss_De_Eng.doc`.

Appendix

1 Supplementary data for the extended FH-set

Iext	Length (bohr)			Angle (deg)		
	0	1	2	0	1	2
IBO exponent $p = 4$						
MAE	0.0018	0.0002	0.0000	0.040	0.006	0.000
RMS	0.0027	0.0004	0.0000	0.057	0.008	0.000
MAX	0.0092	0.0018	0.0000	0.252	0.034	0.002
IBO exponent $p = 2$						
MAE	0.0018	0.0002	0.0000	0.041	0.006	0.000
RMS	0.0027	0.0004	0.0000	0.060	0.009	0.000
MAX	0.0092	0.0018	0.0000	0.286	0.042	0.002
PM						
MAE	0.0017	0.0002	0.0000	0.040	0.005	0.000
RMS	0.0026	0.0004	0.0000	0.061	0.008	0.000
MAX	0.0089	0.0016	0.0000	0.291	0.031	0.002

Table 1: Group 1 DF-LMP2/AVTZ' errors relative to DF-MP2/AVTZ'.

Iext	Length (bohr)			Angle (deg)		
	0	1	2	0	1	2
IBO exponent $p = 4$						
MAE	0.0027	0.0006	0.0002	0.047	0.018	0.011
RMS	0.0041	0.0010	0.0003	0.068	0.028	0.018
MAX	0.0148	0.0042	0.0016	0.599	0.287	0.184
IBO exponent $p = 2$						
MAE	0.0028	0.0006	0.0002	0.048	0.018	0.011
RMS	0.0043	0.0010	0.0003	0.068	0.028	0.018
MAX	0.0161	0.0041	0.0016	0.586	0.288	0.184
PM						
MAE	0.0028	0.0006	0.0002	0.050	0.018	0.011
RMS	0.0043	0.0010	0.0003	0.073	0.028	0.018
MAX	0.0231	0.0039	0.0015	0.589	0.285	0.183

Table 2: Group 2 DF-LMP2/AVTZ' errors relative to DF-MP2/AVTZ'.

Iext	Length (bohr)			Angle (deg)		
	0	1	2	0	1	2
IBO exponent $p = 4$						
MAE	0.0031	0.0008	0.0003	0.062	0.023	0.014
RMS	0.0051	0.0013	0.0005	0.104	0.039	0.025
MAX	0.0215	0.0063	0.0031	1.048	0.211	0.128
IBO exponent $p = 2$						
MAE	0.0033	0.0008	0.0003	0.061	0.024	0.014
RMS	0.0055	0.0014	0.0005	0.103	0.040	0.025
MAX	0.0215	0.0063	0.0031	1.018	0.211	0.128
PM						
MAE	0.0033	0.0008	0.0003	0.069	0.024	0.014
RMS	0.0054	0.0014	0.0005	0.113	0.040	0.025
MAX	0.0220	0.0064	0.0031	0.992	0.206	0.129

Table 3: Group 3 DF-LMP2/AVTZ' errors relative to DF-MP2/AVTZ'. Anthracene not included.

Iext	Length (bohr)			Angle (deg)		
	0	1	2	0	1	2
IBO exponent $p = 4$						
MAE	0.0038	0.0014	0.0006	0.069	0.023	0.020
RMS	0.0063	0.0020	0.0009	0.116	0.040	0.034
MAX	0.0246	0.0068	0.0033	0.603	0.210	0.166
IBO exponent $p = 2$						
MAE	0.0038	0.0014	0.0006	0.068	0.024	0.020
RMS	0.0062	0.0020	0.0008	0.114	0.041	0.034
MAX	0.0236	0.0067	0.0033	0.595	0.207	0.164
PM						
MAE	0.0043	0.0014	0.0006	0.104	0.027	0.021
RMS	0.0068	0.0021	0.0009	0.159	0.045	0.037
MAX	0.0244	0.0072	0.0032	0.755	0.218	0.181

Table 4: Group 4 DF-LMP2/AVTZ' errors relative to DF-MP2/AVTZ'.

Orb	Energy	Centres and Charges
8	-0.814583	C 1 1.130 H 2 0.731 C 3 0.073 C 6 0.026 C 7 0.025
9	-0.429650	C 3 0.993 C 1 0.954 C 4 0.034
10	-0.429650	C 3 0.993 C 1 0.954 C 4 0.034
11	-0.803734	C 3 0.987 C 4 0.732 C 1 0.224 H 2 0.023 (other: 0.035)
12	-1.022870	C 4 0.603 C 5 0.473 C 3 0.338 C 1 0.304 C 6 0.166 C 7 0.105
13	-0.433448	C 4 0.958 C 5 0.950 C 1 0.033 C 7 0.021 (other: 0.037)
14	-0.433448	C 4 0.958 C 5 0.950 C 1 0.033 C 7 0.021 (other: 0.037)
15	-1.046350	C 5 0.574 C 4 0.530 C 3 0.251 C 6 0.244 C 7 0.220 C 1 0.152 C 8 0.022
16	-1.016391	C 7 0.529 C 6 0.469 C 1 0.374 C 3 0.332 C 8 0.105 C 4 0.102 C 5 0.069
17	-0.850561	C 6 0.948 C 5 0.845 C 7 0.106 C 8 0.044 C 4 0.022 (other: 0.035)
18	-0.429191	C 6 1.017 C 7 0.916 C 5 0.029 C 4 0.023
19	-0.429191	C 6 1.017 C 7 0.916 C 5 0.029 C 4 0.023
20	-0.754714	C 7 1.072 C 8 0.764 C 6 0.127 C 5 0.021
21	-0.692865	C 8 1.145 H 10 0.826 (other: 0.029)
22	-0.692865	C 8 1.145 H 9 0.826 (other: 0.029)
23	-0.692867	C 8 1.145 H 11 0.826 (other: 0.029)

Table 5: Orbitals of HC≡C−C≡C−C≡C−CH₃ generated after geometry optimization using a PM localization scheme based on IAO partial charges. Energy in a.u., print threshold for centres 0.20.

Orb	Energy	Centres and Charges
8	-0.984119	C 3 1.008 C 1 0.974
9	-0.974285	C 5 0.997 C 4 0.994
10	-0.973640	C 6 1.000 C 7 0.992
11	-0.912094	C 4 0.999 C 3 0.990
12	-0.908643	C 5 1.005 C 6 0.985
13	-0.820525	C 7 1.071 C 8 0.925
14	-0.754003	C 1 1.231 H 2 0.766
15	-0.688438	C 8 1.152 H 9 0.826 (other: 0.022)
16	-0.688438	C 8 1.152 H 11 0.826 (other: 0.022)
17	-0.688438	C 8 1.152 H 10 0.826 (other: 0.022)
18	-0.434094	C 4 0.973 C 5 0.935 C 7 0.026 C 3 0.026 C 1 0.023
19	-0.434094	C 4 0.973 C 5 0.935 C 7 0.026 C 3 0.026 C 1 0.023
20	-0.427753	C 6 1.025 C 7 0.903 C 5 0.036 (other: 0.035)
21	-0.427753	C 6 1.025 C 7 0.903 C 5 0.036 (other: 0.035)
22	-0.425589	C 3 0.983 C 1 0.965 C 5 0.024 C 4 0.024
23	-0.425589	C 3 0.983 C 1 0.965 C 5 0.024 C 4 0.024

Table 6: Orbitals of $HC\equiv C-C\equiv C-C\equiv C-CH_3$ generated after geometry optimization using a IBO $p = 4$ localization scheme. Energy in a.u., print threshold for centres 0.20.

Orb	Energy	Centres and Charges
8	-0.976254	C 3 1.007 C 1 0.984
9	-0.973734	C 5 0.997 C 4 0.995
10	-0.971984	C 6 0.998 C 7 0.995
11	-0.911489	C 4 0.998 C 3 0.992
12	-0.908476	C 5 1.004 C 6 0.986
13	-0.817608	C 7 1.069 C 8 0.927
14	-0.762701	C 1 1.222 H 2 0.775
15	-0.688891	C 8 1.151 H 10 0.828 (other: 0.021)
16	-0.688889	C 8 1.151 H 11 0.828 (other: 0.021)
17	-0.688889	C 8 1.151 H 9 0.828 (other: 0.021)
18	-0.435557	C 4 0.968 C 5 0.940 C 3 0.025 C 1 0.024 C 7 0.023 (other: 0.020)
19	-0.435557	C 4 0.968 C 5 0.940 C 3 0.025 C 1 0.024 C 7 0.023 (other: 0.020)
20	-0.427828	C 6 1.018 C 7 0.912 C 5 0.031 C 4 0.024
21	-0.427828	C 6 1.018 C 7 0.912 C 5 0.031 C 4 0.024
22	-0.425923	C 3 0.984 C 1 0.964 C 4 0.024 C 5 0.023
23	-0.425923	C 3 0.984 C 1 0.964 C 4 0.024 C 5 0.023

Table 7: Orbitals of $HC\equiv C-C\equiv C-C\equiv C-CH_3$ generated after geometry optimization using a IBO $p = 2$ localization scheme. Energy in a.u., print threshold for centres 0.20.

No	PM0	PM1	PM2	IB0	IB1	IB2	Canon
1	0.0047	0.0072	0.0076	0.0046	0.0072	0.0076	0.0077
2	0.0067	0.0104	0.0108	0.0064	0.0104	0.0108	0.0108
3	0.0060	0.0094	0.0097	0.0058	0.0093	0.0097	0.0098
4	0.0082	0.0106	0.0110	0.0096	0.0107	0.0110	0.0110
5	0.0066	0.0099	0.0104	0.0067	0.0099	0.0104	0.0104
6	0.0061	0.0084	0.0088	0.0061	0.0084	0.0088	0.0089
7	0.0051	0.0067	0.0072	0.0051	0.0067	0.0072	0.0074
8	0.0047	0.0062	0.0067	0.0047	0.0062	0.0067	0.0068
9	0.0050	0.0070	0.0073	0.0050	0.0070	0.0073	0.0074
10	0.0058	0.0077	0.0082	0.0057	0.0077	0.0082	0.0083
11	0.0050	0.0071	0.0075	0.0050	0.0071	0.0075	0.0077
12	0.0074	0.0091	0.0095	0.0073	0.0091	0.0095	0.0097

Table 8: RMS in bohr of DF-(L)MP2/AVTZ' relative to DF-CCSD(T)/AVTZ'. PM localization with Iext= $0, 1, 2$ denoted as PM0, PM1, and PM2 respectively. IBO $p = 4$ localization equivalently denoted as IB0, IB1, and IB2, and canonical DF-MP2 as Canon. Calculations performed on 12 systems as listed in tab. 6.6.

2 Supplementary data for the Ionization Potentials

Molecule	A/1	A/2	A/3	A/4	A/5	A/6	A/7	A/8
Acridine	8.67	7.86	(M)	8.68	-	-	-	-
Anthracene	10.93	12.62	10.42	7.36	11.68	11.11	8.50	9.21
Azulene	10.90	8.43	11.73	7.32	-	-	-	-
Benzonitrile	12.58	9.72	11.88	9.91	-	-	-	-
Benzoquinone	14.27	14.91	11.00	13.44	10.38	10.14	10.97	(M)
Borondipyrromethene		6.68*	-	-	-	-	-	-
Dichlone	10.31	9.62	10.07	9.81	-	-	-	-
Dinitrobenzonitrile	11.77	10.87	(M)	11.18	-	-	-	-
Fumaronitrile	12.96	11.19	13.15	13.54	-	-	-	-
Maleic Anhydride	11.89	11.83	11.13	14.30	-	-	-	-
mDCNB	12.55	10.42	12.39	10.22	-	-	-	-
Naphthalenedione	10.00	9.71	9.75	9.63	-	-	-	-
NDCA	11.35	9.58	10.18	8.94	-	-	-	-
Nitrobenzene	11.07	10.01	10.39	9.94	-	-	-	-
Nitrobenzonitrile	11.50	10.38	10.82	10.54	-	-	-	-
Phenazine	8.66	12.08	10.23	11.92	11.08	8.87	8.29	9.53
Phthalic Anhydride	11.27	10.65	10.31	10.28	-	-	-	-
Phthalimide	10.70	9.84	10.03	9.91	-	-	-	-
TCNE	14.04	13.89	14.06	13.53	11.71	14.06	14.77	13.86
TCNQ	(M)	13.08	12.80	12.81	9.38	11.51	11.06	13.08
Cl$_4$-Benzoquinone	12.62	11.98	10.95	10.73	10.62	12.64	9.89	12.89
Cl$_4$-Isobenzofurandione	(M)	10.04	10.72	9.71	-	-	-	-
F$_4$-Benzenedicarbonitrile	13.67	13.73	13.16	13.20	12.78	10.75	10.30	17.18
F$_4$-Benzoquinone	15.02	16.05	11.40	11.44	11.46	14.24	10.70	17.10

Table 9: Adiabatic IPs in eV of 24 different molecules for up to 8 irreps, denoted A/1 to A/8. Tab. 10 lists the names of all irreps used above. Geometry optimizations performed using (R)MP2/AVTZ' gradients, single point energies calculated on UCCSD(T)/AVTZ' or (*) DF-LUCCSD(T) level. (M) indicates a multi-reference state.

No	D_{2h}	C_{2v}	C_{2h}	C_s
1	A_g	A_1	A_g	A'
2	B_{3u}	B_1	A_u	A''
3	B_{2u}	B_2	B_u	-
4	B_{1g}	A_2	B_g	-
5	B_{1u}	-	-	-
6	B_{2g}	-	-	-
7	B_{3g}	-	-	-
8	A_u	-	-	-

Table 10: Irreps of point groups D_{2h}, C_{2v}, C_{2h}, and C_s with enumeration as in MOLPRO.

Molecule	V/F12a	V/F12b	A/F12a	A/F12b
Acridine	7.96	7.95	7.92	7.91
Anthracene	7.45	7.44	7.41	7.40
Azulene	7.51	7.50	7.38	7.37
Benzonitrile	9.91	9.90	9.79	9.78
Benzoquinone	10.29	10.27	10.22	10.22
Dichlone	10.06	10.05	9.88	9.87
Dinitrobenzonitrile	11.10	11.09	10.96	10.94
Fumaronitrile	11.38	11.36	11.28	11.26
Maleic Anhydride	11.30	11.29	11.24	11.22
mDCNB	10.40	10.39	10.31	10.29
Naphthalenedione	9.88	9.86	9.70	9.68
NDCA	9.11	9.10	9.02	9.01
Nitrobenzene	10.17	10.16	10.01	10.00
Nitrobenzonitrile	10.58	10.56	10.46	10.45
Phenazine	8.40	8.38	8.36	8.34
Phthalic Anhydride	10.54	10.53	10.35	10.34
Phthalimide	10.06	10.05	9.91	9.90
TCNE	11.87	11.85	11.82	11.80
TCNQ	9.48	9.46	9.47	9.45
Cl_4-Benzoquinone	10.08	10.07	9.95	9.93
Cl_4-Isobenzofurandione	9.96	9.95	9.78	9.77
F_4-Benzenedicarbonitrile	10.71	10.70	10.38	10.37
F_4-Benzoquinone	11.07	11.05	10.78	10.76

Table 11: IPs in eV for 23 different molecules, with V/F12a and A/F12a the respective vertical and adiabatic IPs on UCCSD(T)-F12a/AVTZ level, and V/F12b and A/F12b on UCCSD(T)-F12b/AVTZ level. Irreps default to the relaxed cations smallest IP, tab. 6.8.

3 Supplementary data for FeC$_{72}$N$_2$H$_{100}$

Geometry of FeC$_{72}$N$_2$H$_{100}$ obtained using partly density-fitted algorithm, converged to 10^{-5} hartree and a norm of 10^{-3} a.u..

Fe	-0.0001014904	-0.0000252171	-0.0000107314
N	0.0063572732	-0.0094449009	1.9603710019
N	-0.0063567007	0.0094107787	-1.9603713425
C	1.0739434415	-0.0096441712	2.8422574678
C	2.4084946885	-0.0243443282	2.3435861960
C	3.5078377676	-0.0361154604	3.2188943834
C	3.3379315893	-0.0319915696	4.6068127497
C	2.0329769965	-0.0033656818	5.1079298773
C	0.9087326356	0.0086661075	4.2618677531
C	2.7107883347	-0.0196884674	0.8717064253
C	3.1802984515	-1.2098749435	0.2394797730
C	3.7186391169	-1.1275144838	-1.0527992499
C	3.8462157054	0.0962648337	-1.7352333710
C	3.3069788005	1.2429420286	-1.1339068622
C	2.7359253674	1.2097912057	0.1549047508
C	3.2301265360	-2.5435477714	0.9855998330
C	4.6809443632	-2.9185694590	1.3299805870
C	2.5502487477	-3.6826855376	0.2154954488
C	4.6215843477	0.1356295328	-3.0503346894
C	6.0733632961	-0.3183384163	-2.8168701227
C	4.6140004503	1.5026521447	-3.7367022578
C	2.3098110843	2.5183661905	0.8267224290
C	1.5812061155	3.4816255436	-0.1215962682
C	3.5290389134	3.2054157996	1.4599131111
C	-0.4378473554	0.0792272824	4.9227003330
C	-1.0001333105	-1.0830599534	5.5242324113
C	-2.1922896825	-0.9556046965	6.2553413705
C	-2.8456590476	0.2792240309	6.4171899404
C	-2.2815026862	1.4100370921	5.8104500398
C	-1.0825022701	1.3333003486	5.0746036789
C	-0.3117560193	-2.4433742585	5.3788313450
C	-0.6570252933	-3.4394986480	6.4920668652
C	-0.5878912883	-3.0620856549	3.9993263854

C	-4.0794177190	0.3588082684	7.3101021168
C	-5.0989341449	1.4185792376	6.8778048673
C	-3.6577772644	0.5775947543	8.7724364267
C	-0.4886882092	2.6141351505	4.4909470774
C	-0.2412906427	3.6762642486	5.5721453292
C	-1.3579209781	3.1734145905	3.3560880372
C	-1.0739343349	0.0096191359	-2.8422529979
C	-2.4084868852	0.0243235714	-2.3435778195
C	-3.5078349461	0.0361058660	-3.2188788625
C	-3.3379404584	0.0319894270	-4.6067996472
C	-2.0329875538	0.0033596218	-5.1079250831
C	-0.9087317735	-0.0086824489	-4.2618683490
C	-2.7108055452	0.0196714094	-0.8717045602
C	-3.1803091444	1.2098485415	-0.2394865390
C	-3.7186524878	1.1274951992	1.0527795427
C	-3.8462427913	-0.0962704582	1.7352163841
C	-3.3070225050	-1.2429412213	1.1338873524
C	-2.7359722502	-1.2097943367	-0.1549098386
C	-3.2301117104	2.5435210999	-0.9856020827
C	-4.6809235281	2.9185769399	-1.3300005752
C	-2.5502206124	3.6826503740	-0.2154919028
C	-4.6216031963	-0.1356229481	3.0503314681
C	-6.0733847120	0.3183489948	2.8168840369
C	-4.6140184332	-1.5026391299	3.7367099756
C	-2.3098646376	-2.5183538277	-0.8267198421
C	-1.5812641441	-3.4815919754	0.1215916139
C	-3.5290703915	-3.2054083919	-1.4599170262
C	0.4378599131	-0.0792292923	-4.9226963049
C	1.0001499032	1.0830607251	-5.5242181426
C	2.1923094342	0.9556145236	-6.2553229557
C	2.8456849932	-0.2792097576	-6.4171745963
C	2.2815328960	-1.4100257204	-5.8104358277
C	1.0825222158	-1.3332988460	-5.0746058409
C	0.3117664867	2.4433673572	-5.3788167106
C	0.6570168444	3.4394982187	-6.4920511497
C	0.5878848036	3.0620855312	-3.9993088872
C	4.0794445844	-0.3587887435	-7.3100857327
C	5.0989684879	-1.4185511241	-6.8777851703
C	3.6578071929	-0.5775848279	-8.7724194579

C	0.4887042859	-2.6141494380	-4.4909884100
C	0.2413554473	-3.6762623287	-5.5722124894
C	1.3579226410	-3.1734393508	-3.3561201673
H	-0.8787763982	0.0197108004	2.4671634041
H	4.5141351510	-0.0381904874	2.7881912230
H	4.1993738513	-0.0402380081	5.2789731464
H	1.8609884874	0.0176553935	6.1891491317
H	4.0995644140	-2.0364728857	-1.5273757480
H	3.3527919739	2.1944257166	-1.6650193948
H	2.6890366145	-2.4135617379	1.9339922423
H	4.7081098472	-3.8569126842	1.9058620372
H	5.1656360353	-2.1353403114	1.9286607572
H	5.2752145504	-3.0636693240	0.4133485955
H	3.0827500057	-3.9146414141	-0.7196506694
H	1.5107859037	-3.4311244517	-0.0375362696
H	2.5393368721	-4.5970903672	0.8286449019
H	4.1396647044	-0.5861615566	-3.7332087136
H	6.6347758362	-0.3185693989	-3.7638247432
H	6.1267795142	-1.3311693838	-2.3918517386
H	6.5790417901	0.3675841244	-2.1188734457
H	5.1342215870	2.2549234210	-3.1219310742
H	3.5926488539	1.8507893890	-3.9373140263
H	5.1389317031	1.4386182868	-4.7010450007
H	1.6151202414	2.2556808811	1.6415519239
H	1.1782972315	4.3335555686	0.4476885345
H	0.7477994349	2.9896509260	-0.6466544412
H	2.2681717609	3.8890498346	-0.8793257416
H	4.2850812291	3.4349838178	0.6911545627
H	3.9928879927	2.5613740476	2.2209025872
H	3.2350485749	4.1500619545	1.9437782735
H	-2.6316287025	-1.8357493276	6.7318129056
H	-2.7644431077	2.3832500985	5.9293041419
H	0.7726993008	-2.2597896669	5.4358692027
H	-0.5078947391	-3.0011520201	7.4897931701
H	-0.0100721308	-4.3256389636	6.4086542511
H	-1.6986545665	-3.7881278024	6.4216665842
H	-1.6618899148	-3.2737620872	3.8746791992
H	-0.0418970001	-4.0124771524	3.8884282689
H	-0.2733765103	-2.3879075505	3.1913658692

H	-4.5775215883	-0.6256857380	7.2514500881
H	-4.7052587649	2.4364144426	7.0197631742
H	-6.0133735693	1.3343435418	7.4841477437
H	-5.3770597055	1.3041914076	5.8202439329
H	-3.1374460218	1.5424366400	8.8792209944
H	-2.9727112719	-0.2144938089	9.1087085297
H	-4.5348858020	0.5828426341	9.4385724207
H	0.4928068147	2.3571135862	4.0630545057
H	-1.1854103830	4.0290175661	6.0153871548
H	0.2686402583	4.5500400384	5.1367462139
H	0.3883368465	3.2771403709	6.3811891607
H	-1.4688552463	2.4353364544	2.5501363751
H	-0.9002629985	4.0802990740	2.9291344916
H	-2.3629194675	3.4421916483	3.7199860754
H	0.8787692022	-0.0197378940	-2.4671197793
H	-4.5141300761	0.0381869616	-2.7881610957
H	-4.1993898762	0.0402459239	-5.2789500851
H	-1.8609989269	-0.0176537615	-6.1891445753
H	-4.0995622783	2.0364563646	1.5273616902
H	-3.3528388135	-2.1944184876	1.6650020062
H	-2.6890215123	2.4135232302	-1.9339775575
H	-4.7080530115	3.8569221011	-1.9058801777
H	-5.1656265870	2.1353638661	-1.9286939298
H	-5.2752027879	3.0636997344	-0.4133722087
H	-3.0827236036	3.9146113597	0.7196517794
H	-1.5107622209	3.4310722624	0.0375478280
H	-2.5392913920	4.5970571256	-0.8286367739
H	-4.1396670162	0.5861666879	3.7331968940
H	-6.6347865568	0.3185835585	3.7638437716
H	-6.1268187903	1.3311834306	2.3918681546
H	-6.5790768098	-0.3675709140	2.1188952343
H	-5.1342540299	-2.2549124185	3.1219520985
H	-3.5926679582	-1.8507780423	3.9373218640
H	-5.1389454466	-1.4385850637	4.7010538574
H	-1.6151714129	-2.2556658626	-1.6415354501
H	-1.1783369006	-4.3335215989	-0.4476901282
H	-0.7478679132	-2.9896092368	0.6466521882
H	-2.2682191652	-3.8890239949	0.8793177989
H	-4.2851203477	-3.4349903040	-0.6911688150

H	-3.9929224083	-2.5613764340	-2.2209087069
H	-3.2350725140	-4.1500546615	-1.9437816003
H	2.6316453331	1.8357656352	-6.7317857268
H	2.7644784378	-2.3832358862	-5.9292919859
H	-0.7726853732	2.2597647873	-5.4358631432
H	0.5078820460	3.0011511176	-7.4897764959
H	0.0100495989	4.3256276688	-6.4086321526
H	1.6986414215	3.7881431599	-6.4216628500
H	1.6618768102	3.2737913407	-3.8746523764
H	0.0418651978	4.0124627450	-3.8884102179
H	0.2733879698	2.3878984419	-3.1913485153
H	4.5775411113	0.6257090824	-7.2514379095
H	4.7053006092	-2.4363891923	-7.0197438990
H	6.0134086954	-1.3343095498	-7.4841260237
H	5.3770906379	-1.3041603797	-5.8202240000
H	3.1374850592	-1.5424318770	-8.8792015918
H	2.9727350118	0.2144965339	-9.1086959218
H	4.5349172909	-0.5828274962	-9.4385535398
H	-0.4928029569	-2.3571545304	-4.0631075697
H	1.1854946229	-4.0289859214	-6.0154361291
H	-0.2685624063	-4.5500588437	-5.1368383675
H	-0.3882613915	-3.2771389017	-6.3812645467
H	1.4688318996	-2.4353797602	-2.5501467919
H	0.9002696879	-4.0803399671	-2.9291944064
H	2.3629323397	-3.4421955948	-3.7200014092

4 Supplementary data for Noncovalent Intercations

Equilibrium geometries of the invesitgated dimers on CP-DF-MP2/cc-pVTZ level as originally published in [129]. Other geometries used in our work can be found by scaling the main interaction coordinate by factors of $0.90, 0.95, 1.05, 1.10, 500$.

	Water-Water		
O	-0.702196054	-0.056060256	0.009942262
H	-1.022193224	0.846775782	-0.011488714
H	0.257521062	0.042121496	0.005218999
O	2.268880784	0.026340101	0.000508029
H	2.645502399	-0.412039965	0.766632411
H	2.641145101	-0.449872874	-0.744894473
	AcOH-AcOH		
C	-1.061709204	1.297140572	0.292060003
O	-0.358161116	2.270458613	0.531812668
O	-0.589303516	0.094917758	0.003788813
H	0.404435659	0.127722621	0.018411838
C	-2.558427798	1.342549823	0.296257320
H	-2.895997978	2.347464002	0.518316340
H	-2.932889278	1.022390451	-0.672995551
H	-2.937211960	0.644910433	1.039557084
C	2.799564974	1.108464452	0.271261944
O	2.095946609	0.135149964	0.031474342
O	2.327138640	2.310899840	0.559040415
H	1.333350100	2.278001606	0.544639911
C	4.296277422	1.062561706	0.269297549
H	4.633856986	0.061242513	0.031772054
H	4.677775967	1.772914645	-0.460171349
H	4.667793733	1.365256223	1.245352910

Benzene-Benzene ππ

C	0.712645325	1.120995701	0.060540783
H	1.357841649	1.986399167	0.127737169
C	1.258235731	-0.159251901	0.124233518
H	2.324954277	-0.287099878	0.246743035
C	0.426884963	-1.274526662	0.042650428
H	0.850444649	-2.268432680	0.094749952
C	-0.949577845	-1.110074058	-0.100313595
H	-1.594455696	-1.976273703	-0.163713480
C	-1.495525640	0.171050561	-0.161546018
H	-2.563782791	0.299221149	-0.273703115
C	-0.663827601	1.286642887	-0.083401433
H	-1.086900697	2.281000204	-0.132886135
C	1.949488213	1.110116294	3.600833554
H	2.594333337	1.976300037	3.664584272
C	2.495441339	-0.171034805	3.662353287
H	3.563648223	-0.299181855	3.775097506
C	1.663791859	-1.286634905	3.583702858
H	2.086873566	-2.280987340	3.633356521
C	0.287390298	-1.120999876	3.438986110
H	-0.357712298	-1.986410120	3.371353478
C	-0.258169573	0.159232871	3.375020282
H	-1.324797607	0.287062084	3.251841521
C	0.573107377	1.274513633	3.457091226
H	0.149582495	2.268418667	3.404722296

Benzene-Benzene TS

C	0.729188666	1.113101217	0.326728253
H	1.303215897	2.014222336	0.159160270
C	1.375087369	-0.119366352	0.412776946
H	2.450514736	-0.174623998	0.313307203
C	0.635039807	-1.280553386	0.629385409
H	1.136334479	-2.236017467	0.700217157
C	-0.750985629	-1.209654296	0.757890338
H	-1.324525898	-2.111412827	0.924198912
C	-1.397034430	0.022670814	0.673089633
H	-2.472425369	0.078488260	0.773997991
C	-0.656897314	1.184296216	0.458338585
H	-1.157828445	2.140587131	0.395096082
C	0.153204042	0.145707432	4.043919807
H	0.275330449	0.371190888	2.993493373
C	-0.937877526	-0.609191179	4.471256076
H	-1.658382055	-0.965705436	3.747561655
C	-1.098577507	-0.903316502	5.824206143
H	-1.945685094	-1.489285066	6.154453684
C	-0.166694946	-0.442263122	6.752700221
H	-0.290588442	-0.670229283	7.802707720
C	0.924890153	0.312838932	6.327459937
H	1.648009238	0.670672112	7.047842591
C	1.083694047	0.606323951	4.973968620
H	1.930951965	1.192398746	4.643921295

Ethene-Pentane

C	0.666400380	0.183810777	0.419736827
H	1.228881823	-0.329883014	1.186259711
H	1.228035558	0.697208130	-0.347609893
C	-0.665973577	0.182973428	0.419611910
H	-1.227921712	-0.331498899	1.186103344
H	-1.228184271	0.695645746	-0.347748081
C	-2.532764928	-0.397981112	4.211823937
H	-2.562258371	-1.011001895	3.310634058
H	-2.568898877	-1.072201731	5.067440951
H	-3.433936285	0.213035316	4.229069882
C	-1.271328442	0.454694304	4.247641874
H	-1.271734307	1.074787875	5.147035818
H	-1.262940095	1.141602620	3.398581462
C	-0.000054181	-0.382863267	4.220698667
H	-0.000208236	-1.069535974	5.072530681
H	0.000086886	-1.010441104	3.324056175
C	1.271166226	0.454723162	4.248103204
H	1.271439228	1.074533913	5.147588614
H	1.262971401	1.141797812	3.399195577
C	2.532617606	-0.398001350	4.212279020
H	2.562241077	-1.010857849	3.310969842
H	3.433795716	0.212934818	4.229857059
H	2.568535967	-1.072457431	5.067784731

Ethyne-Ethyne TS

C	-0.601729956	-0.028570118	0.384934916
H	-1.663735430	-0.028526566	0.379014311
C	0.610109174	-0.028663644	0.388163788
H	1.672135444	-0.028793082	0.387967520
C	-0.007422226	0.101064182	4.163366909
H	-0.004027846	0.067329130	3.100070027
C	-0.011358649	0.139354205	5.374832292
H	-0.014624881	0.172730086	6.435743710

Data used to generate the plots in chapter 7. Card. is the cardinal number of the underlying AVnZ' basis and CP refers to counterpoise corrected values (Yes/No). All methods are density-fitted and local methods use IBO $p = 4$ localization with Iext=0 (/0) or Iext=1 (/1).

AcOH-AcOH

Card.	CP	MP2	LMP2-F12/0	LMP2-F12/1	MP2-F12	LMP2/0	LMP2/1
2	N	1.678524	1.670719	1.667608	1.665130	1.730050	1.709979
3	N	1.671650	1.676205	1.673016	1.669326	1.702908	1.689653
4	N	1.669291	1.674279	1.671914	1.670404	1.688581	1.680512
5	N	1.669765	1.673655	1.671632	1.670560	1.682445	1.677011
CBS	N	1.669901					
2	Y	1.714147	1.668987	1.664798	1.671428	1.733731	1.718991
3	Y	1.689569	1.673729	1.671145	1.671400	1.703233	1.691464
4	Y	1.679308	1.673424	1.671152	1.671224	1.688769	1.680747
5	Y	1.675433	1.673372	1.671332	1.670976	1.682683	1.677089
CBS	Y	1.671722					

Benzene-Benzene $\pi\pi$

Card.	CP	MP2	LMP2-F12/0	LMP2-F12/1	MP2-F12	LMP2/0	LMP2/1
2	N	3.600202	3.694262	3.677961	3.634451	3.847957	3.724535
3	N	3.633352	3.697043	3.672082	3.656776	3.762764	3.705263
4	N	3.655599	3.691607	3.670091	3.663196	3.727746	3.683675
5	N	3.661882	3.685531	3.668596	3.665062	3.707149	3.678263
CBS	N	3.667043					
2	Y	3.765264	3.713775	3.680169	3.681027	3.866452	3.786888
3	Y	3.701855	3.707137	3.682598	3.668627	3.764392	3.715278
4	Y	3.681989	3.695965	3.674035	3.666882	3.727947	3.687196
5	Y	3.674336	3.687268	3.670188	3.666423	3.707259	3.678439
CBS	Y	3.666560					

Benzene-Benzene TS

Card.	CP	MP2	LMP2-F12/0	LMP2-F12/1	MP2-F12	LMP2/0	LMP2/1
2	N	2.416937	2.468567	2.457897	2.434219	2.576741	2.497074
3	N	2.430371	2.466550	2.455593	2.443669	2.510230	2.476385
4	N	2.444747	2.464309	2.454765	2.451013	2.487428	2.464487
5	N	2.449246	2.461806	2.454463	2.452373	2.474560	2.462265
CBS	N	2.452652					
2	Y	2.527811	2.480429	2.462085	2.464452	2.589832	2.545573
3	Y	2.478051	2.472434	2.462106	2.454191	2.512197	2.484162
4	Y	2.464171	2.466144	2.456536	2.453510	2.487673	2.464837
5	Y	2.458560	2.462547	2.455165	2.453100	2.474672	2.462386
CBS	Y	2.452445					

| | | | Ethene-Pentane | | | | |
Card.	CP	MP2	LMP2-F12/0	LMP2-F12/1	MP2-F12	LMP2/0	LMP2/1
2	N	3.720652	3.716966	3.702426	3.675485	3.951051	3.844140
3	N	3.685958	3.729942	3.714219	3.684396	3.809808	3.743497
4	N	3.689566	3.709534	3.698714	3.692103	3.752243	3.718600
5	N	3.693067	3.704225	3.694970	3.694061	3.727948	3.708329
CBS	N	3.695786					
2	Y	3.871952	3.746697	3.721989	3.726100	3.982276	3.911584
3	Y	3.752627	3.740222	3.724906	3.697931	3.813541	3.758779
4	Y	3.719247	3.712701	3.701960	3.696217	3.752859	3.719702
5	Y	3.706921	3.706615	3.697365	3.695434	3.728194	3.708777
CBS	Y	3.694216					
			Ethyne-Ethyne TS				
Card.	CP	MP2	LMP2-F12/0	LMP2-F12/1	MP2-F12	LMP2/0	LMP2/1
2	N	3.720652	3.716966	2.640914	2.635929	2.744306	2.681370
3	N	3.685958	3.729942	2.647025	2.645428	2.683328	2.664647
4	N	3.689566	3.709534	2.657087	2.654889	2.677884	2.670801
5	N	3.693067	3.704225	2.656975	2.657756	2.667329	2.665360
CBS	N	3.695786					
2	Y	3.871952	3.746697	2.647295	2.670085	2.780546	2.781313
3	Y	3.752627	3.740222	2.661313	2.659362	2.699769	2.701915
4	Y	3.719247	3.712701	2.658932	2.659320	2.677588	2.671589
5	Y	3.706921	3.706615	2.658610	2.658893	2.667428	2.665523
CBS	Y	3.694216					
			Water-Water				
Card.	CP	MP2	LMP2-F12/0	LMP2-F12/1	MP2-F12	LMP2/0	LMP2/1
2	N	1.959783	1.946406	1.954712	1.948163	2.013835	1.987792
3	N	1.953854	1.952422	1.951137	1.951195	1.983767	1.972558
4	N	1.950069	1.950924	1.948690	1.953073	1.968686	1.962261
5	N	1.951318	1.953281	1.951731	1.954189	1.963034	1.960049
CBS	N	1.951784					
2	Y	2.007456	1.948328	1.947753	1.959128	2.016360	2.012152
3	Y	1.976347	1.954123	1.953155	1.955624	1.985934	1.978044
4	Y	1.964251	1.951367	1.949131	1.955092	1.969249	1.962861
5	Y	1.959849	1.953570	1.951983	1.954858	1.963201	1.960137
CBS	Y	1.955290					
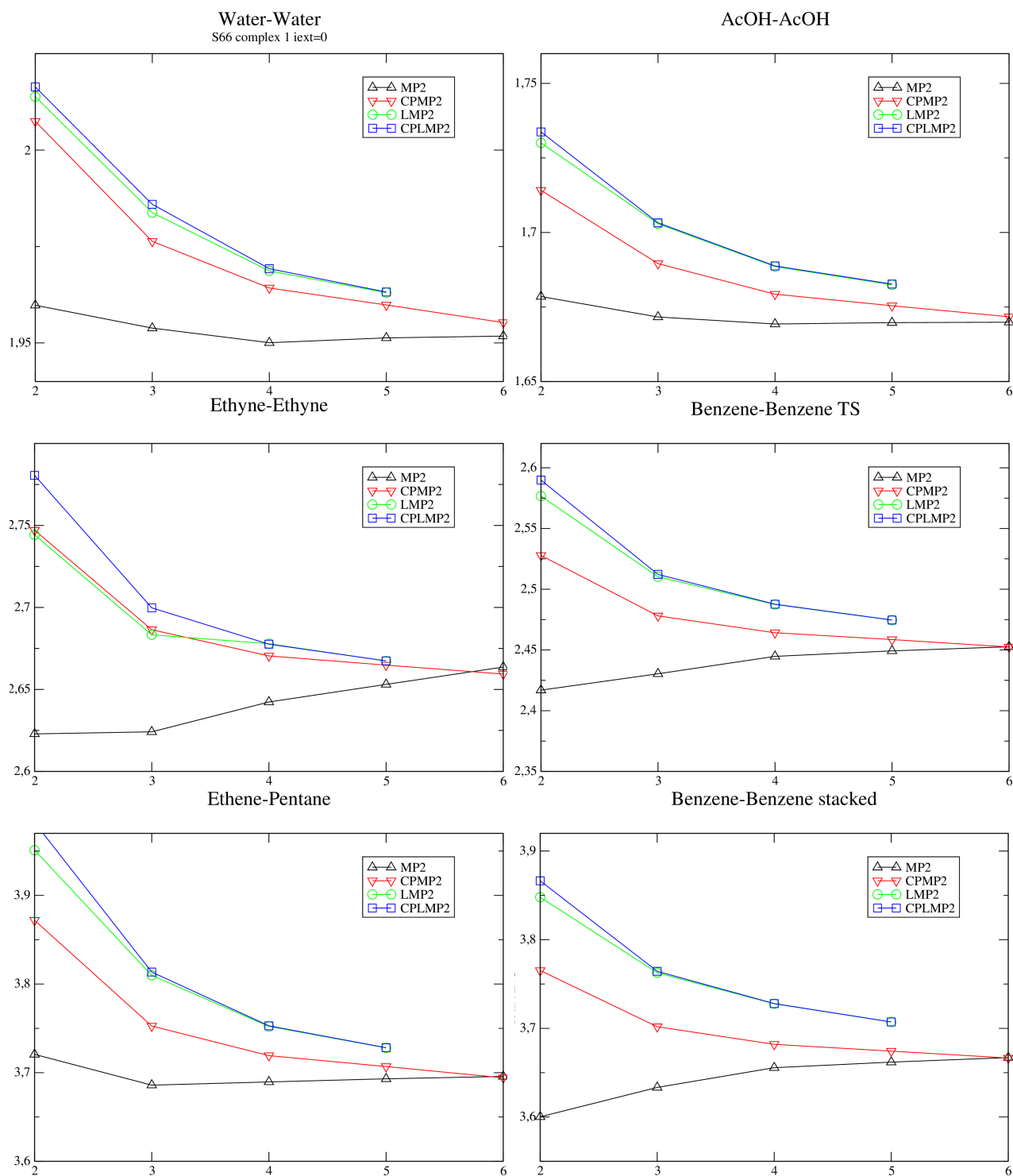
Figure 1: Convergence of the intermolecular equilibrium distance (Angstrom) as a function of the basis set size. x-axis: numbers $n = 1 - 5$ are cardinal numbers in AVnZ', 6 is extrapolation to the CBS limit. Depicted: MP2 (black), CP-MP2 (red), LMP2 (green), and CP-LMP2 (blue). All methods density-fitted using IBO $p = 4$, Iext=0 localization.

Erklärung über die Eigenständigkeit der Dissertation Ich versichere, dass ich die vorliegende Arbeit mit dem Titel *Analytical Energy Gradients for Open-Shell Local Second-Order Møller-Plesset Perturbation Theory and Applications to large Molecules* selbständig verfasst und keine anderen als die angegebenen Quellen und Hilfsmittel benutzt habe; aus fremden Quellen entnommene Passagen und Gedanken sind als solche kenntlich gemacht [135].

Declaration of Authorship I hereby certify that the dissertation entitled *Analytical Energy Gradients for Open-Shell Local Second-Order Møller-Plesset Perturbation Theory and Applications to large Molecules* is entirely my own work except where otherwise indicated. Passages and ideas from other sources have been clearly indicated [135].

Stuttgart, den 3. August 2018

_____

Mark Dornbach